

Development and distribution of soil properties on marine terraces on Central Spitsbergen

Comparing performance and results of two models



Marijn van der Meij
February, 2015



WAGENINGEN UNIVERSITY
WAGENINGEN UR

Development and distribution of soil properties on marine terraces on central Spitsbergen

Comparing performance and results of two models

W.M. (Marijn) van der Meij

91 11 25 563 010

A thesis submitted to Wageningen UR in partial fulfilment of the degree of Master of Science:

Earth and Environment, specialisation: Soil Geography and Landscape

Wageningen, February 2015

Supervisors:

dr.ir. A.J.A.M. (Arnaud) Temme
Soil Geography and Landscape group
Wageningen UR, Netherlands

dr.ir. G.B.M. (Gerard) Heuvelink
Soil Geography and Landscape group
Wageningen UR, Netherlands

Abstract

The effects of climate change on the arctic system influence soil forming processes. In order to study the effect of these short term changes (~100 years) on soil development, knowledge on long term soil development (~10.000 years) is needed. A general approach in studying soil forming processes and soil properties is the use of models. This study explored the use and performance of a static statistical Structural Equation Model (SEM) and a new dynamic mechanistic model (LORICA) for explaining and predicting spatial and temporal distribution of soil properties in arctic soils. A chronosequence of raised marine beaches located in central Spitsbergen provided opportunity to study both temporal as spatial variation. A literature study was used to get insight in different arctic soil forming processes. Data from 30 randomly selected locations was used for parameterization, calibration and validation of both models. Processes influencing soil development were isostatic rebound, aeolian deposition, weathering, silt translocation and organic matter uptake. SEM was the best predictive model and resulted in an unbiased prediction of observed properties. Parameters estimated by SEM could be explained on basis of the occurring processes. This shows the possibility of applying SEMs as explanatory and predictive models in soil science. Predictions from LORICA were biased and inaccurate when considering soil properties in individual horizons. LORICA does simulate general trends which were also observed in the field data when taking together properties of the individual horizons. Both models contributed in their own way to understanding spatial and temporal distribution of soil properties. SEM gave insight in distribution of soil properties. LORICA contributed in the understanding of underlying processes. The gained knowledge contributes to our general understanding of arctic soil formation and forms a basis for further research on variation in soil properties in the arctic.

Acknowledgements

This thesis was my last adventure as a student at the Wageningen UR. When I started in Wageningen over 5 years ago, I did not expect to end up on Spitsbergen for my master thesis research. First of all, I would like to thank 'the other student' Christian de Kleijn for coming up with the great idea of going to Spitsbergen. A big thanks also goes out to the researchers of the Adam Mickiewicz University, Poznan, for giving us the opportunity to stay at their research facility in the Ebba valley and for the spatial data of the area.

I like to thank Arnaud and Gerard for their supervision during this thesis. Your guidance and useful remarks helped me to structure all the work I have done and bring it together in this report.

Lotte, thank you for your patience when I had to continue working in evenings and weekends. Your support certainly helped me finishing this thesis.

Merlijn and Christian, thank you for the numerous games of chess.

At last, I like to thank the staff of the SGL group and all other people who helped me for the possibility to use the OSL lab, general guidance and the search for the right thesis template.

Contents

1	Introduction.....	1
1.1	General.....	1
1.2	Statistical and static modelling.....	1
1.3	Mechanistic and dynamic modelling.....	1
1.4	Research objective and questions.....	2
1.5	Reading guide.....	2
2	Study area.....	3
2.1	General.....	3
2.2	Local climate.....	3
2.3	Geology.....	4
2.4	Marine terraces.....	4
2.4.1	Isostatic uplift.....	4
2.4.2	Beach ridges and beach valleys.....	5
2.4.3	Position in the landscape.....	6
3	Soil development on marine terraces.....	7
3.1	Soil forming processes.....	7
3.1.1	Erosion and deposition.....	7
3.1.2	Cryogenic processes.....	8
3.1.3	Physical weathering.....	9
3.1.4	Chemical processes.....	10
3.1.5	Organic matter accumulation.....	10
3.1.6	Transport in the soil.....	11
3.1.7	Other soil Arctic soil forming processes.....	12
3.2	Conceptual model.....	12
4	Materials and methods.....	15
4.1	Available maps.....	15
4.2	Fieldwork.....	15
4.2.1	Sampling scheme.....	15
4.2.2	Field materials.....	16
4.2.3	Observations.....	16
4.2.4	Sampling method.....	16
4.2.5	Bulk density.....	17
4.3	Laboratory analysis.....	17
4.3.1	Moisture content.....	17
4.3.2	Particle size distribution.....	17
4.3.3	Organic matter fraction.....	18
4.4	Map preparations.....	18
4.4.1	Correcting the DEM.....	18
4.4.2	Vegetation index.....	19
4.4.3	Age map.....	19
4.5	Structural equation modelling.....	20
4.5.1	Introduction to the model.....	20
4.5.2	Model structure.....	21
4.5.3	Input data.....	23
4.6	LORICA.....	23
4.6.1	Model structure.....	24
4.6.2	Input data.....	26
4.6.3	Translating model output into horizons.....	27
4.7	Variation in the measurements.....	28

4.7.1	Variance in measuring thickness	28
4.7.2	Variance in laboratory measurements.....	29
4.8	Validation of model results	29
5	Results.....	31
5.1	Data analysis	31
5.1.1	Summary of sampling locations	31
5.1.2	Horizon thickness	32
5.1.3	Gravel fraction	32
5.1.4	Silt fraction	33
5.1.5	Organic matter.....	34
5.2	Structural equation model	34
5.2.1	Variance in measurements.....	34
5.2.2	Parameterization	35
5.2.3	Visualizing model performance	35
5.2.4	Predictions for the study area.....	37
5.2.5	Validation.....	37
5.3	LORICA	38
5.3.1	Parameterization and calibration.....	39
5.3.2	Prediction.....	39
5.3.3	Validation.....	42
6	Discussion	47
6.1	Processes and observed properties on the marine terraces.....	47
6.2	Predicting soil properties with SEM	48
6.3	Simulating soil forming processes and predicting soil properties with LORICA.....	48
6.4	Synthesis.....	49
6.4.1	Comparing model results	49
6.4.2	Performance of SEM.....	50
6.4.3	Performance of LORICA	51
7	Conclusions	53
8	References	55
	Appendix A: Field form	59
	Appendix B: R-scripts used for SEM	61
	B1: Horizon 2A	61
	B2: Horizon 2B/	61
	B3: Horizon 2BC	62
	B4: Applying model on field data.....	62
	B5: Cross validation	63
	Appendix C: adapted scripts used in LORICA	65
	C1: Isostatic rebound	65
	C2: Aeolian deposition	65
	C3: Physical weathering.....	66
	C4: Silt eluviation	67

List of figures

Figure 1: Location of the Ebba Valley in Central Spitsbergen.....	3
Figure 2: Geological map of the Ebba valley.....	4
Figure 3: Scatter plot of datings from Long et al. (2012).....	5
Figure 4: Aerial photograph of the Ebba valley showing the location of the marine terraces.....	6
Figure 5: Different aeolian landforms in the Ebba valley.....	8
Figure 6: Observed evidence of cryogenic processes in the Ebba valley.	9
Figure 7: Silt cap covering the top of a rock and calcitic pendants attached to the bottom of a rock	10
Figure 8: Different stages of silt morphologies as defined by Forman and Miller.....	11
Figure 9: Different stages of carbonate coatings as used by Forman and Miller.....	11
Figure 10: Conceptual model of interactions between soil forming processes and environmental and other external factors.	13
Figure 11: Conceptual model of dominant processes on marine terraces on central Spitsbergen.	14
Figure 12: The different main strata used for the sampling scheme.	15
Figure 13: Study area with all sampling locations.....	15
Figure 14: Scatterplot theodolite measurements and altitudes derived from the DEM.	18
Figure 15: Boxplot of RGB values for the sampling locations, sorted by different morphological unit.	19
Figure 16: Scatterplot of observed vegetation cover versus calculated vegetation index.	19
Figure 17: Model script of the SEM of horizon 1A.	22
Figure 18: Pictures of the current beach, consisting of gravelly and sandy material.....	27
Figure 19: Scatterplot of gravel fraction versus sand fraction, for the 2A and 2B/ horizons.	28
Figure 20: Plot of the silt fractions of the 2B/ and 2BC horizons observed in the field.....	28
Figure 21: Boxplot of the horizon thickness for different terrace levels.	32
Figure 22: Boxplot of gravel fractions from field data.....	32
Figure 23: Boxplot of silt fraction from field data.	33
Figure 24: Total amount of silt observed in the field.	33
Figure 25: Boxplot of organic matter fraction from field data..	34
Figure 26: Scatterplot of total amount of organic matter observed in 1A horizons.....	34
Figure 27: Schematic overview of the fitted SEM model for the 1A horizon.	35
Figure 28: Visualization of how SEM reacts on different combinations of age and VI.....	36
Figure 29: Properties of the 1A horizon in the valley positions, simulated by SEM.	38
Figure 30: Scatterplots of simulations by SEM versus field observations..	38
Figure 31: Scatterplot of the thickness of the 1A horizon versus age of the soils.....	39
Figure 32: Map showing change in altitude due to erosion simulation in LORICA.....	40
Figure 33: Scatterplots of soil properties modelled by LORICA versus the age of the soil.....	41
Figure 34: Scatterplot of modelled horizon thickness versus the observed modelled thicknesses.	43
Figure 35: Scatterplots of soil properties simulated by LORICA versus field observations.	44
Figure 36: Picture of soil pit J10..	46
Figure 37: Picture of soil pit J11.	46
Figure 38: Scatterplots of simulated soil properties of 1A horizons by SEM and LORICA.....	50

List of tables

Table 1: Overview of soil forming processes on the marine terraces of the Ebba valley	7
Table 2: Division of samples over the strata.....	16
Table 3: List of materials used in the field.....	16
Table 4: Sampling locations where sampling method did not meet the standard	17
Table 5: Order of actions performed in the laboratory.....	18
Table 6: Overview of input data SEM	23
Table 7: Parameters used as input for the LORICA model.....	27
Table 8: Overview of the horizons present in different morphological settings..	31
Table 9: Summary of the fitted SEM for horizon 1A.	36
Table 10: Summary of simulations resulting from cross-validation SEM.....	37
Table 11: Overview of simulated soil properties by LORICA, sorted per terrace levels.....	41
Table 12: Overview of simulated soil properties by LORICA	42
Table 13: Overview of observed and simulated soil properties by LORICA of locations J10 and J11.....	45
Table 14: Validation statistics of predictions of SEM and LORICA for 1A horizons	50

1 Introduction

1.1 General

Climate change has a large effect on the entire arctic system. Physical, ecological, social and economic changes will occur or are already occurring due to global warming (Arctic Climate Impact Assessment, 2004). Changes evoked by increasing temperatures include increasing rate of glacier melt (Rachlewicz et al., 2007), changes in weather patterns (Forland et al., 2011), increase of vegetation abundance (Sturm et al., 2001), changes in surface albedo, decrease of the permafrost table and earlier snowmelt (Barros et al., 2014).

These processes influence the types and rates of soil forming processes in the arctic, affecting for example the local ecology (Burga et al., 2010) and global carbon cycle (Hobbie et al., 2000). Recent studies aim at elucidating the development of soils in cold regions on decadal time-scales (Kabala and Zapart, 2009; Bárcena et al., 2011; Kabala and Zapart, 2012). These studies indicate faster soil development than would be expected under low arctic temperatures. This rapid soil development is also found in young soils (<1.000 years) in alpine regions, where weathering is kinetically limited instead of supply limited as is the case in old soils (~10.000 years) (West et al. (2005), as stated in Mavris et al. (2010)). This results in weathering rates of 3 to 4 times greater than those in the old soils (Egli et al., 2006; Egli et al., 2014).

Less is known about development and distribution of arctic soils on millennial timescales. Research has been done on current properties of old soils in the arctic (e.g. Pereverzev and Litvinova (2010) and Pereverzev (2012)), but there is a lack of knowledge on underlying soil forming processes and variability of soil properties in the landscape. Examples are weathering rates (Colman, 1981) and rate of silt eluviation. This knowledge contributes to general understanding of arctic soil development and the arctic system. Next to that, it can serve as baseline to bring changes in soil development due to accelerated global warming into perspective and help quantify these changes.

A common method to get insight in the spatial variation and distribution of soil properties is the use of different types of explanatory or predictive models. Distinction can be made between statistical and mechanistic models and between static and dynamic models. Whereas mechanistic models are based on theoretical concepts and connections and are widely applicable, statistical models are calibrated on data from a given study area and can typically be used only in that specific area. Dynamic models include time-dependent changes, resulting in a system whose state is dependent on previous states (e.g. Heuvelink et al. (2006)), whereas the state of static models does not vary in time (e.g. Hoffmann et al. (2014)). Different modelling approaches can result in comparable results (Egli et al., 2014). This raises the question whether it is necessary to develop large, complicated models, or that simpler models can also give the required insight in the spatial distribution of soil properties.

1.2 Statistical and static modelling

Statistical models are widely used in soil science. A new development is the use of structural equation modelling (SEM) in environmental sciences. SEMs can be used to study theoretical concepts using statistical techniques (Grace et al., 2010). Commonly they are used in the social sciences, to investigate complex networks of relationships between non-observable variables, which are inferred from several measured variables (Grace et al., 2010). Applications in environmental sciences are thus far restricted to ecology (e.g. (Arhonditsis et al., 2006; Grace and Keeley, 2006; Grace et al., 2010)). SEM is used sporadically in soil science (Kane et al., 2015) and has not yet been applied on examining and predicting the distribution of soil properties. SEMs can be used in dynamic and static mode.

1.3 Mechanistic and dynamic modelling

A mechanistic model simulates interactions between detailed described physical processes, using parameters estimated from field observations (Sonneveld et al., 2006). Mechanistic models are in general dynamic models, where the state of a system determines the rates and of the processes in the model. This modelling approach enables to study the interactions between different soil forming processes, as well as the interactions between pedogenesis and landscape altering processes (Vanwalleghem et al., 2013).

Topography is the main driving factor behind soil development in pro-glacial areas (Egli et al., 2006). Next to relief, time also plays an important role, according to the variation in weathering rates found by Egli et al. (2014). Although time cannot explain the complete variability of soil properties in an area (Temme and Lange, 2014), it is expected that incorporating time into a model ends up in more accurate predictions, because time is one of the main drivers of soil formation. Both time and topography are soil forming factors included in the soilscape model LORICA (Temme and Vanwalleghem, 2015).

1.4 Research objective and questions

The objective of this study is **to explore the use and performance of a structural equation model and of soilscape model LORICA to explain and predict the spatial and temporal distribution of soil properties in old arctic soils**. The study was performed on a series of marine terraces on central Spitsbergen.

The following questions are answered in order to reach the objective:

1. Which processes play a role in the development of soils on marine terraces on central Spitsbergen?
2. Which properties do soils on marine terraces on Spitsbergen have and how are they distributed in the soil profiles and in the landscape?
3. Which distribution of soil properties on marine terraces on Spitsbergen does a Structural Equation Model simulate?
4. Which distribution of soil properties on marine terraces on Spitsbergen does the soilscape model LORICA simulate and how is the distribution influenced by geomorphic processes?
5. Which of the studied models is most suitable for predicting the distribution of soil properties on the marine terraces of central Spitsbergen?

1.5 Reading guide

This report starts with a description of the study area (Chapter 2). After that, a short literature study on different soil forming processes in the arctic is presented (Chapter 3). This chapter closes with a conceptual framework which is the basis for the two model studies. Chapter 4 contains the materials and methods section and describes fieldwork, laboratory analysis, available datasets and methods for the two models. The results are presented in Chapter 5. It starts with an exploratory data analysis, showing trends in the data. After that, parameters, predictions and validation of SEM and LORICA are presented. Chapter 6 contains the discussion of the results and compares performance of both models. The report ends with a list of conclusions drawn from this study (Chapter 7).

2 Study area

2.1 General

Fieldwork for this thesis was performed on the marine terraces located in the Ebba valley. This valley, created by the retreating Ebba glacier, is located in the centre of the island West-Spitsbergen, which is part of the Spitsbergen archipelago (Figure 1). The valley is bounded by mountain ranges in the north and south, the Ebba glacier in the west and the Petunia bay in the east. The southern mountain range is called the Wordiekammen (Figure 2).



Figure 1: Location of the Ebba Valley in Central Spitsbergen. Source of image: Long et al. (2012)

The Ebba valley and its surroundings have been subject of research for many years. The Adam Mickiewicz University from Poznan, Poland, has a research station in this valley. Their research focuses on response of the cryosphere of Spitsbergen to changing environmental conditions. Their main areas of interest are geomorphology, glaciology and permafrost fluctuations. Also geology and hydrology of the area have been studied extensively (Gulinska et al., 2003; Rachlewicz et al., 2007; Rachlewicz and Szczuciński, 2008; Elster and Rachlewicz, 2012; Szpikowski et al., 2014).

2.2 Local climate

Average annual temperature in the Ebba valley is $-5.6\text{ }^{\circ}\text{C}$. In July and August temperatures around $5\text{ }^{\circ}\text{C}$ occur. In winter, temperatures decrease to about -15 to $-20\text{ }^{\circ}\text{C}$ on average, with extremes below $-30\text{ }^{\circ}\text{C}$ (Rachlewicz and Szczuciński, 2008; Láska et al., 2012). Precipitation in the Ebba valley is low compared to the well-studied west coast. Annual rainfall is 200 mm. In summer, precipitation falls as light drizzle, in winter as snow. Permanent snow cover occurs from October until June (Láska et al., 2012).

The most frequent wind direction is south, while there is also a high frequency of wind coming from the valley, from the north-east to north-north-east. The strongest winds also come from the valley, with wind speeds up to 6 m s^{-1} . Wind speeds from other directions are in general lower, with speeds of about 3 m s^{-1} (Láska et al., 2012). The wind is mainly dominated by large-scale circulations, with some local influences from channelling effects by the fjords and katabatic winds over the mountain ridges (Esau and Repina, 2012).

The active layer of permafrost in the area varies between 0.5 and 2.5 meter. Depth of the permafrost is mainly influenced by air temperature (Rachlewicz and Szczuciński, 2008).

2.3 Geology

Spitsbergen contains a very geology. This is also the case for the geology surrounding the Ebba valley. Due to its location in the active Billefjorden fault zone, geological layers with a wide range of ages and properties are cropping out. This information is summarized in the Geological Map of Billefjorden (Dallmann et al., 2004). Figure 2 displays the Ebba valley on the geological map.



Figure 2: Geological map of the Ebba valley. Geological formations: 9: Gipshuken formation; 11: Wordiekammen formation; 13: Minkinfjellet formation; 14: Fortet member; 17: Trikolorfjellet member; 18: Ebbaelva member; 19: Hultberget formation; 20: Billefjorden group; 33: Smutsbreen unit; 34: Eskolabreen unit. Map source: Dallmann et al. (2004).

The oldest formations date from the Precambrian, and consist of metamorphic rocks. These formations are found on the sides of the Ebba glacier. Above these formations, early Carboniferous sandstones, conglomerates, shales and coals can be found, which were deposited as fluvial and shore clastic sediments. Sides of mountain ranges surrounding the valley consist of late Carboniferous sandstones, shales, conglomerates, limestones, dolomites and anhydrites.

Quaternary deposits in the area are colluvial, alluvial, glacio-fluvial and gravelly and sandy marine deposits, consisting of the same material as the surrounding mountains. These last deposits are located in the study area, with a thickness of 1-2 m (Zwolinski et al., 2013).

2.4 Marine terraces

This study is performed on marine terraces (raised beaches) on the shores of the Petuniabukta. In this section I describe the processes responsible for creating these terraces and the position of the terraces in the landscape.

2.4.1 Isostatic uplift

The terraces were formed through the process of isostatic uplift after the melting of the Spitsbergen – Barents Sea ice-sheet (Rachlewicz and Szczuciński, 2008; Ingólfsson and Landvik, 2013). With accumulation of ice during the last ice age, the earth crust below got compacted by the heavy weight on top. Melting of the ice-sheet decreased pressure, resulting in expansion of the earth crust. This in turn results in a decreasing relative sea level (RSL) and the formation of several beach terraces at different altitudes.

Relation between altitude and age of marine terraces in the Ebba valley

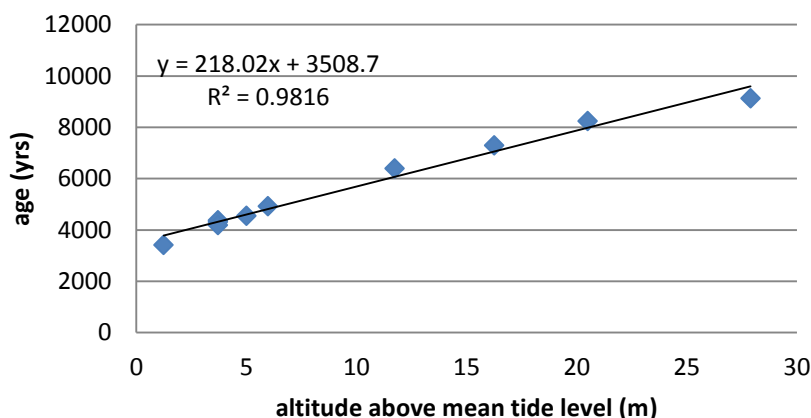


Figure 3: Scatter plot of the dates Long et al. (2012) found from dating shells on the different terrace levels. The black line is the fitted trend-line.

Uplift rate is not constant over the Spitsbergen region (Forman et al., 2004). Different changes in ice-volume cause different uplift rates (Mémin et al., 2012). Because of this variable uplift rate, it is not possible to use well-documented uplift rates from other areas in our study area. Long et al. (2012) dated different terrace levels in the Ebba valley, using juvenile specimens of a shell called *Astarte Borealis*. Uplift rates and different terrace ages were derived from these datings (Figure 3). A linear trend indicates that the youngest soils in the area are around 3500 years old. This age agrees with the cooling of the climate during the Holocene, which started around 3000 years ago. The cooling resulted in the Little Ice Age. The increasing mass of the glaciers from that time lowered the area again (Zwolinski et al., 2013). Current glacier melt triggered a new episode of isostatic rebound. Beaches younger than 3.000 years were flooded again by isostatic depression (Lambeck, 1995, 1996; Long et al., 2012).

2.4.2 Beach ridges and beach valleys

During isostatic uplift different beach levels were created. Beaches typically consist of a ridge and valley. Ridges are created during moderate to strong wave-action and sea-level fluctuations (Scheffers et al., 2012). Coarse material is thrown on the shoreline, creating a ridge in the landscape. Behind the ridge a calm depositional area is formed, which is called the beach valley. The ridges rise in the landscape due to isostatic rebound, creating a new shoreline where a new ridge is created. This process results in a stair-like landscape pattern, consisting of beach ridges and valleys.

Winds coming from the glacier cover sheltered valley positions with a layer of aeolian sand and silt, kept in place by tundra vegetation (Figure 5c) (Scheffers et al., 2012; Zwolinski et al., 2013). Beach ridges usually do not contain vegetation.

Not all beach ridges are prominently present in the landscape. Several smaller ridges can be found in between the large ridges, which are barely higher than the depressions in between them (Brückner and Schellmann, 2003). Ridges can be distinguished from the valleys by the amount of vegetation. Ridges are drier and contain less vegetation than the more moist depressions and therefore have a lighter colour than the surrounding vegetated valleys.

2.4.3 Position in the landscape



Figure 4: Aerial photograph of the Ebba valley showing the location of the marine terraces. Indicated are the 6 main terrace levels and important units in the vicinity of the terraces. the aerial photograph is from 2009.

Figure 4 shows the position of the marine terraces in the landscape. The white/grey colours are beach ridges. The surface consists of sediments consolidated by a microbial layer. There is no or minimal vegetation. The darker grey/reddish colours are beach valleys, vegetated by tundra vegetation, like *Salix Polaris*, *Saxifraga oppositifolia*, *Saxifraga cernua*, *Polygonum viviparum* and *Cassiope tetragone* (Gulińska et al. (2003), as stated in Rachlewicz and Szczuciński (2008)).

The northern border of the terraces is formed by a plain eroded by the Ebba river. This plain is inundated a few days per year, during the melting season (A. Stach, personal communication). In the north east, a large gully has eroded part of the highest terraces. The study area reaches to the point where the terraces are influenced by this gully. The southern and eastern borders of the highest terrace level (6) consist of alluvial material resulting from gullies originating in the Wordiekammen. Prominent gullies dissecting the terraces were outside the area of interest (Figure 4).

3 Soil development on marine terraces

This chapter discusses different soil forming processes that occur on marine terraces in the Ebba valley and concludes with a conceptual framework of how the different soil forming processes interact and how they react to external input. This framework is the basis of the two model studies presented in the subsequent chapters.

The speed of most soil forming processes is known to be strongly influenced by temperature and water availability, usually in a positive way. There is a significant amount of soil forming in the Arctic, despite the low temperatures. Some of these processes are typical for arctic areas, like cryogenic processes. Other processes occur in soils all over the world, such as organic matter accumulation and gleying.

3.1 Soil forming processes

Much is known about soil forming processes in Arctic areas. Some literature sources give a broad overview of processes that occur all over the Arctic. Other sources focus on one specific process. Table 1 lists different soil forming processes that can be found in Arctic areas. The first column indicates what type of process it is.

Table 1: Overview of soil forming processes on the marine terraces of the Ebba valley

Type of process	Process
Erosion and deposition	Aeolian erosion and deposition Fluvial erosion and deposition Marine erosion and deposition
Cryogenic processes	Cryoturbation Frost heaving Surface cracking Forming of ice wedges Patterned ground forming Mass movement (solifluction)
Physical weathering	Frost Hydration
Chemical processes	Dissolution Oxidation Gleying Changing pH
Accumulation	Organic matter accumulation
Transport	Silt translocation Carbonate leaching and precipitation

3.1.1 *Erosion and deposition*

Due to continuous retreat of glaciers on Spitsbergen (Rachlewicz et al., 2007), unconsolidated material is uncovered and deposited in pro-glacial outwash plains (sands). This material is easily available for further transportation. When the surface is dry and frozen, during fall, fine material (fine sand and silt) is taken up by **aeolian activity** and eventually deposited when wind speed decreases or when it becomes mixed with fresh snow (Rachlewicz, 2010). Next, the deposited material is relocated again by the wind, where beach ridges, created by **marine deposition**, end up as a deflation surface and fine material accumulates by tundra vegetation on the flat terrace valleys located on the lee side of the ridges (Figure 5a) (Zwolinski et al., 2013). Horizontal layers of organic matter in the sandy deposits are evidence of accumulation by, and later on burying of, vegetation. Fine material from the surface is blown away, leaving surface gravels standing on pedestals (Figure 5b). Aeolian sediments are deposited on beach valleys, creating thick sandy covers (Figure 5c). Aeolian activity especially occurs with strong winds coming from the north and north-east, with speeds over 5 m s⁻¹. This reflects in the different forms of aeolian accumulation, individual ventifacts and shapes formed by corrosion in the surface of rocks (Paluszkiwicz (2003) and Górska-Zabielska (2008), as stated in Zwolinski et al. (2013)).

Gully **water** coming from the Wordiekammen has to cross the marine terraces in order to reach the sea. Because beach ridges protrude in the landscape, most water flows adjacent to the ridges, creating more moist conditions in the beach valleys. At some points the gullies cross the beach ridges in order to reach the lower terraces. This leads to deep dissected trenches in the beach ridges.

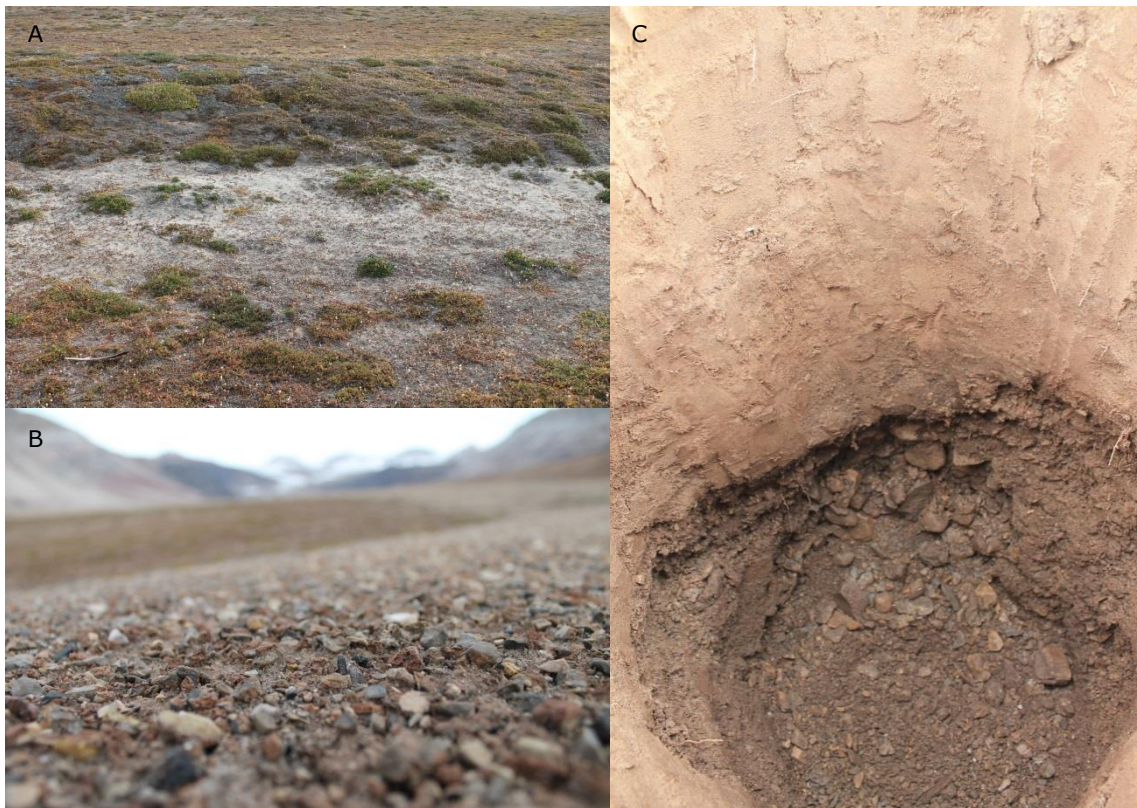


Figure 5: Different aeolian landforms in the Ebba valley. A: layer of sand on the lee side of a ridge. B: surface pebbles located on pedestals of finer material. C: Sandy A horizon located on top of the marine deposits.

3.1.2 Cryogenic processes

Climate has a major effect on soil forming processes, also in Spitsbergen. Due to the cold climate and occurrence of permafrost, several cryogenic processes occur in soils on the marine terraces (Jones et al., 2009). All these processes are driven by the availability of water in the soil layer above the permafrost. Most processes have a mixing effect on the soil material.

Cryoturbation is the term for processes that mix different horizons in a soil. One of the main processes causing cryoturbation is called **frost heaving or frost thrusting** (Forman and Miller, 1984), where soil material gets displaced by freezing and thawing of the soil. When water freezes, it expands. Soil particles move upward by the pressure caused by expansion of water. The speed of the uplift increases with particle size, causing a sorting of different textures. Upward movement causes vertical orientation of stones in the soil and eventually at the surface (Jones et al., 2009) (Figure 6a). By mixing of the soil, new weatherable materials reach the surface, causing constant weathering processes (Forman and Miller, 1984).

Sorting by frost heaving causes different patterns at the surface. Examples are patterned ground and mud boils. **Patterned ground** occurs in many different forms, depending on the properties of the soil material below it. Drew and Tedrow (1962) made an overview of the different kind of patterned ground found in the Arctic, connected to certain soil properties. Different patterns includes stripes of rocks and vegetation, stone polygons and stone nets. Properties depend, amongst others, on drainage and vegetation. **Mud boils** are a special kind of patterned ground, where fine material (mud) is moved upward and gets separated from the stones in the soil (Figure 6b and c). This creates small hills in the area, with vegetated depressions in between. Mud boils tend to move downslope, by which they capture

the vegetation in the depressions, which turn into horizontal organic matter layers. Mud boils generally form in fine sediments, located on top of a permafrost layer (Shilts, 1978).

Cooling of Arctic soils can lead to **surface cracking**, comparable to the drying of clay soils. Surface of the soil shrinks, when cooled down, causing cracks in the surface. These cracks get larger when water accumulates in the cracks and freezes again, creating **ice wedges** (Jones et al., 2009).

Waterlogged soils located on sloping areas undergo mass movement during the thawing of the soil, a process called **solifluction** (Harris et al., 2008). About half a meter of the top soil gently moves downslope, creating lateral solifluction lobes (Figure 6d). Saturated soil slides down over the impermeable permafrost layer, with a speed up to 15 cm per year on slopes of 0.5 degrees and steeper (Jones et al., 2009).

There is not a lot of water available in the soil in the study area for the above-mentioned processes, because of good drainage and limited precipitation. However, some places show many traces of cryogenic processes. These places were usually more saturated with water.

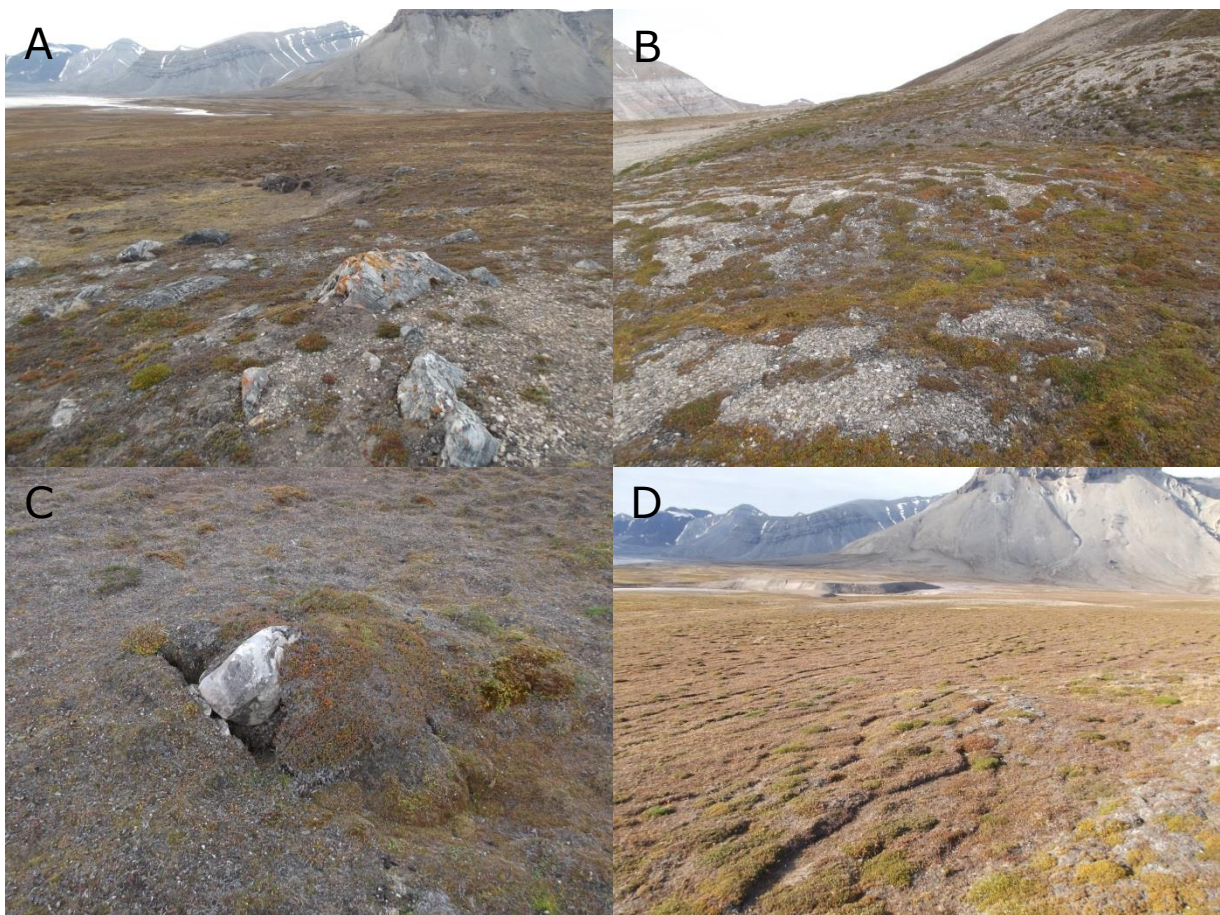


Figure 6: Observed evidence of cryogenic processes in the Ebba valley. A: tilted and elevated stones, by frost heaving. B: Mud boils on the highest terraces. C: A rock occurring in a mud boil. D: solifluction lobes on a sloping terrace.

3.1.3 *Physical weathering*

Forman and Miller (1984) mention several physical weathering processes. The first is **frost weathering** or frost shattering of sand particles, where expanding freezing water located in cracks of a particle make the particle break. Soils which freeze and thaw regularly are most subject to frost weathering, because expansion of freezing water is the highest when temperatures reach just below zero (Matsuoka et al., 2003).

Forman and Miller (1984) also mention **hydration weathering**, where rocks saturated with adsorbed water expand. The amount of adsorption and expansion depends on the temperature, which is in the same range as soil temperatures during freezing and thawing (Dunn and Hudec, 1966). Due to multiple cycles of sorption and desorption the rocks break, by fatigue of the rock material (Hudec, 1973). Dunn and Hudec (1966) claim that weathering in cold areas mainly is a product of hydration weathering and that frost weathering is a secondary process, because pore water does not freeze, but adsorbs to the rock. White (1976) questions this hypothesis, because not all criteria for hydration weathering are met in reality. These are presence of water in a closed system, which is not likely in a pore system, and rocks that are strong enough to resist the pressure that the water emits when it freezes. Rocks cannot handle that kind of internal pressure, and would simply shatter, due to the frost weathering.

3.1.4 Chemical processes

Although physical weathering processes produce silt particles, Forman and Miller (1984) favour dissolution as primary process of silt production in soils on marine beaches on Spitsbergen. **dissolution** of carbonate-rich rocks releases primary sand and silt particles which were captured in the rocks. This is supported by D.H. Mann in Ugolini (1986), who provides evidence that silt on the marine terraces studied by Forman and Miller results from dissolution of dolomite. Etzelmuller and Sollid (1991) showed a silt-rich residue after treating dolomitic bedrock with HCl. On the contrary, other studies show that silt production due to dissolution of dolomite is negligible (e.g. C'iric' and Senic' (1985)). Leaching and precipitation of dissolved carbonates is discussed later.

Permafrost acts as an impermeable layer in soils, where percolating groundwater stagnates and eventually starts a more horizontal flow. This stagnating water causes **reduced conditions**. The resulting oxygen deficit forces ferric iron in the soil to convert into ferrous iron, which has a greyish colour (Jones et al., 2009). The soils can also become more red, by the **oxidation** of iron-rich minerals. This can result in a red iron-coating around soil particles, which are visible as iron mottles or as red colours in the soil (Margesin, 2009).

pH on the marine terraces lies between 7 and 8, due to carbonate-rich parent material (Jones et al., 2009). Kabala and Zapart (2009) state that soil pH can change by dissolution of carbonates and by colonization of the soil with plants, which produce humic acids. Most of the horizons of soils encountered during fieldwork (Section 4.2) had a strong to extreme reaction to HCl, indicating an abundance of calcaric material in the soil. This reaction was the same over the complete profile, except for a possible aeolian cover, which reacted moderately to HCl. Due to these findings, it can be expected that pH will not fluctuate much in the soil profiles.

3.1.5 Organic matter accumulation



Figure 7: Silt cap covering the top of a rock (A) and calcitic pendants attached to the bottom of a rock (B).

Organic matter in soils on marine terraces results from the decaying of plant material, dead animals and animal excrements. Kabala and Zapart (2012) show that carbon accumulation starts immediately after occupation of sediments by plants, leading to a steady increase of organic matter in the first 80 years of soil development on moraines of a retreating glacier. Schüllli-Maurer et al. (2007) show that this

increase continues also on longer time-scales (2000-12000 years) on marine terraces in Southern Norway. Organic matter accumulates in the top horizon, where most biological activity takes place. This can be seen in soil descriptions on marine terraces on the Billefjorden coast by Pereverzev (2012).

According to Kabala and Zapart (2012), organic matter accumulation does not start at an organic matter content of zero, but at a certain threshold, which can be caused by palaeosols, initial carbon in marine sediments, organic matter coming from parent material and by aeolian deposition (Hawes, 2008).

3.1.6 *Transport in the soil*

Silt formed by physical weathering migrates through the coarse-textured soil, by water that becomes available from snow-melt (Ugolini, 1986). Although **translocation of silt** occurs both on vegetated and non-vegetated areas, it is likely that more silt can be found in the vegetated parts, due to the trapping of aeolian silt by vegetation and because vegetated areas are usually located at a lower position, thus accumulating more snow and water.

Forman and Miller (1984) created a classification system of the amount of silt in a horizon (Figure 8). First traces of silt translocation are silt caps on top of larger clasts in the soil (Figure 7a). Stages 1 to 4 indicate these silt caps, with an increasing thickness and cover percentage. At stage 5, silt is not only located on top of the clasts, but is also connected to other silt caps. At stage 6, the complete matrix is enriched with silt. Because of the considerable amount of silt available at stages 5 and 6, Forman and Miller (1984) decided to name horizons where this occurs a B/ horizon, with the italic I as a symbol for silt. We also used this classification system in our soil descriptions.

Dissolved **carbonates** are also **transferred** through the soil. Dissolution is mainly controlled by the partial CO₂ pressure (carbonic acid). Most of the dissolution occurs in summer months, when biological activity increases the CO₂ in the soil (Courty et al., 1994). High permeability of coarse fragmented marine material causes leaching through the profile (Ugolini, 1986).

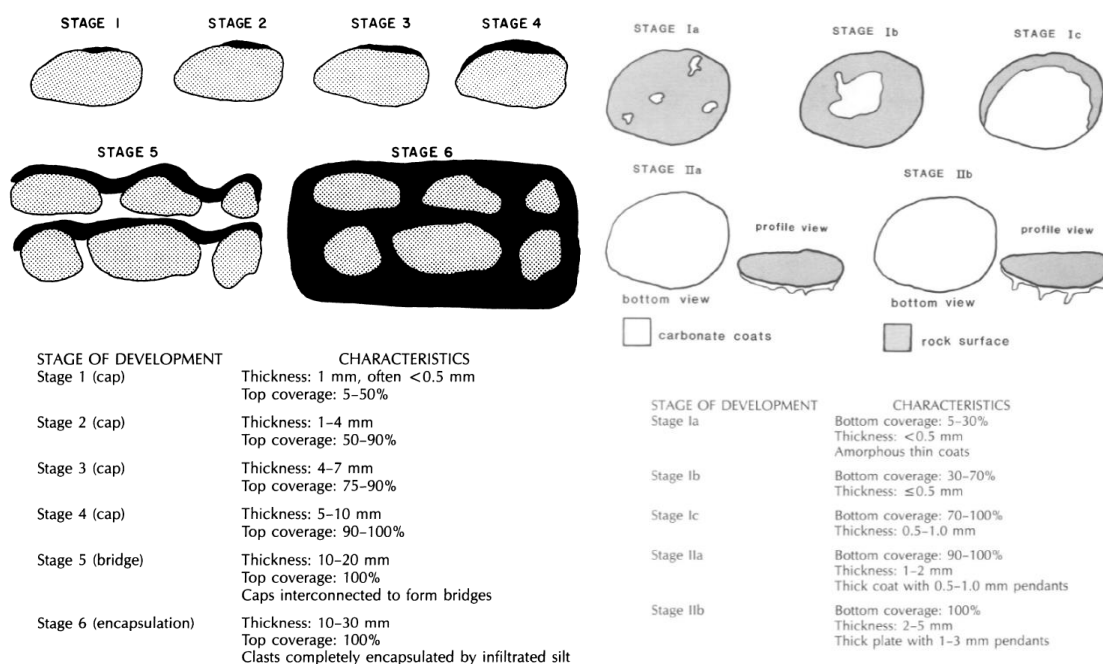


Figure 8: Different stages of silt morphologies as defined by Forman and Miller. Source: Forman and Miller (1984)

Figure 9: Different stages of carbonate coatings as used by Forman and Miller. Source: Forman and Miller (1984)

Precipitation of carbonates can be caused by several processes. The first process is a decrease of partial CO₂ pressure in the soil water, reducing the amount of carbonates that can be dissolved. Second is an increase of concentration of carbonates in solution due to evaporation. The last process is exclusion of carbonates from the solution, because the solution freezes (Ugolini, 1986). Accumulation of secondary carbonates happens on the downside of the clasts, creating a coating (Figure 7b). Precipitation occurs on these locations, because the water flux is limited below the larger clasts (Courty et al., 1994).

Forman and Miller (1984) used a part of a classification which was originally created to classify carbonate coatings in desert soils (Gile et al., 1966), to classify carbon coatings they observed (Figure 9). Stage I coatings do not cover the complete clast. Stage II coatings do. When stage II coatings are present, the horizon is called a calcaric horizon, with the addition of the symbol k (e.g. Bk).

Secondary carbonates can be divided in 5 different types of layers, whose properties like colour and chemical composition can be led back to different stable soil forming conditions in the Arctic, such as differences in vegetation, moisture conditions and temperature (Courty et al., 1994).

3.1.7 Other soil Arctic soil forming processes

Some processes described in literature do not apply to the study area. These are for example clay destruction, clay translocation and salinization. The required pH for these processes is respectively <5, 5-7 and >9. pH in soils on marine terraces in Spitsbergen is expected to be in between 7 and 8, as can be seen in the results of Forman and Miller (1984) and Pereverzev (2012). These processes do not occur, because the pH-requirement is not met. We also found no traces of these processes during the fieldwork. Podsolization also does not occur on the marine terraces, due to good drainage of the coarse material (Pereverzev, 2012).

3.2 Conceptual model

Processes described in section 3.1 are summarized in a conceptual model, which links the soil forming processes to environmental and other external factors (Figure 10). This shows a complex network of relations between different variables and processes.

A selection of this conceptual model was used as a basis of both model studies described in this report (Figure 11). The selection was based on properties observed in the field and on possibility to model these processes. Most common observed properties in the field were aeolian deposits in valley positions, gullies formed by fluvial erosion, decay in gravel fraction due to weathering, B/ horizons enriched in silt and dark top horizons due to organic matter accumulation. Calcitic pendants were also observed but are not considered in the models, because the models were not designed to model ordinal variables. The mechanistic model simulated these processes in order to predict soil properties. The statistical used the field observations to predict soil properties, based on regressions between different properties and external factors like age and vegetation presence.

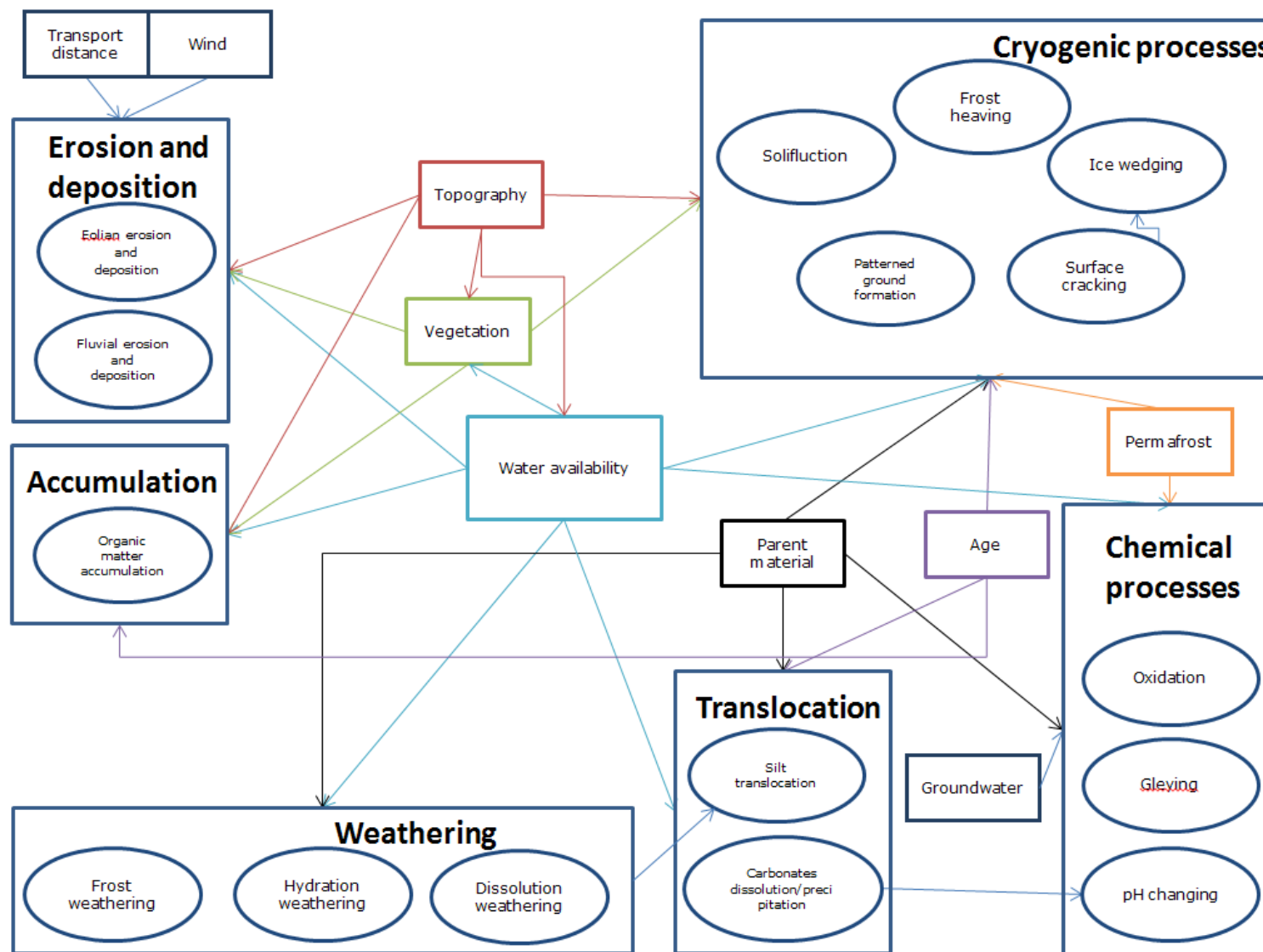


Figure 10: Conceptual model of interactions between soil forming processes and environmental and other external factors.

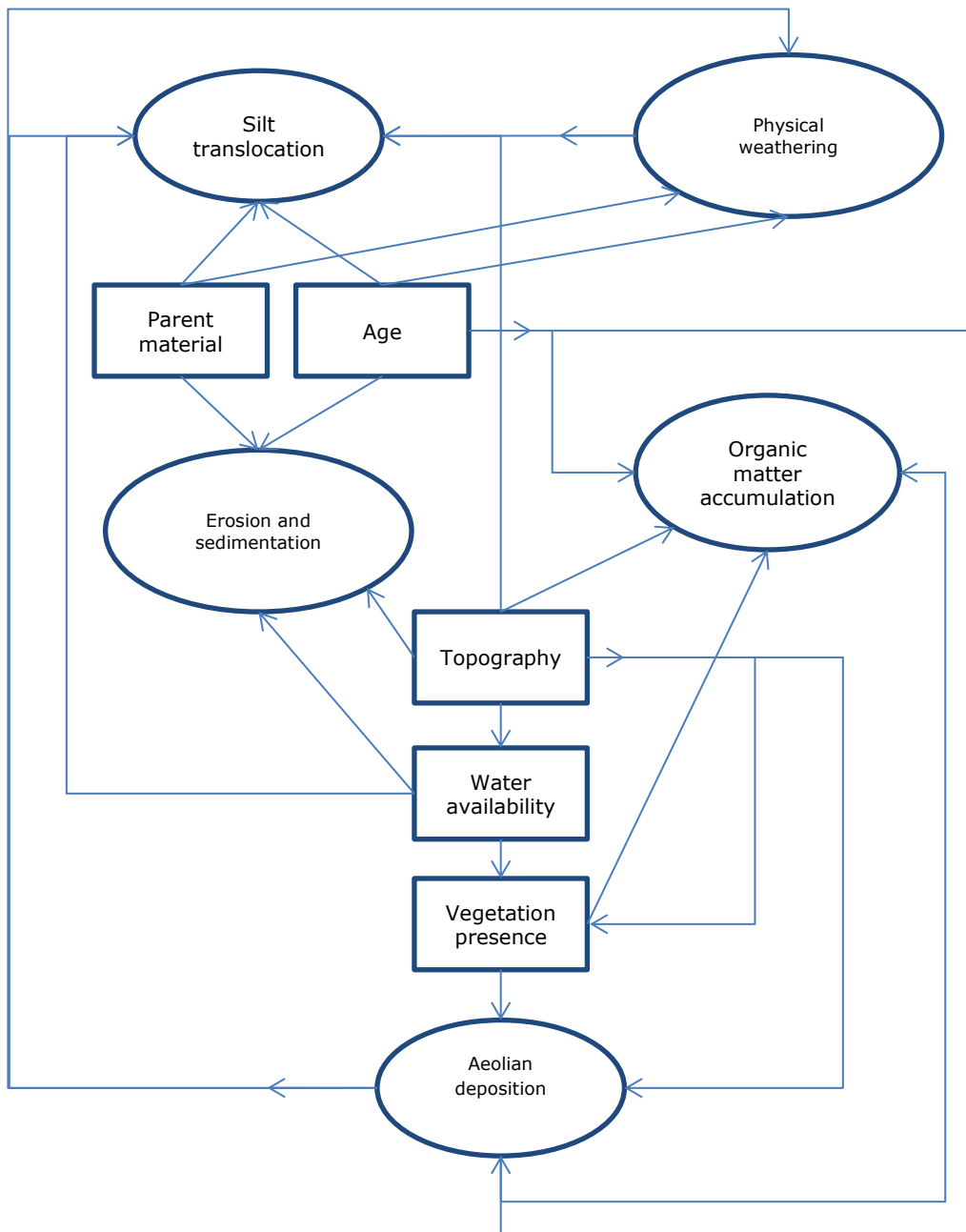


Figure 11: Conceptual model of dominant processes on marine terraces on central Spitsbergen.

4 Materials and methods

4.1 Available maps

Maps used in this study come from the researchers of the Adam Mickiewicz University. The spatial reference is WGS1984, UTM zone 33N.

The aerial photograph taken in 2009 covers the south-east side of the Ebba valley, where the marine terraces are located. Cell size is 0.44 by 0.44 meters. The photo was probably taken in the end of summer, regarding the absence of snow.

The used DEM has a cell size of 10 by 10 meters. It covers the complete Petunia bay, with some adjacent glacier valleys, including the Ebba valley. DEM derivatives show patterns which indicate that the DEM is created from contour lines. Small scale elevation differences (e.g. ridge-valley systems) are not captured by the DEM. Simulated streams do not match the locations of streams on the aerial photograph, indicating that the DEM is not properly projected on the area. The border of the fjord in the DEM does not match the border on the aerial photograph. Other available DEMs had a cell size of 30 or 40 meters, but they displayed less detail than the used DEM.

4.2 Fieldwork

4.2.1 *Sampling scheme*

A stratified random sampling scheme was used to sample the marine terraces, in order to avoid preferential sampling and facilitate statistical validation, while also distributing the soil samples fairly uniformly over different terraces. The study area was divided in three strata, with almost equal sizes (Figure 12). Each stratum was then subdivided in substrata with and without vegetation, using the aerial photograph. Cells with a redness larger than 70 were classified as areas without vegetation, the other cells were classified as vegetated areas.

Ten random sampling locations were appointed to each stratum. For strata 2 and 3, the distribution of samples over vegetated and non-vegetated areas was done following the ratio between ridge and valley cells (Table 2). This was not the case in stratum 1, where there was much more vegetated area. Here I chose to sample at least two non-vegetated locations, to say something about the variance in non-vegetated areas on lower terraces.



Figure 12: The different main strata used for the sampling scheme. Every stratum was separated in vegetated (dark) and non-vegetated parts (light).



Figure 13: Study area with all sampling locations. The red lines indicate the different main terrace levels. Points starting with an R are randomly selected points. Points indicated with a J are judgementally chosen.

Figure 13 shows the final sampling locations. Points indicated with letter R are random points used for this study. The points beginning with letter J are judgemental points, selected by the other student who participated in the fieldwork. These points are on extraordinary locations with specifications which were not yet captured by the random samples. These are for instance locations outside the marine terraces or locations which were mentioned in other studies (e.g. the locations where Long et al. (2012) collected their dating samples). Two of these points were used in the validation of LORICA.

Table 2: Division of samples over the strata

		vegetated	non-vegetated	total
stratum 1	Cells in raster	644029	46218	690247
	Fraction	0.93	0.07	
	Division of locations	8	2	
stratum 2	Cells in raster	570381	121467	691848
	Fraction	0.82	0.18	
	Division of locations	8	2	
stratum 3	Cells in raster	323835	329701	653536
	Fraction	0.50	0.50	
	Division of locations	5	5	

4.2.2 *Field materials*

Table 3 shows a list of materials used during fieldwork. Soil pits were dug using a shovel and trays to get loose material out. Soil material was collected on garbage bags, in order to put all material back in the pit. Optionally present vegetation was removed in one piece, so that it could be placed back on the top of the pit.

Horizon properties were described using FAO standards (FAO, 2006) and the Munsell Color book. A bulk density ring with a volume of 100 cm³ was filled with material from each horizon and weighed using a small field-scale (precision = 0.1 g). Every horizon was tested on presence of CaCO₃ using HCl. Soil moisture is measured using a soil moisture meter. The exact altitude of most sampling locations was measured using a Zeiss delta R55 theodolite, except for locations which were not visible from the position of the theodolite (Figure 13).

Table 3: List of materials used in the field

Shovel
Buckets
Garbage bags
FAO guidelines for soil description
Munsell color book, 2009 revisited
Bulk density ring (volume = 100 cm ³ , empty weight = 95 g)
Scale, precision = 0.1 gram
Sample bags
HCl
Theta probe soil moisture sensor sm150, hh2 delta 2 moisture meter
Zeiss elta R55 theodolite

4.2.3 *Observations*

For every location, a field form (Appendix A) was filled in, noting position, general landscape settings, soil profile description and general remarks. Soil horizons were described in detail. Horizon descriptions were aggregated to match the horizons described below.

4.2.4 *Sampling method*

Per sampling location, different soil horizons were sampled by scraping a bulk density ring over the entire length of the horizon, creating a composite sample of the complete horizon. The collected material was captured in a sampling bag.

The sampled horizons were:

- 1A: top horizon located on beach valleys. This horizon consists of aeolian sands and silts, captured by vegetation in the valleys;
- 2A: top horizon developed in marine terrace material, characterised by a relatively low gravel fraction;
- 2B: horizon located between 2A horizons and the layer where accumulated silt can be found. The horizon exists of alternating layers of gravel and coarse sand, which were mixed in the composite sample;
- 2B/: horizon where silt illuviation caused the soil to change from a clast supported soil to a (partly) matrix supported soil. These horizons were classified as stage 5 or 6, according to the silt morphologies (Figure 8);
- 2BC: lowest horizon visible in the soil pit, consisting of coarse sand and gravel where (almost no) soil forming took place. Silt morphologies reach below 5, indicating some eluviation of silt. Also calcitic pendants can still be present. The BC horizon was not sampled for each location, because it was assumed that there is not much variation in the parent material. The sample for the BC horizon was generally taken from the top 30 cm of the layer.

Aeolian deposits always got prefix 1 and horizon in marine deposits always got prefix 2, in order to make an easier reference to a certain parent material.

For some locations, sampling was not done according to the method described above (Table 4). These samples were left out of the analysis.

Table 4: Sampling locations where sampling method did not meet the standard

Sample number	Inconsistency
R2	Horizons 2A and 2B/ collected in one sample
R4	Horizons 1A and 2A collected in one sample
R8	Horizons B and B/ collected in one sample
R9	Two B/ were identified, with a B layer in between. B/1 and B are collected in one sample. B/2 was sampled individually
R18	Horizons 1A and 2A are sampled together. Horizon 2A does not resemble other 2A horizons, because of the low percentage of rocks in the horizon. So these could be treated as a single horizon

4.2.5 *Bulk density*

Bulk density was calculated by subtracting the weight of an empty bulk density ring (95 g) from a ring filled with soil material. The remaining mass was divided by the volume of the ring (100 cm³), resulting in the bulk density in g/cm³. Multiplication with 1000 gives the bulk density in kg/m³.

4.3 Laboratory analysis

Samples collected in the field were analysed in the laboratory in Wageningen. Variables measured were moisture content, particle size distribution and organic matter fraction. Table 5 shows in which order the proceedings in the lab were performed.

4.3.1 *Moisture content*

Before the other analyses were performed, the moisture was removed from the sample, by drying the samples overnight at 105 °C.

4.3.2 *Particle size distribution*

The dried sample was sieved for two minutes by hand to determine its particle size distribution. The used mesh sizes were 2000 µm for the sand fraction and 63 µm for the silt fraction. The weight of the three particle sizes (gravel, sand and silt) was divided by the total weight of the sample, resulting in mass fractions of the different sizes.

Before sieving the samples were grinded, to break up silty aggregates and silt caps on gravels.

4.3.3 Organic matter fraction

The organic matter fraction was measured using the loss on ignition (LOI) method. A weighed sample was heated with 2 °C per minute up to a temperature of 550 °C. The sample stayed for three hours in the oven at this temperature. The slow heating was to avoid inflammation of the organic matter. The difference in weight before and after heating, divided by the initial weight, resulted the organic matter fraction of the sample.

This analysis was performed on the finer fractions (<2000mm), because the larger fractions consisted only of gravels. After the analysis, the organic matter content was multiplied by the fraction of finer materials, to result in the total organic matter fraction.

Table 5: Order of actions performed in the laboratory

Action	Analysis
Weighing aluminium can	Moisture content
Weighing initial sample	
Drying sample at 105 °C	
Weighing dried sample	
Grinding the sample	Particle size distribution
Sieving for 2 minutes	
Weighing sand and silt fraction	
Mixing sand and silt fraction	
Weighing LOI cup	Organic matter content
Weighing initial LOI sample (sand + silt)	
Weighing gravel fraction	Particle size distribution
Burning LOI sample	Organic matter content
Weighing burned LOI sample	

4.4 Map preparations

Using the available digital data and field observations, input maps for the two models were created. This section describes the methods performed to create these maps.

4.4.1 Correcting the DEM

For 27 sampling locations the elevation was measured using a theodolite. The theodolite measurements show that the values which are in the original DEM are underestimated by approximately 6% (Figure 14). The DEM was corrected using the linear regression between theodolite measurements and DEM values.

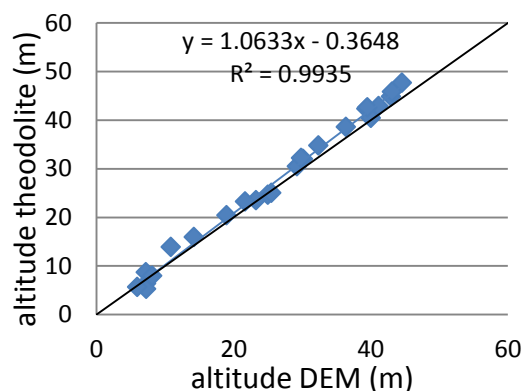


Figure 14: Scatterplot of measurements by a theodolite versus the values resulting from the DEM with cell size of 10 meters, including the trendline with its equation and fit. The black line indicates the 1:1 line.

The inconsistencies in the DEM were not removed. Multiple attempts resulted in new errors to occur and did not show satisfactory improvement.

4.4.2 Vegetation index

A vegetation index (VI) is an indicator of vegetation presence in an area or raster cell. Most existing vegetation indices make use of near infra-red reflectance (e.g. NDVI), but NIR images were not available for our study area. Indices using only RGB (red, green and blue bands of an image) do exist, but they are still in development and empirically calibrated for regions with different vegetation than present in the study area (PHL, 2014). Finding the right calibration for the study area was beyond the scope of this thesis research. Moreover, most existing vegetation indices focus on green vegetation, while tundra vegetation in the study area is more red/brown. That is why I decided to create my own vegetation index for the study area, using the available aerial photograph.

Vegetated parts in the area all have a lower R, G and B value on the aerial photograph compared to the barren ridges (Figure 15). A higher R, G or B value thus indicates less vegetation. To amplify the differences between different locations, the RGB-values for every cell were multiplied to create the vegetation index (VI), according to the following equation:

$$VI = Redness * Greenness * Blueness$$

Calculations were performed on different bands of the aerial photograph. The created map is aggregated to match the DEM with cell size of 10 meter. Aggregation was achieved by taking the median within a 10 by 10 m cell, to ignore extremes and anomalies such as dark rocks and buildings. If values were larger than $2 \cdot 10^6$ or smaller than $8.5 \cdot 10^4$, the cell got a new value, which equals the average of the 9 surrounding cells, including its own value. This was done to remove extremes with a larger extent.

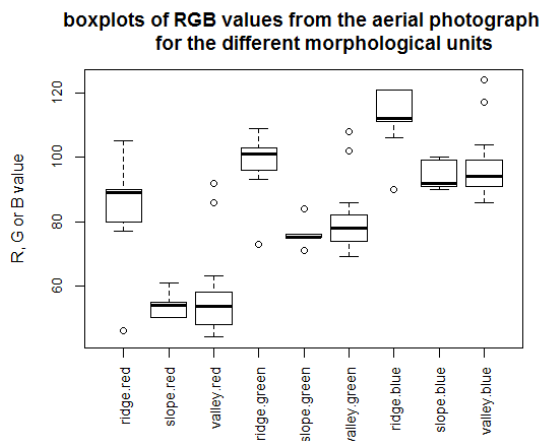


Figure 15: Boxplot of RGB values for the sampling locations, sorted by different morphological unit. The RGB values come from the aerial photograph from 2009.

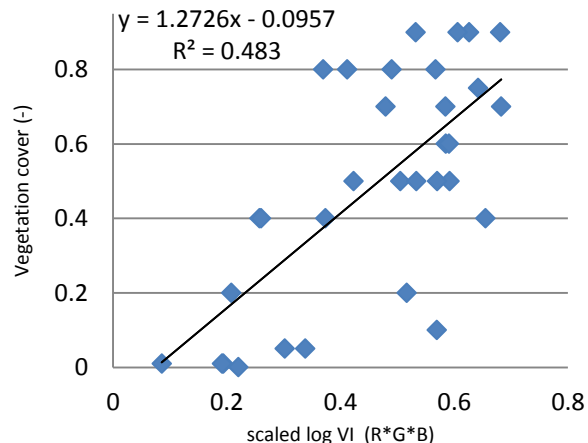


Figure 16: Scatterplot of observed vegetation cover versus calculated vegetation index.

Resulting VI-values gave an exponentially decreasing relation with vegetation cover estimated in the field. A log transformation resulted in the best linear fit with observed vegetation cover. To reach an index ranging from 0 to 1, the following formula was applied to scale the $\log(VI)$ values:

$$scaled\ VI = 1 - \frac{(\log(VI)) - \min(\log(VI))}{(\max(\log(VI)) - \min(\log(VI)))}$$

The scaled VI was defined such that it increased with observed vegetation cover (Figure 16). Cells with a VI higher than 0.45 were classified as valley. Other cells were classified as ridge.

4.4.3 Age map

The conceptual model shows that age is an important variable in the soil forming processes in the study area (Figure 11). Higher locations are older than lower locations. The age was deduced from the

regression with elevation in order to create an area-covering map (Figure 3). Absence of small scale elevation differences results in a DEM with continually increasing altitudes towards higher terraces, what provides the opportunity of creating a continually increasing age map.

4.5 Structural equation modelling

4.5.1 *Introduction to the model*

Structural equation modelling (SEM) is designed to analyse interactions in a system, by calculating both direct and indirect effects of different variables on each other (Grace and Keeley, 2006). A SEM generally consists of two parts, a measurement model and path model (Iacobucci, 2009). The measurement model defines relations between measured variables and non-observable latent variables. The path model is similar to a regression model, where different latent variables are correlated with each other. Advantages of SEM over traditional (multiple) linear regression are that both direct and indirect effects between variables can be studied. Also effects of target variables on each other can be taken into account. Another advantage is that SEMs can split the variances of measurement model and path model. This way it is easier to determine where model improvements can be obtained. SEMs search for correlations in data, they do not show causal relations (Iacobucci, 2009).

4.5.1.1 *Measurement model*

Latent variables represent abstract variables that are not directly observable. Examples are biodiversity or customer satisfaction. The measurement model relates one or more measured variables to these latent variables, in order to get a value for the latent variables. This analysis is also known as factor analysis. Residuals from these calculations are characterised by variances of measurements. Calculations are done according to the following equation (Iacobucci, 2009):

$$x = C * d + r$$

With the following terms:

- x : a vector of e measured variables;
- C : $e * f$ matrix of factor loadings of the measured variables on the latent variables;
- d : a vector of f latent variables;
- r : vector of variance in the measurements, assumed to be normally distributed with zero mean and variance-covariance matrix G .

4.5.1.2 *Path model*

In the path model different latent variables are related to other latent variables. Two different variables can be distinguished. Exogenous variables are latent variables which are not influenced by other latent variables. They do influence other latent variables, which are called endogenous. Endogenous variables can be influenced both by exogenous variables and other endogenous variables.

The path analysis is as follows (Iacobucci, 2009):

$$n = B * n + A * p + j + s,$$

with following terms:

- n : vector of k endogenous variables;
- B : $k * k$ matrix of coefficients of the relationships between the different endogenous variables;
- A : $k * l$ matrix of coefficients of the relationships between the exogenous variables and endogenous variables;
- p : vector of l exogenous variables;
- j : vector of intercepts of k intercepts of endogenous variables;
- s : vector of k residual variances in the endogenous variables, assumed normally distributed with zero mean and variance-covariance matrix H .

Latent variables captured in vectors n and p combined form vector d from the measurement model. Vector j is not mentioned in Iacobucci (2009). j is added, because the intercepts are needed for the prediction with SEM.

4.5.1.3 Parameterization

SEM has to estimate parameters of matrices C , A and B . Matrix C contains the factor loadings of the measurement on the latent variables. To obtain a unique estimate for the latent variables, the first factor loading and variances should be fixed. If one latent variable is reflected in multiple measured variables, the factor loading of the first measured variable is set to 1 by default. When all factor loadings can be freely estimated, no unique estimate for the latent variable exists. The remaining factor loadings are estimated relative to the fixed first factor loading. Estimated variances and covariances by SEM are stored in matrices G and H .

Regression coefficients estimated by SEM are stored in matrix A or B , depending if the independent variable is exogenous or endogenous. The coefficient is only estimated when the user indicates that there is a relation between two variables. the same goes for covariances in Matrices G and H .

4.5.1.4 Prediction

The path model can be rewritten into an prediction equation: $n = (I - B)^{-1} * (A * p) + j$. Matrices B and A were based on the regression coefficients from the model fit.

4.5.2 Model structure

The work with SEM was performed in the statistical program R, using the package *lavaan* (Rosseel, 2012). *Lavaan* is an open-source tool to define and calibrate a SEM. For working with raster data, the packages *raster* (Hijmans, 2014) and *rasterVis* (Lamigueiro and Hijmans, 2014) were used. Functions used in R are marked italic in the text.

Lavaan works with list-wise deletion (deletion of an entire row) when there are NoData values in the dataset. This is the case when a horizon was not present at a certain location or when a horizon was not sampled. This led to a calibration on two sampling locations, when SEM was applied on each horizon simultaneously. That is why a SEM was made for every individual horizon. That way every model has sufficient data to fit and run the model. As an example, the SEM of horizon 1A is discussed in this report. The used model is displayed in Figure 17.

The function *lavaan()* was used to fit the model. All code necessary for fitting the model should be defined in the model script when using this function. Nothing is added automatically, what does happen when using other fit functions.

4.5.2.1 Measurement model

In this study, latent variables are soil variables of interest. These variables are measured, but the measurements are subject to measurement error. The measurement model links the measured variables with the latent variables. A single factor loading of 1 was used, because each measurement is related 1 to 1 with a latent variable. An example is the thickness of a horizon: *measured thickness = real thickness + measurement error*.

The following syntax was used to link the measured variables with latent variables: *latent variable = ~ 1 * measured variable*. With the syntax *measured variable ~ var * measured variable*, the variance in the measurements (*var*) was assigned to the measurements. Covariances in the measurements were assumed zero. This calculations of this variance are discussed in Section 4.7.

The measured variables in the 1A horizon were thickness, silt fraction and organic matter fraction. They are mentioned as *thick_1A*, *silt_1A* and *OM_1A* in the model.

The matrix with factor loadings C has the following form, because all factor loadings are set to 1: $\begin{bmatrix} 1 \\ 1 \\ 1 \end{bmatrix}$.

Variables age and VI were not considered in the measurement model, because it was assumed that the age and VI maps were without variance. Therefore, they could be used direct in the path model.

```

Horizon 1A

#creating the model
LAVAAN_horA1 <- '          #name of the model

# measurement model          #Indicate in what manner the latent variables depend on the measured variables
thick_1A_r =~ 1*thick_1A      #multiplication by 1 sets factor loading to 1
silt_1A_r =~ 1*silt_1A
OM_1A_r =~ 1*OM_1A

# variances observed variables          #indicate the variance in the measurements, as
                                          #indicator of measurement error

thick_1A~~1*thick_1A
silt_1A~~0.00302*silt_1A
OM_1A~~0.0385*OM_1A

# path analysis (regressions)          #indicates the regressions between the different latent variables
thick_1A_r ~ age+veg_index
silt_1A_r ~ thick_1A_r+age
OM_1A_r ~ age+veg_index+thick_1A_r

#factor variances          #Requests residual variances of endogenous variables
thick_1A_r ~~ thick_1A_r
silt_1A_r ~~ silt_1A_r
OM_1A_r ~~ OM_1A_r

#Intercepts          #This code indicates that intercepts should be taken into account with
                        #the regression

thick_1A_r~1
silt_1A_r~1
OM_1A_r~1
'

#fitting the model
fit1A1 <- lavaan(LAVAAN_horA1, data=V_data) #Fit the model with the data

summary(fit1A1,standardized=T)          #summary of the model fit

```

Figure 17: Model script of the SEM of horizon 1A. Text behind a # indicates a comment on the line before.

4.5.2.2 Path model

Regressions between the different latent variables were described according to the following syntax: *endogenous latent variable* ~ *exogenous latent variables* + *endogenous latent variable*. Exogenous variables in horizon 1A were age and vegetation index (VI), endogenous variables were thickness, silt fraction and organic matter fraction. They are mentioned as age_hy, VI, thick_1A_r, silt_1A_r and OM_1A_r in the model. The r indicates that this is the true, error-free value.

The following syntax indicated that the variance in the latent variables should be calculated: *latent variable_i*~~*latent variable_i*. No value was assigned in the syntax, in order to let *lavaan* calculate the variance. The covariances were assumed to be zero. *Lavaan* always calculates intercepts of the endogenous variables. *Endogenous variable* ~ 1 indicated that *lavaan* should also present these intercepts in the model output.

The choice of explanatory variables was based on the conceptual model (Section 3.2). SEM has a function to search for other variables which have a high correlation with the target variable and can increase the accuracy of the fit. This function was used to find extra explanatory variables. Variables found in this way were only added if their involvement could be explained by soil forming processes in the area. The syntax for this function was the following:

```
mi <- modindices(fit_model)
```

$mi[mi\$op == "~",]$

This function returned a list of all possible combinations of involved variables, with an indicator of how much a certain combination would add to the total fit of the regression of the target variable.

Matrix A, with correlation coefficients between exogenous and endogenous variables, is a 3*2 matrix with

the following structure: $A = \begin{bmatrix} thickness \sim age & thickness \sim VI \\ silt \sim age & 0 \\ OM \sim age & OM \sim VI \end{bmatrix}$.

Correlation matrix B is a 3*3 matrix, with the following structure: $B = \begin{bmatrix} 0 & 0 & 0 \\ silt \sim thickness & 0 & 0 \\ OM \sim thickness & 0 & 0 \end{bmatrix}$

4.5.3 Input data

The data file for the model consisted of 20 rows, each indicating one sampling location in a valley position. Ridge positions were left out, due to their lack of aeolian cover. Columns were ordered per horizon and contained information on thickness, silt, gravel and sand fraction and organic matter fraction. The last columns contained the VI, altitude and age of the sampling locations. The output of *lavaan* presents the coefficients with a maximum of three decimal places. The order of magnitude for some variables was changed in order to get a proper display of the coefficients (Table 6).

Table 6: Overview of data included in the input file + summary and units of data used for the SEM model of horizon 1A

	Variable	Unit	Range of data for horizon 1A in valley positions
Information per horizon	Thickness	cm	0-45
	Silt fraction	%	5.6-18.6
	Sand fraction	-	Not used
	Gravel fraction	-	Not used
	Organic matter fraction	%	1.7-6.4
General information	Altitude	Meters	6.5-47.0
	Age	100 years	49.2-137.6
	Vegetation index	%	41.2-68.3

Model performance was visualized by applying the model on different combinations of age and VI, in the form of 50x50 rasters. The age raster contained values ranging from 0 to 140, separated over the different columns. The VI raster contained VI values ranging from 40-100, divided over the different rows. Combining both rasters resulted in a different combination of age and VI for every cell.

Variances in the measurements is calculated using methods described in Section 4.7.

4.6 LORICA

MILESD (Model for Integrated Landscape Evolution and Soil Development) was developed to fill the need for an integrated soil-landscape model (Vanwallegem et al., 2013). Soil forming processes included in this model are bedrock weathering, physical weathering, chemical weathering, neo-formation of clay, clay eluviation, bioturbation and the carbon cycle. MILESD used a basic landscape evolution model. In their discussion they stated that the soil-part of MILESD should be coupled with a state-of-the-art landscape evolution model, to improve the landscape-evolution part of their model. That is why the soil-part of MILESD was coupled with LAPSUS (Landscape Process modeling at multi-dimensions and Scales), a landscape evolution model which takes into account several erosion and sedimentation processes, like for example water erosion and deposition, tillage, landsliding, solifluction and tectonics (Schoorl et al., 2002). Coupling these two models improved the understanding of the dynamics and relations between soil development and landscape evolution (Vanwallegem and Temme, 2014).

The model used to predict the development of the particle size distribution in the study area is LORICA (Temme and Vanwallegem, 2015). LORICA is a further development of MILESD. LORICA works with the preservation of mass. Weathering of a certain mass of a certain fraction results in the same mass of a finer fraction. The same goes for geomorphic processes as erosion and deposition.

4.6.1 *Model structure*

Not all processes available in LORICA were used in this study, because some processes do not occur in the study area. Other processes were added, to take into account processes which were not yet available in LORICA. The used modules, and possible adjustments, are described below.

4.6.1.1 *Isostatic rebound*

To account for isostatic rebound in the area, an extra piece of code was added in LORICA (Appendix C1). The trend between age and elevation was used to calculate a threshold which determined which parts of the study area were present above sea level at a certain time step. Elevations lower than the calculated threshold were set to no data. This way the areas of the DEM which were considered below sea level at a certain moment in time were not subject to landscape and soil forming processes. Locations were affected by different processes from the moment of emerging until the end of the model run.

The used trend comes from the shell datings from Long et al. (2012) (Figure 3). The trend is: $age\ location = 218.02 * elevation + 3508.7$. Transforming this equation resulted in: $elevation = (age\ location - 3508.7)/218.02$. The linear trend was extrapolated to the highest terrace (terrace level 6 in Figure 4). This beach ridge is the oldest undisturbed ridge in the study area and for that reason chosen as the initial shoreline for the model run. The lowest elevation on this terrace is 47 meter, which corresponds to an age of 13755 year.

The following formula was added to LORICA:

$$IF\ DEM_{i,j} > \left(\frac{(13755 - timestep) - 3508.7}{218.02} \right) \& DEM_{i,j} == NoData, THEN\ DEM_{i,j} = DEM_{original_{i,j}}$$

Where i and j refer to a certain cell in the study area. DEM is the map which LORICA uses for its calculations at a certain time step. DEM_original is the DEM of the study area which is used as input in the model.

4.6.1.2 *Water erosion and sedimentation*

LORICA generates run-off and infiltration by applying rainwater on the grid cells. Run-off flows downhill, collecting sediments on its way. When the amount of sediments transcends the sediment capacity of the water, the sediments start to be deposited. Sediments can also be transported out of the study area. Mass of eroded material is equal to mass of deposited material in the study area and mass of sediments transported out of the area. Vegetation and coarse material decrease the mass of material that can be eroded. An extensive explanation of this module is provided in Temme and Vanwalleghem (2015).

Initial values were used for almost all parameters in this module. Exceptions were erosion threshold and bio protection constant/vegetation cover. Erosion threshold indicates how much transport capacity must be available before erosion occurs. Field observations indicate some traces of erosion. That is why this parameter was set to zero, in order to let some erosion occur. The original values for the bio protection constant and vegetation cover are 1. Because of the scarce and low vegetation, bio protection constant was set to 0.5.

4.6.1.3 *Aeolian deposition*

LORICA is not designed to model aeolian processes. That is why an extra module was added (Appendix C2). In the first time step, gravel content of the first soil layer in valley positions was set to zero. Sand content was set to a very small amount (10^{-10} kg), to make sure that the layer kept existing. Removed material was added to the lowest layer, to avoid loss of material. The amount of sand added every time step was calculated using the slope of linear regression between the increase of thickness of the 1A horizons in valley positions with age.

This thickness was converted to an amount in kilograms using the bulk density of the aeolian sand cover, which was calculated by taking average bulk density of buried 1A2 horizons, described separately in the field. These buried horizons are less affected by plant growth and other surface processes.

4.6.1.4 Physical weathering

Through physical weathering, gravel content in the soil changes to sand. Sand then again changes to silt. Decrease in gravel fraction is used to determine the weathering rate, using the following formula: $Gravel_t = Gravel_0 * (1 - C_0)^t$, where $Gravel_t$ is the gravel fraction at time t , $Gravel_0$ is the initial gravel fraction and C_0 is the weathering rate at the surface (y^{-1}). The intensity of weathering decreases with depth in the soil (Vanwalleghem et al., 2013), following the formula $C_d = C_0 * e^{kd}$, with C_d (y^{-1}) the weathering rate at depth d (m) and k the depth decay constant (m^{-1}).

Initial weathering rate and initial gravel fraction were derived from comparing weathering rates in 2B/ and 2BC horizons, by performing linear regression on the logarithm of gravel content in both horizons, according to the following formula:

$$\log(\text{gravel}_{\text{horizon}}) = \log(\text{Gravel}_0) - C_{\text{horizon}} * t$$

Rewriting these formula results in:

$$\text{gravel}_{\text{horizon}} = \text{Gravel}_0 * (1 - C_{\text{horizon}})^t$$

Depth of 2B/ horizons was calculated by adding the thickness of overlying horizons with half of the thickness of the 2B/ horizons. Depth of 2BC horizons was calculated by adding 0.15 meters to the cumulative thickness of overlying horizons. Only locations where both a 2B/ and 2BC horizon were observed were considered in these calculations. Weathering rates of both horizons, combined with average depth of the horizons, resulted in the depth decay constant k and initial weathering rate C_0 . The

depth decay constant k was calculated as $k = \frac{\ln \frac{C_{2B/}}{C_{2BC}}}{d_{2B/} - d_{2BC}}$. With a known k , C_0 was calculated.

Smaller particles have a larger reactive surface, so physical weathering processes happen faster for smaller particles. This was implemented in LORICA using the following formula:

$$\frac{-\text{Particle size constant}}{\log_{10}(\text{upper particle size})}$$

Where particle size constant indicates how strong the effect of a smaller particle size is.

As input for the particle sizes of gravel, sand and silt, the initial values were used. These are 0.01 m, 0.002 m and 0.00005 m. They serve as upper limits of the particles in the model and were based on USDA classification (Vanwalleghem et al., 2013). Upper limit of silt particles measured in the laboratory is 67 μ m, but this was overlooked when filling in the parameters for the model. Particle size constant was kept on the initial value of 5 (Vanwalleghem et al., 2013).

Combining all formulas affecting physical weathering results in the following equation, which was used in LORICA:

$$\text{Weathered mass}_{\text{fraction}} = \text{total_mass}_{\text{fraction}} * C_0 * e^{k * \text{depth}} * \frac{-\text{particle size constant}}{\log_{10}(\text{upper particle size})}$$

All gravel weathered only to sand and all sand weathered only to silt. The weathering stopped at the silt fraction, because there were no traces of finer material in the soils. The script is located in Appendix C3.

4.6.1.5 Silt translocation

Silt in the soil was formed by physical weathering of gravel and sand particles. Silt released by dissolution of parent material was assumed to be negligible (C'iric' and Senic', 1985). A part of the produced silt eluviated through the soil profile via a downward water flux. This eluviation is comparable to eluviation of clay through a soil. That is why the script for clay eluviation was adjusted to calculate silt transport in the soil (Appendix C4). Silt was transported from one layer to the layer below according to the following formula: $\Delta \text{silt} = \text{silt}_{\text{max}}(1 - e^{-k * P_{\text{silt}}}) \Delta t$ (Vanwalleghem et al., 2013), with:

- Δsilt = amount of silt eluviating per time-step;
- silt_{max} : the maximum amount of silt that can eluviate per time-step;

- k: a constant, set to 1 in this study;
- P_{silt} : the mass fraction of silt in the layer where the silt eluviates from.

5 soil pits were selected to calculate the silt_{max} . These pits were sampled on ridge positions without aeolian cover, indicating only vertical water transport and no other sources of silt than silt originating from weathering of the marine deposits. The amount of silt in these soils was calculated using silt fractions, horizon thicknesses and bulk density of horizons 2A, 2B and 2B/.

An input file for LORICA, containing the same altitudes as the selected soil pits, resulted in the simulated amount of silt in the modelled 2A and 2B/ horizons. The silt_{max} was calibrated by searching for the lowest RMSE between silt content in the model output and field data.

4.6.2 Input data

4.6.2.1 *Digital elevation model*

Aeolian cover was subtracted from the DEM in order to simulate initial conditions of the area. Thickness of the aeolian cover should have been based on regression between thickness and age (Figure 31), like the aeolian deposition. However, something went wrong in the map preparations, where a regression between the square root of thickness and square root of age was used. This regression produced a better fit, with a higher R^2 . Analysis on the model results was already performed when I found this out. Due to time constraints this error could not be fixed in time and analysis was performed on the output resulting from the wrong input DEM. This DEM was calculated using the following formula:

$$DEM_{\text{without aeolian sand}} = DEM_{\text{original}} - (\sqrt{218.02 * DEM + 3508.7 * 0.0072 - 0.1442})^2$$

Besides the study area, also a part upstream of the marine terraces was used as input, in order to let sediments enter the study area from higher located areas.

Due to inconsistencies in the DEM, a part of the flat sea surface was included in the DEM when it was clipped by the terrace levels. This flat area led to errors in LORICA, because it cannot handle flat surfaces at the borders of an area. Also permafrost lakes located on T1 and T2 produced errors, because they were present as sinks in the DEM. Both the permafrost lakes as the flat sea surface were removed from the DEM, to prevent errors in LORICA.

4.6.2.2 *Map of ridges and valleys*

To indicate which cells receive aeolian sand, a map of ridges and valleys, indicated with 0 and 1, was used. Cells with a VI higher than 0.45 were indicated as valley, cells with a VI lower than 0.45 were indicated as ridge.

4.6.2.3 *Input parameters*

Annual precipitation in the Ebba valley is 200 mm, from which the most part falls as snow (Strzelecki, 2012). In summer, precipitation falls as very light drizzle. Due to the absence of the sun in the winter months, very small amounts of precipitation in summer and melting of precipitation in solid phase in a short time window, I assumed the evaporation to be negligible.

There is no information available on the exact infiltration amounts in the study area. The soils in the study area are dry and coarse-textured. Average soil moisture content in the samples examined in the lab was 9.5%, with a standard deviation of 7.6 %. According to Gray et al. (2001), these dry and coarse soils can be sorted in the group with unlimited infiltrability. Because of visible gullies in the area it is clear that not all water infiltrates, but also overland flow occurs. That is why I chose infiltration to be 75% of the precipitation.

Initial composition of marine deposits was deduced from the initial gravel content calculated using the formulas in Section 4.6.1.4, which is 0.90 for the 2B/ horizon and 0.89 for the 2BC horizon. Marine sediments only consist of coarse materials, no silt is deposited in situ. This is also visible in the deposits on the current beach (Figure 18). This resulted in an initial distribution of 90 % gravel and 10 % sand in the beach deposits.



Figure 18: Pictures of the current beach, consisting of gravelly and sandy material.

Initial soil depth in the terraces was set to 100 meters. That way soil development is not limited by the available amount of soil material. The number of soil layers in LORICA was set to 10.

The model was run for 13755 years, corresponding to the minimum age of the highest terrace in the area. The model runs from the past to the present. Table 7 contains an overview of all parameters used as input.

Table 7: Parameters used as input for the LORICA model

General		Number of soil layers		10
		Initial soil depth (m)		100
		Precipitation (m y^{-1})		0.2
		Evaporation (m y^{-1})		0
		Infiltration (m y^{-1})		0.15
Initial composition of the soil		Gravel (%)	90	
		Sand (%)	10	
		Silt (%)	0	
Geomorphic processes	Water erosion and deposition	p (multiple flow factor)		2
		m (exponent of overland flow)		1.67
		n (exponent of slope)		1.3
		K (erodibility)		0.0003
		Erosion threshold		0
		Rock protection constant		1
		Bio protection constant		0.5
Selectivity change constant		0		
Soil forming processes	Physical weathering	Weathering rate constant (y^{-1})		$4.06 \cdot 10^{-5}$
		Depth decay constant (m^{-1})		-2.22
		Particle size constant (m)		5
	Silt translocation	Particle size	Coarse fraction (m)	0.01
			Sand fraction (m)	0.002
			Silt fraction (m)	0.00005
Silt translocation	Maximum eluviation (kg)		0.172	
	Saturation constant		1	

4.6.3 *Translating model output into horizons*

X and Y coordinates of the sampling locations in the field were used to select which soil profiles LORICA had to give as output. The 10 soil layers in the outputs were translated in 4 horizons (1A, 2A, 2B/ and 2BC) to compare them with the field observations. Criterion for 1A horizons was a gravel fraction lower than 0.05, which indicates the sandy/silty nature of the horizon. Most 2A horizons observed in the field have a sand fraction larger than the gravel fraction (Figure 19). For 2B/ horizons, gravel fraction is in

general larger. Separation was thus based on which of the fractions dominated in the output layers of LORICA. This border is displayed by the 1:1 line in Figure 19. The lower boundary of 2B/ horizons was based on silt fraction (Figure 20). A border of 2.5% separates almost all 2B/ horizons from the 2BC horizons. 2BC horizons with a silt fraction higher than 2.5% were in general located on higher terraces (Figure 23).

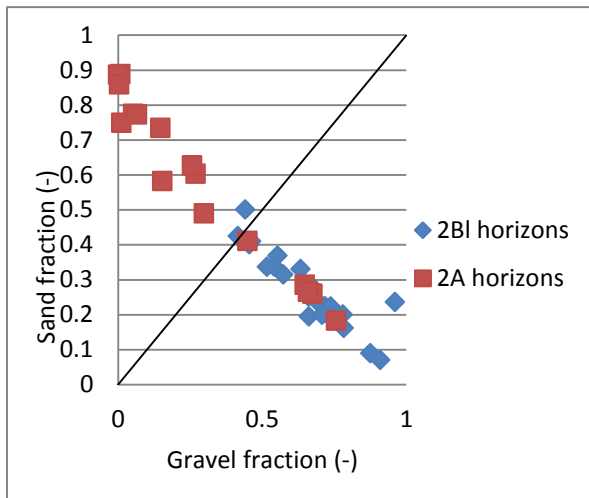


Figure 19: Scatterplot of gravel fraction versus sand fraction, for the 2A and 2B/ horizons observed in the field. Points above the black line have a sand fraction higher than the gravel fraction. Points below the black line have a higher gravel fraction.

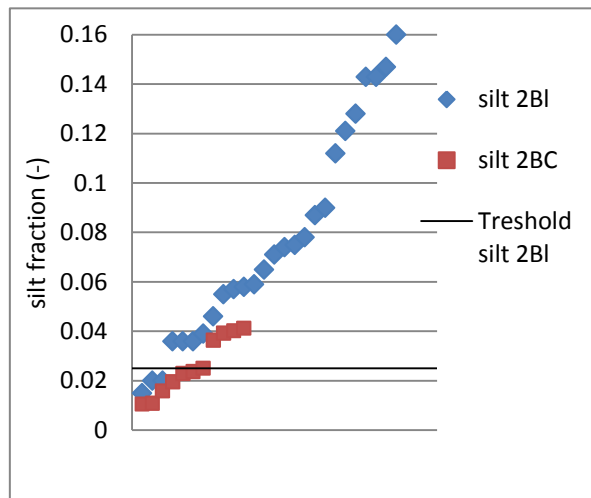


Figure 20: Plot of the silt fractions of the 2B/ and 2BC horizons observed in the field, in ascending order. The black line indicates the chosen threshold of 2.5% silt as boundary of the 2B/ horizons.

Decision rules were applied in following order:

1. Gravel fraction < 0.05 → 1A horizon
2. Sand fraction > gravel fraction → 2A horizon
3. Gravel fraction > sand fraction → 2B/ horizon
4. Silt < 0.025 → 2BC horizon

Horizon thickness was calculated by adding thicknesses of the layers appointed to a certain horizon. The same was done for mass of present gravel, sand and silt. Fractions of gravel, sand and silt were calculated by averaging fractions of the layers appointed to a certain horizon.

LORICA worked with cells of 10 by 10 meters in this study. In order to compare quantities of soil material from the model with field observations, the quantities of modelled soil material were divided by 100, to get the results per square meter.

4.7 Variation in the measurements

A part of the variation in the measurements was caused by devices used to measure the data. This variation is quantified using variances in the measurements. Horizon thickness was measured using a tapeline. Results in the laboratory were all measured with a scale. When a sample was placed on a scale, it took a while before the given weight was steady. After it became steady, the value could still shift. Some cups used for the LOI were weighted multiple times.

4.7.1 Variance in measuring thickness

Standard deviation in thickness measurements using the tapeline was estimated to be 1 cm. This error can be caused due to the following processes:

- Positioning the base of the tapeline wrong (e.g. not exactly on the end of the previous horizon), the thickness could be both underestimated or overestimated;

- Rounding the measurements to whole cm.

4.7.2 Variance in laboratory measurements

Two scales were used in the laboratory. A paired T-test showed that there is no significant difference between output of the two scales. Variance of the measurement errors for one single measurement with a scale was calculated by taking the weighted average of variances of the cups calculated with Excel, according to the following formula:

$$\text{Variance scale measurements } (g^2) = \frac{\sum_{i=1}^n \text{var}_i * \text{obs}_i}{\sum_{i=1}^n \text{obs}_i}$$

With the number of cups n that is weighted more than once, var_i as the variance in cup i and obs_i as the amount of observations for that cup.

Variance propagates through calculations of target variables. Resulting variance in target variables was calculated using standard procedures for error propagation. This is done for every observation. Per horizon (1A, 2A, 2B, 2Bl and 2BC), the average variance for each property is taken.

4.8 Validation of model results

SEM was validated using cross validation (Appendix B6). One sample was removed from the input file. The model was then fitted on the remaining samples. The fitted model was applied on the age and VI of the removed sample. Resulting thickness, silt content and organic matter content were compared to measured values from the removed sample.

Results of the models were plotted against observations in the field. Comparing scatterplots with the identity line indicated if trends in the model results matched observed trends. It also showed if the model overestimated or underestimated certain variables by the position of scatter-points above or below the identity line. This bias was quantified by the mean prediction error: $MPE = \frac{1}{n} \sum_{i=1}^n [\hat{y}_i - y_i]$, with \hat{y} as the predicted value and y as the observed value in the field (Hengl et al., 2004).

Accuracy of the models was tested using the Root Mean Squared Error (RMSE). The RMSE is the square root of the mean squared error: $RMSE = \sqrt{\frac{1}{n} \sum_{i=1}^n [\hat{y}_i - y_i]^2}$.

For SEM, validation statistics were performed on results of the cross-validation and field observations. For LORICA, the validation was performed on the output of the 30 sampling locations and corresponding field data.

The output of LORICA was compared to two judgmentally chosen locations (J10 and J11), to see how the model performs on locations not taken into account in the calibration (J10) and located just outside the study (J11).

5 Results

5.1 Data analysis

Data collected during the fieldwork and in the laboratory were used for calibration of the two models. This section describes trends that can be seen in field and lab results. First, a summary of the data is given. After that, trends in different variables are treated using graphical illustrations. Variables considered are horizon thickness, gravel fraction, silt fraction and organic matter fraction.

5.1.1 Summary of sampling locations

Table 8 provides an overview of the occurrence of different horizons on different morphological settings, ordered per terrace level. Most 1A horizons occur in valleys and on sloping terrain. A few exceptions are located on a ridge positions. These points are located in small depressions on ridges, where still some aeolian sand is accumulated, due to present vegetation. This is shown by the relatively small thickness of the 1A horizon on the ridges compared to the 1A horizons in valley positions, for terrace level 5.

Only 5 sampling points contain a 2B horizon. This is in contrast with the hypothesis that between the A horizons and B/ horizon a layer with less silt is located, which acted as transport layer for the silt. Due to this low occurrence, 2B horizons were not considered in the model studies.

Table 8: Overview of the horizons present in the different sampling locations, divided over the different morphological settings on the different terrace levels. Between brackets the average thickness of those horizons is mentioned.

Terrace level	Horizon	ridges	slopes	valleys	Total
1	1A			2 (12)	2
	2A			2 (12)	2
	2B				0
	2BI			1 (12)	2
	2BC			2	1
	Total samples			2	2
2	1A	1 (10)	1 (10)	2 (13.5)	4
	2A	2 (10)	1 (11)		3
	2B		1 (20)		1
	2BI	2 (23)	1 (29)	2 (35)	6
	2BC	3	1	2	5
	Total samples	3	2	2	7
3	1A		2 (26)		2
	2A	1 (7)	1 (20)		2
	2B	1 (23)	1 (26)		2
	2BI	1 (25)	1 (10)		3
	2BC	1	2		2
	Total samples	1	2		3
4	1A		1 (7)	8 (32.75)	9
	2A	1 (6)		4 (20)	5
	2B				0
	2BI	1 (69)	1 (8)	4 (40.75)	7
	2BC	1	1	5	6
	Total samples	1	1	8	10
5	1A	2 (11)		5 (31.4)	7
	2A	2 (15)		1 (36)	3
	2B	1 (38)		1 (30)	2
	2BI	2 (35)		4 (22.5)	6
	2BC	2		4	6
	Total samples	3		5	8
Total per morphological setting		8	5	17	30

5.1.2 *Horizon thickness*

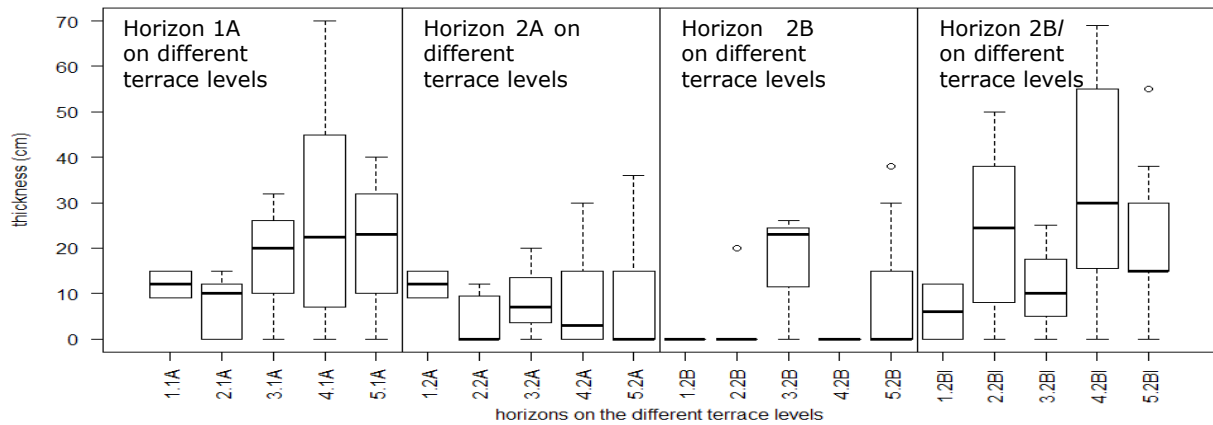


Figure 21: Boxplot of the horizon thickness for different terrace levels.

In general, the thickness of 1A and 2BI horizons increase with age. For horizon 2A it seems that the thickness decreases (Figure 21). When a horizon was absent in a soil pit, it got a thickness of 0. This happened especially for 2A and 2B horizons.

5.1.3 *Gravel fraction*

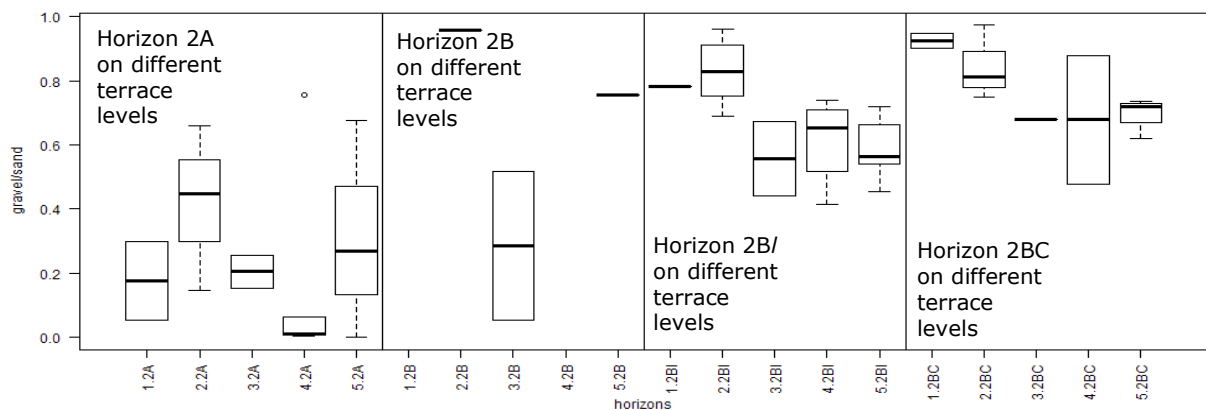


Figure 22: Boxplot of gravel fraction in the horizons formed in marine sediments, on different terrace levels.

Gravel fraction can decrease by physical weathering and dissolution. This is visible in the reduction of gravel fraction in horizons 2B/ and 2BC (Figure 22). The 2B/ horizon shows a steeper trend and lower gravel fractions compared to the 2BC horizon, showing faster weathering processes in higher horizons. Changes of gravel fraction in horizons 2A and 2B show no trend with age.

5.1.4 *Silt fraction*

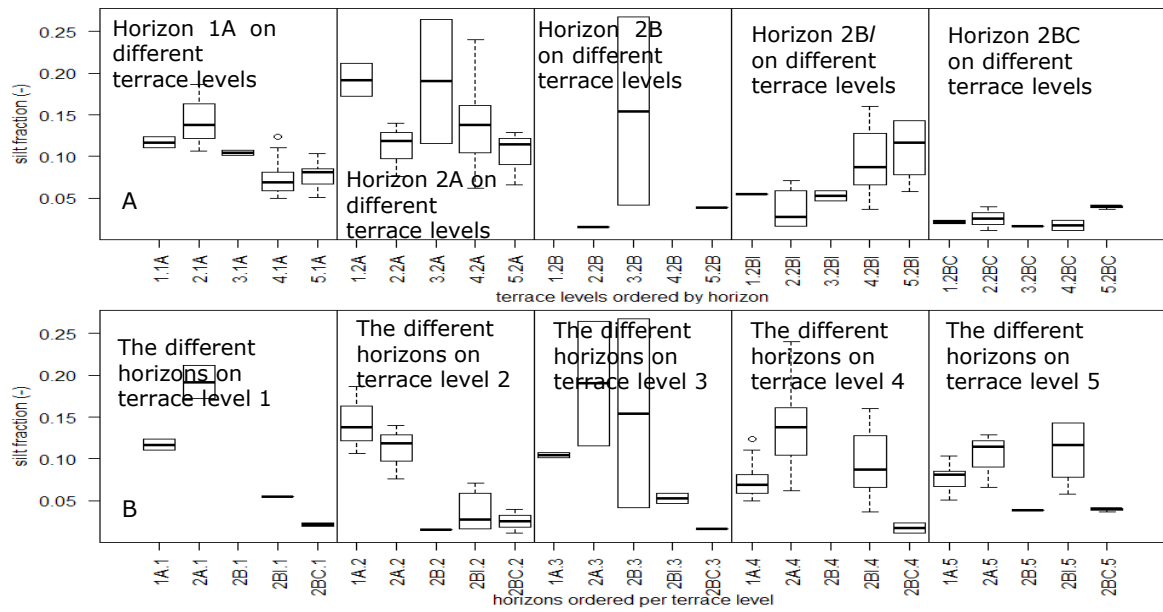


Figure 23: Boxplot of silt fraction in different horizons on different terrace levels (A) and in a vertical profile on each terrace level (B).

Silt fractions in 1A and 2A horizons decrease towards higher terraces. For lower lying 2B/ and 2BC horizons, silt fractions increase with altitude (Figure 23). No trend is visible for 2B horizons. The total amount of silt in 2B/ horizons increases faster than the total amount of silt in both 2A horizons combined (Figure 24).

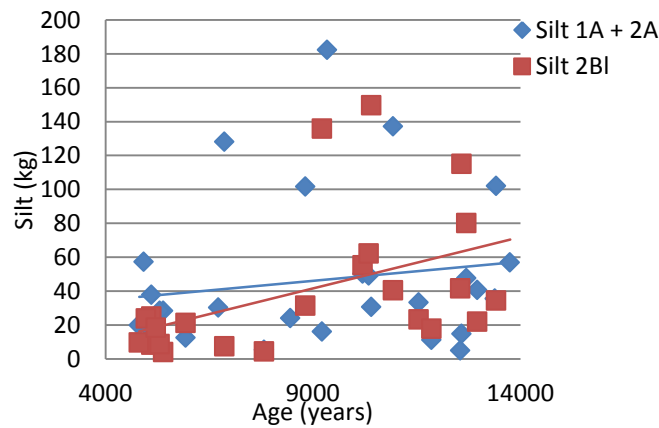


Figure 24: Total amount of silt observed in the field, for both A horizons combined and for the 2B/ horizon

5.1.5 Organic matter

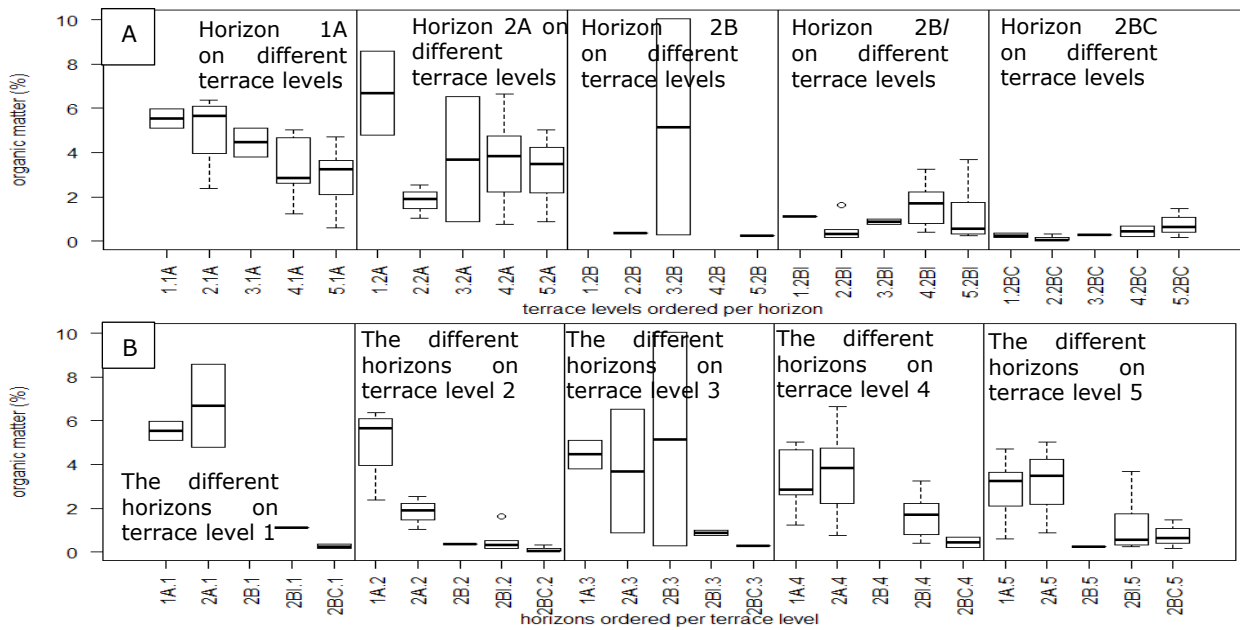


Figure 25: Boxplot of organic matter fraction in different horizons on the different terrace levels (A) and in a vertical profile on each terrace (B).

Boxplots in Figure 25a show that organic matter fraction decreases with age in 1A and 2A horizons. Total amount of organic matter in the 1A horizons increases with age (Figure 26). For horizons 2B/ and 2BC the organic matter fraction increases with age. There is still a lot of fluctuation in the trends. The OM fraction in the soils decreases with depth (Figure 25b). Both A horizons show a significantly higher OM fraction than the B horizons on all terrace levels (save for the 2B horizon).

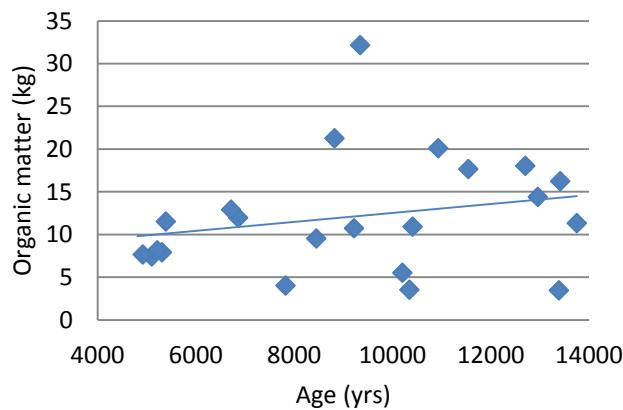


Figure 26: Scatterplot of total amount of organic matter observed in 1A horizons, calculated with bulk density, organic matter fraction and horizon thickness.

5.2 Structural equation model

5.2.1 Variance in measurements

Variance per measurement with laboratory scales is $4.5 \cdot 10^{-3} \text{ g}^2$. This variance propagates through the calculations of the variables of the 1A horizon. The variance in thickness is 1 cm^2 . For the percentage of silt and percentage of organic matter, the variances are $3.02 \cdot 10^{-3}$ and $3.85 \cdot 10^{-2}$. These variances were used in the input of the SEM.

5.2.2 Parameterization

Table 9 shows the summary of the fitted SEM for horizon 1A. A schematic overview is provided in Figure 27. The model used 17 of 20 samples, because three samples contain NoData due to errors in sampling or because of absence of a 1A horizon. Model fit is quite good, considering the high P-value (0.625).

Thickness of 1A horizons increases with age, with $0.178 \text{ cm}/100 \text{ years} = 1.78 \cdot 10^{-5} \text{ m/year}$. It also appears that vegetation has a negative effect on thickness. Remaining variance in thickness is 79.5 cm^2 . Variance in the original data is 170.4 cm^2 . A substantial amount of the variance is thus removed by applying this model. Best indicators for silt fraction in 1A horizons are age and horizon thickness. Age has a very significant negative effect on the silt content, while thickness has a positive effect. Variance in silt fractions is brought back from 11.1 to 5.3. Organic matter can best be explained by age, VI and horizon thickness. Both increasing age and thickness have a negative effect, while an increasing VI has a positive effect.

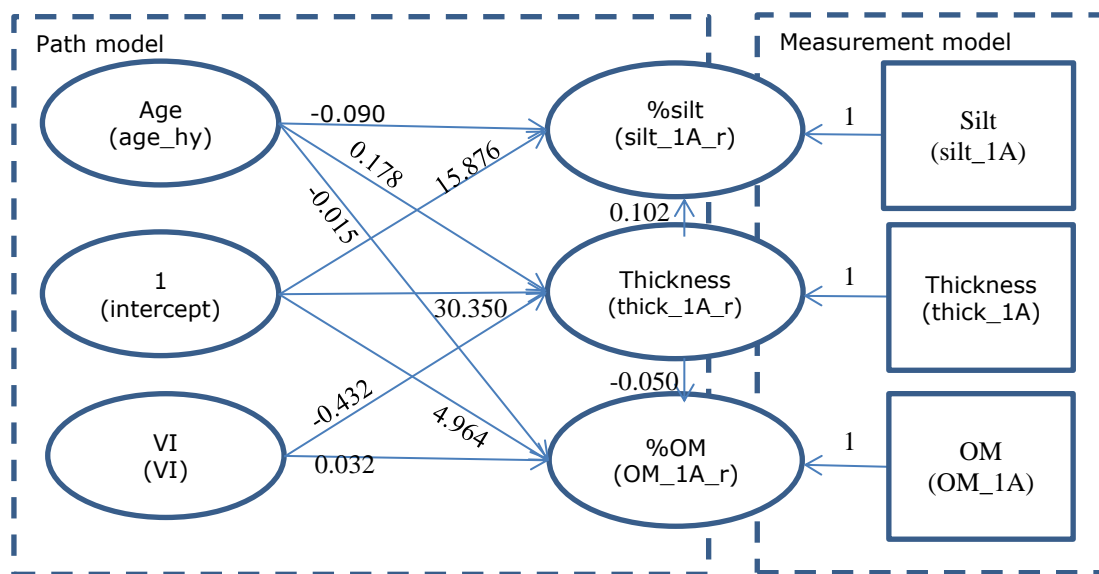


Figure 27: Schematic overview of the fitted SEM model for the 1A horizon. Rectangles indicate field measurements. Oval shapes indicate the latent variables. The terms used in the model are displayed between brackets (Table 10). The numbers are coefficients resulting from fitting the SEM. Exogenous variables in this study (age and VI) are known exhaustively in space and are used as input for the prediction model.

5.2.3 Visualizing model performance

For a combination of young soils and high VIs, the model results in negative thicknesses (Figure 28a). Soil with ages and VIs corresponding to these negative thicknesses are not present in the study area. The negative thicknesses are a result of extrapolation of the model. Effect of VI on thickness is similar to effect of age on thickness, because the horizontal variation in the figure is similar to vertical variation.

Although VI has no direct influence on the silt fraction through the regressions, there are indirect influences, such as through thickness. However, this effect is much smaller than the effect of age, as evidenced by the larger horizontal variation in Figure 28b.

Influence of age and VI on organic matter is also similar, just as with thickness. Effect of exogenous variables is however opposite than their effect on thickness. This results in low values for old soils with a low vegetation index and high values for young soils with a high vegetation index.

Table 9: Summary of the fitted SEM for horizon 1A.

```
lavaan (0.5-16) converged normally after 112 iterations
```

	Used	Total
Number of observations	17	20

Estimator	ML
Minimum Function Test Statistic	0.941
Degrees of freedom	2
P-value (Chi-square)	0.625

Parameter estimates:

Information	Expected
Standard Errors	Standard
	Estimate Std.err Z-value P(> z)

Latent variables:

thick_1A_r =~				
thick_1A	1.000			
silt_1A_r =~				
silt_1A	1.000			
OM_1A_r =~				
OM_1A	1.000			

Regressions:

thick_1A_r ~				
age_hy	0.178	0.079	2.237	0.025
VI	-0.432	0.309	-1.398	0.162
silt_1A_r ~				
thick_1A_r	0.102	0.062	1.645	0.100
age_hy	-0.090	0.023	-3.857	0.000
OM_1A_r ~				
age_hy	-0.015	0.006	-2.579	0.010
VI	0.032	0.021	1.533	0.125
thick_1A_r	-0.050	0.016	-3.172	0.002

Intercepts:

thick_1A_r	30.350	21.973	1.381	0.167
silt_1A_r	15.876	1.747	9.086	0.000
OM_1A_r	4.964	1.477	3.361	0.001
thick_1A	0.000			
silt_1A	0.000			
OM_1A	0.000			

Variances:

thick_1A	1.000		
silt_1A	0.003		
OM_1A	0.038		
thick_1A_r	79.482	27.605	
silt_1A_r	5.702	1.960	
OM_1A_r	0.285	0.112	

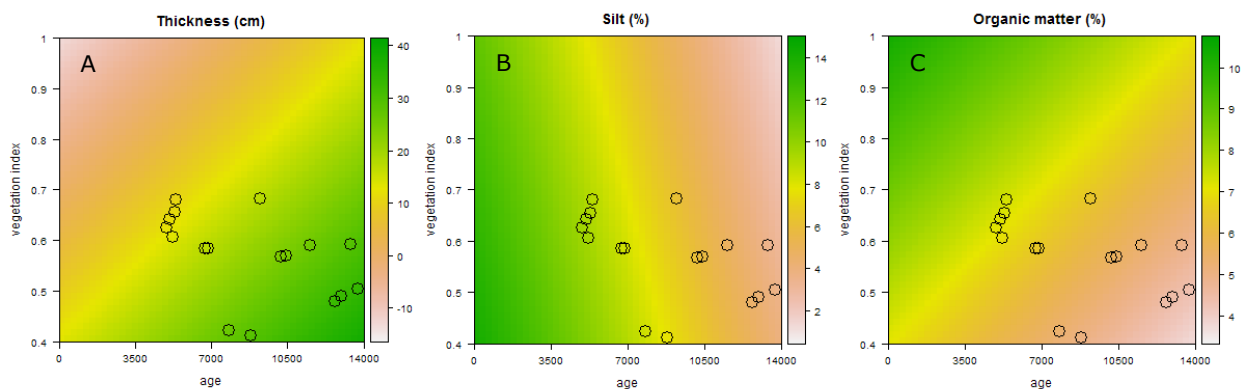


Figure 28: Visualization of how SEM reacts on different combinations of age and VI. Circles indicate the age and VI combinations of field data.

5.2.4 *Predictions for the study area*

The trends visible in Figure 28 also occur in model results for the study area (Figure 29).

Modelled thickness of the 1A horizon (Figure 29a) increases from approximately 5 cm near the current coastline to 40 cm on the highest terraces. Local variation is caused by variation in vegetation index. Second and third terrace level show some lines of higher thickness, parallel to the terrace border, which coincide with cryoturbation patterns with a lower vegetation index. Thicknesses appear to be quite constant on the three lower levels, around the 15 cm. In the 4th terrace the thickness strongly increases towards 25 cm on the 5th terrace level.

Silt fraction in 1A horizons decreases gradually towards higher horizons (Figure 29b). VI causes small scale variability, disturbing the general trend in the area. Highest silt fractions, around 10%, can be found on the lowest terrace. This fraction decreases to approximately 3% on the highest terrace.

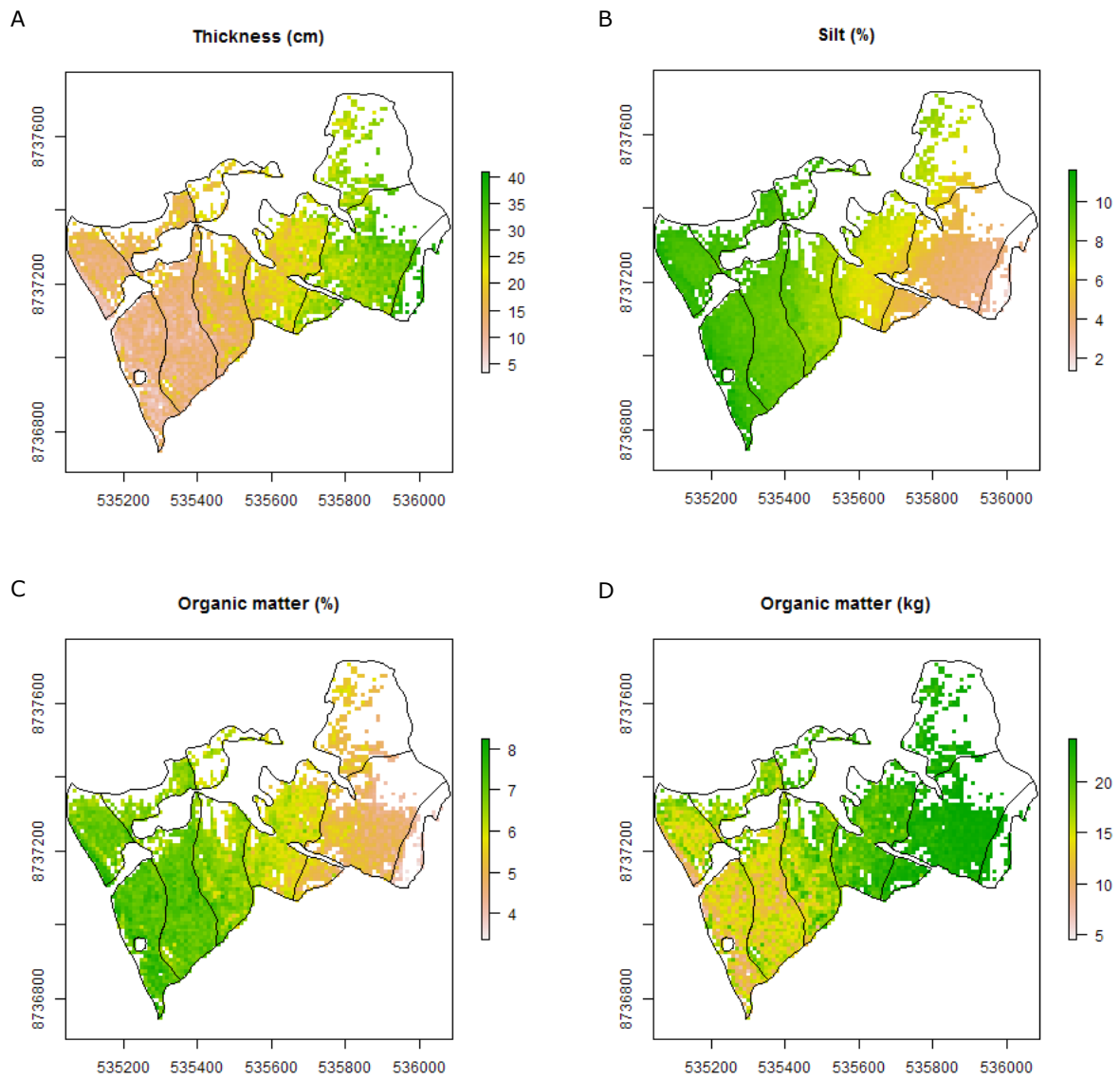
Organic matter fraction also decreases towards higher terrace levels (Figure 29c). Visible patterns resemble those of thickness, as they are caused by the same exogenous variables. But where thickness would increase due to a low VI, OM content decreases. Values range from approximately 6% for the lowest horizon to 3.5% for the highest terraces. Total organic matter content, calculated by multiplying the fraction with thickness of the horizon and bulk density of aeolian deposits, increases with age (Figure 29b).

5.2.5 *Validation*

Table 10: Summary of simulations resulting from cross-validation of samples from the 1A horizons located in valley positions.

	Average	Standard deviation	Min	Max	RMSE	RMSE/ average	MPE	MPE/ average
Thickness (m)	2.14E-01	8.66E-02	1.02E-01	3.70E-01	1.21E-01	5.67E-01	1.42E-04	6.62E-04
Silt fraction (-)	6.93E-02	2.40E-02	2.97E-02	1.03E-01	4.35E-02	6.27E-01	-3.12E-02	-4.50E-01
OM fraction (-)	6.22E-02	1.27E-02	3.86E-02	8.21E-02	2.00E-02	3.22E-01	1.77E-02	2.84E-01

Table 10 shows summary statistics and validation statistics for cross-validation results. The high RMSE of thickness indicates a low accuracy of the model. Figure 30a indicates this through the large scatter around the identity line. The simulations are almost unbiased, according to the MPE of $1.42 \cdot 10^{-4}$ m. The model underestimated the silt fraction in the 1A horizons, according to the negative MPE and positioning of the scatter-points below the identity line (Figure 30b). With a RMSE of 0.044 (64 % of predicted average) the prediction is also not very accurate. An RMSE of 0.020 (relative to predicted average: 0.323) indicates a relatively high accuracy. The scatter-points in Figure 30c follow a clear trend. The simulations are overestimated, according to the scatter-points above the identity line and the positive MPE.



5.3

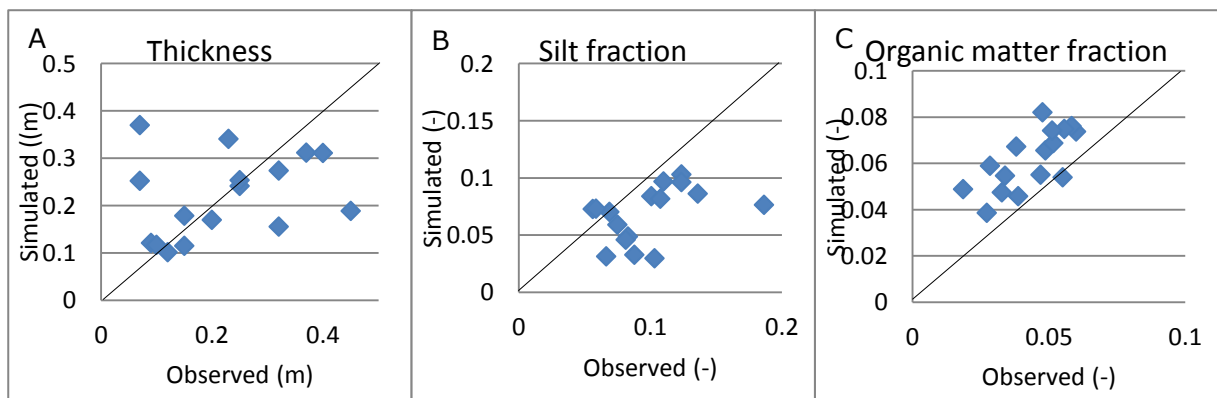


Figure 30: Scatterplots of simulations by SEM versus field observations for thickness (A), silt fraction (B) and organic matter fraction (C). The black line indicates the identity line.

LORICA

5.3.1 Parameterization and calibration

Most parameters were retrieved from field and laboratory data. Parameters for silt translocation were calibrated using multiple model runs.

5.3.1.1 *Aeolian deposition*

Regression shows that per year, averaged over valley positions, $2 \cdot 10^{-5}$ meters of sand is deposited (Figure 31). This increase in thickness corresponds with $3.3 \cdot 10^{-2}$ kg/m²/year, using bulk density of the aeolian cover (1651 kg/m³, standard deviation = 240 kg/m³).

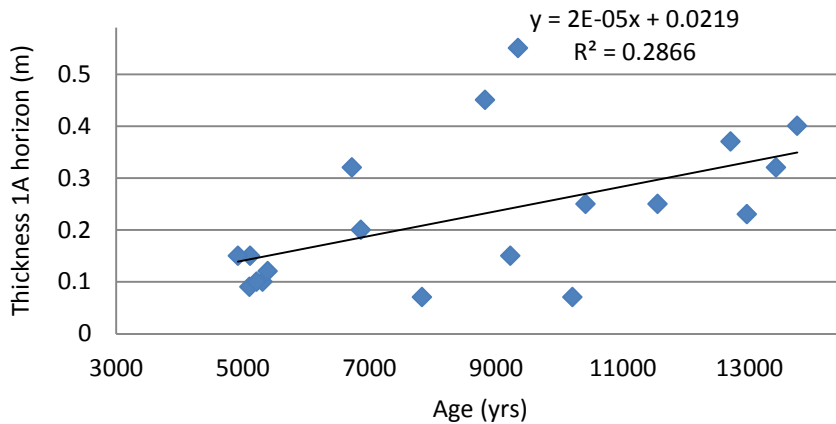


Figure 31: Scatterplot of the thickness of the 1A horizon versus age of the soils, for samples with an 1A horizon present and classified as ridge through their vegetation index.

5.3.1.2 *Physical weathering*

Weathering rates in the 2B/ and 2BC horizon are respectively $1.6 \cdot 10^{-5}$ and $8.6 \cdot 10^{-6}$ y⁻¹, calculated using equations described in Section 4.6.1.4. Average depth calculated by taking the mean of the calculated depths is 0.42 m for the 2B/ horizons and 0.7 m for the 2BC horizons. Combining these parameters results in a k of -2.22 m⁻¹ and an initial weathering rate of $4.06 \cdot 10^{-5}$ y⁻¹.

5.3.1.3 *Silt translocation*

$silt_{max}$ is calibrated to the value which results in the lowest RMSE compared to 5 reference pits on ridge positions. This results in a $silt_{max}$ of 0.172 kg/y⁻¹. There is still a lot of variation between modelled and observed silt content in the reference pits.

5.3.2 Prediction

5.3.2.1 *Landscape*

LORICA did not simulate any sedimentation in the study area. Change in altitude thus shows cumulative erosion in the area (Figure 32). A large difference is visible between ridges and valleys, with largest changes in the latter. Gravel in the ridges acts as shield for erosion processes. The amount of erosion ranges from 0.5 cm to a maximum of 8.5 cm.

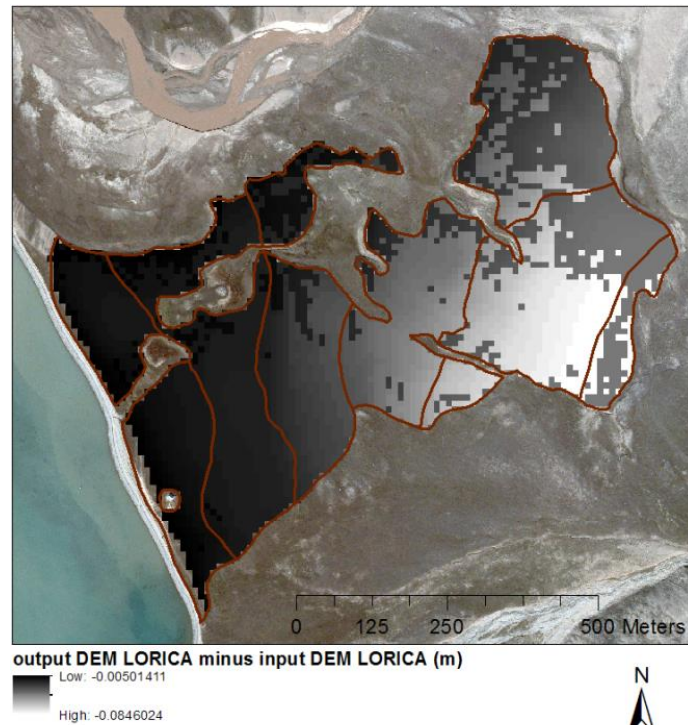


Figure 32: Map resulting from the subtraction of the output DEM resulting from LORICA from the DEM served as input, showing the change in altitude due to erosion. The input DEM is corrected for the aeolian sand cover (Section 4.6.2.1).

5.3.2.2 Soils

The layers in LORICA were translated into a 1A, 2A, 2B/ or 2BC horizon. The upper 9 layers in the output of LORICA were always classified as a 1A, 2A or 2B/ horizon. The lowest layer in LORICA was always classified as 2BC layer. There is illuviation of silt, but the amounts are too small compared to the gravel and sand content, that the silt fraction does not reach above the threshold of 2.5 %.

Only results for 1A, 2A and 2B/ horizons are discussed here. Properties of simulated 2BC horizons are not representative for the field situation, because of the large quantity of gravel and sand.

The simulated 1A horizons have an average thickness of 9.1 cm (Table 12). The large variation in this thickness is caused by the gradient from the lower to higher terraces and absence of aeolian sand on ridge positions (Table 11). The trend in thickness is constant, except for zero thicknesses (Figure 33a). There is no gravel present in this horizon. Silt had formed in situ by weathering of aeolian sand. Silt and sand fraction contain the same standard deviation, indicating that the change in sand fraction is the same change in silt fraction (Figure 33b and c).

The average thickness of the 2A horizons is 6.8 cm, with a standard deviation of 7.7 cm. This large range of thicknesses can be addressed to weathering speed of gravel to sand. The thickest 2A horizons are located on the oldest terraces. No 2A horizons were modelled in soils on the lowest terrace. Also terrace level 3 lacks 2A horizons (Table 11). Thickness is negatively influenced by the presence of a 1A horizon (Figure 33a).

Standard deviation of thickness of 2B/ horizons is smallest both in absolute sense as in relative sense, compared to the other two horizons. The thickest horizons are located on the lowest terraces. Depth of the 1A, 2A and 2B/ horizons stop at the point to where the top 9 layers reach, which is on average 0.56 meters. More gravel was weathered into sand in older soils, creating thicker 2A horizons. Due to the rather constant soil depth, 2B/ horizons decrease in thickness in these older soils (Figure 33a). Gravel fraction of the 2B/ horizons also decreases in these older soils (Figure 33d).

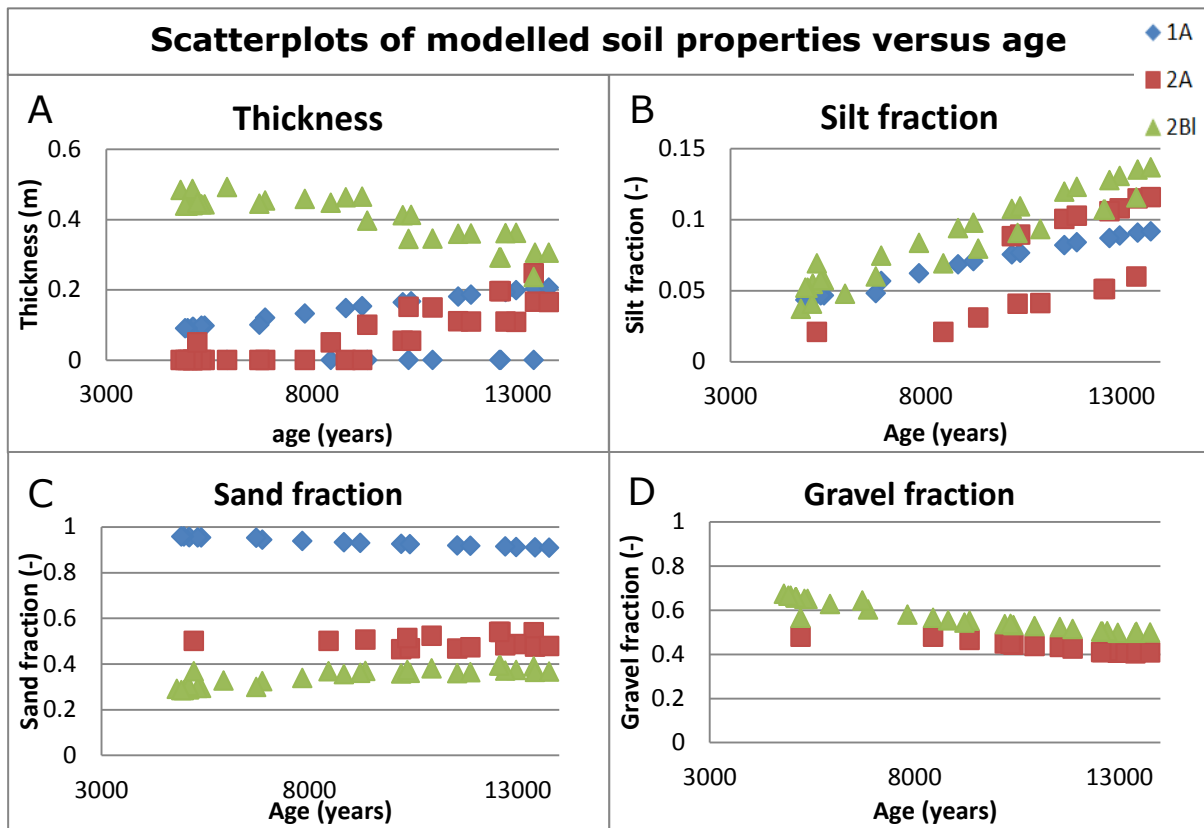


Figure 33: Scatterplots of soil properties modelled by LORICA versus the age of the soil. The blue diamonds are horizon 1A, the red squares are horizon 2A and the green triangles are horizon 2B/.

Table 11: Overview of averaged simulated soil properties, sorted per terrace levels. Zero thicknesses are left out. The horizons modelled indicate how much of the respective horizons are modelled on each terrace level. Between brackets is indicated how many of that horizon are observed in the field.

Horizon	Averaged variable	Terrace level 1	Terrace level 2	Terrace level 3	Terrace level 4	Terrace level 5
1A	Horizons modelled (observed)	2 (2)	4 (4)	2 (2)	5 (9)	6 (6)
	Thickness	0.09	0.10	0.11	0.15	0.19
	Sand fraction (-)	0.96	0.95	0.95	0.94	0.92
	Silt fraction (-)	0.04	0.05	0.05	0.06	0.08
2A	Horizons modelled (observed)	0 (2)	1 (3)	0 (4)	7 (5)	8 (4)
	Thickness		0.05		0.11	0.15
	Gravel fraction (-)		0.48		0.45	0.41
	Sand fraction (-)		0.50		0.50	0.49
	Silt fraction (-)		0.02		0.05	0.10
2B/	Horizons modelled (observed)	2 (1)	7 (6)	4 (3)	10 (8)	8 (7)
	Thickness	0.44	0.46	0.47	0.40	0.32
	Gravel fraction (-)	0.66	0.64	0.62	0.54	0.50
	Sand fraction (-)	0.29	0.30	0.32	0.37	0.37
	Silt fraction (-)	0.05	0.06	0.06	0.09	0.13

Table 12: Summary of the properties of the horizons simulated by LORICA. Included are the validation statistics.

Horizon	Summary statistic	Thickness (m)	Gravel fraction (-)	Sand fraction (-)	Silt fraction (-)	Gravel content (kg)	Sand content (kg)	Silt content (kg)
1A	Average	9.1E-02	-	9.3E-01	6.7E-02	-	2.2E+02	1.7E+01
	Standard deviation	7.8E-02	-	1.9E-02	1.9E-02	-	6.4E+01	9.3E+00
	Max	2.1E-01	-	9.6E-01	9.2E-02	-	3.0E+02	3.1E+01
	Min	0.0E+00	-	9.1E-01	4.4E-02	-	1.4E+02	6.3E+00
	RMSE	2.0E-01	-	6.0E-02	5.5E-02	-	1.8E+02	2.6E+01
	RMSE/average (-)	2.2E+00	-	6.4E-02	8.1E-01	-	8.1E-01	1.5E+00
	MPE	-9.3E-02	-	4.1E-02	-3.1E-02	-	-8.8E+01	-1.6E+01
2A	Average	6.8E-02	4.3E-01	5.0E-01	7.4E-02	1.1E+02	1.3E+02	1.8E+01
	Standard deviation	7.7E-02	2.6E-02	2.7E-02	3.5E-02	4.4E+01	6.0E+01	1.2E+01
	Max	2.5E-01	4.8E-01	5.4E-01	1.2E-01	1.9E+02	2.5E+02	3.7E+01
	Min	0.0E+00	4.0E-01	4.6E-01	2.1E-02	4.8E+01	5.0E+01	2.1E+00
	RMSE	1.0E-01	3.5E-01	2.9E-01	9.5E-02	9.2E+01	2.0E+02	3.1E+01
	RMSE/average (-)	1.6E+00	8.2E-01	5.6E-01	1.6E+00	7.4E-01	1.3E+00	1.9E+00
	MPE	-1.5E-02	1.3E-01	-6.3E-02	-6.3E-02	7.5E+01	-2.2E+01	-1.5E+01
2B/	Average	4.0E-01	5.7E-01	3.4E-01	8.8E-02	5.0E+02	2.9E+02	6.9E+01
	Standard deviation	7.0E-03	6.5E-02	3.6E-02	3.2E-02	1.5E+02	4.2E+01	1.7E+01
	Max	4.9E-01	6.7E-01	3.9E-01	1.4E-02	7.2E+02	3.5E+02	9.6E+01
	Min	2.4E-01	5.0E-01	2.8E-01	3.7E-02	2.4E+02	1.9E+02	4.0E+01
	RMSE	2.9E-01	1.5E-01	1.2E-01	3.5E-02	3.2E+02	1.9E+02	4.8E+01
	RMSE/average (-)	7.2E-01	2.7E-01	3.6E-01	3.9E-01	6.5E-01	6.5E-01	6.7E-01
	MPE	1.3E-01	-9.4E-02	7.5E-02	1.0E-02	1.5E+02	1.5E+02	3.0E+01
Overall	RMSE	2.1E-01	2.2E-01	1.6E-01	5.6E-02	2.8E+02	1.9E+02	3.9E+01
	RMSE/average (-)	2.6E+00	4.1E-01	2.4E-01	7.3E-01	7.0E-01	7.7E-01	8.9E-01
	MPE	6.5E-03	-3.9E-02	4.0E-02	-1.5E-02	1.3E+02	4.1E+01	7.0E+00

5.3.3 Validation

5.3.3.1 Thickness

Figure 34 shows modelled horizon thicknesses plotted against observed thicknesses. All horizons have a relatively high RMSE (Table 12). Ratio between RMSE and average thickness is lowest for 2B/ horizons. Thickness of horizon 1A is underestimated and thickness of horizon 2B/ is overestimated, judging from the MPE and location of scatter-points relative to the identity line (Figure 34). Simulated thicknesses of the 2A horizon has a relatively low MPE.

Combining all horizon thicknesses results in a very low MPE. The RMSE is in the same order of magnitude as the RMSEs of the individual horizons, but is higher relative to the simulated mean.

5.3.3.2 Gravel

Figure 35a shows a large spread in observed gravel fraction in 2A horizons. LORICA does not predict this spread and simulates a quite constant gravel fraction. This inaccuracy also appears in the relatively high RMSE of the 2A horizon. MPE of the gravel fraction in the 2A horizon is positive, where MPE of the 2B/ fractions is negative. RMSE of the 2B/ horizon is relatively small (27% of the average).

Relative RMSEs are high for the modelled gravel content in horizons 2A and 2B/. Gravel content of 2A horizons is overestimated for almost all locations. Overestimation of gravel in the 2B/ horizon is lower, but still for more than half the locations (Figure 35b).

RMSE of combining all gravel fractions combined results in an RMSE in between individual RMSEs. The MPE is lower than both individual MPEs. For gravel content, overall RMSE and MPE are in between individual values.

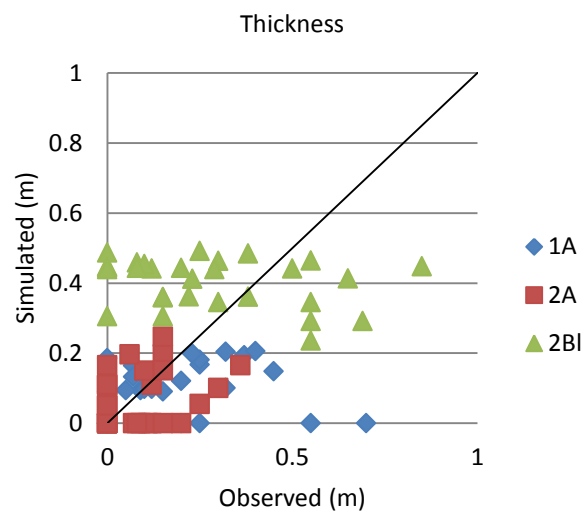


Figure 34: Scatterplot of modelled horizon thickness versus the observed modelled thicknesses, for the 1A (blue), 2A (red) and 2B/ (green) horizons. The black line indicates the identity line.

5.3.3.3 Sand

Sand fraction in 1A and 2B/ horizons is mostly overestimated (Figure 35c). Validation of 1A horizon results in the lowest RMSE (Table 12). The lowest MPE results from validation of sand fraction in 2B/ horizons. Scatter-points of 2B/ horizons are closest to the identity line. There is an overestimation of the amount of sand in the 2B/ horizon. For 1A and 2A horizons, the model underestimates sand content (Table 12).

The overall prediction of sand fraction has a lower MPE than the individual horizons. RMSE is 24% of the estimated mean.

5.3.3.4 Silt

Simulation of silt fractions gives high relative RMSEs. MPE is highest for 2A horizons, which is also evident in the underestimation visible in Figure 35e.

Absolute amount of silt present in the horizons is underestimated for 1A and 2A horizons. Silt content in the 2B/ horizons is overestimated.

Overall prediction of silt fraction and silt content has an MPE closer to zero than the MPEs of the individual horizons. Relative RMSE of the silt content is lower than RMSEs of the 1A and 2A horizons. For the silt fraction, relative RMSE is lower than those of the 2A and 2B/ horizon.

5.3.3.5 Overall prediction

Lowest relative RMSEs result from predictions of thickness and properties of the 2B/ horizon (Table 12). Except for the sand fraction, relative RMSEs are all the lowest for this horizon. Soil properties with lowest relative RMSEs are gravel and sand fraction. Largest relative RMSEs are in the thickness and silt content of the 1A horizon.

Taking all predictions of a certain variable together results in general in a smaller MPE. Relative RMSEs are in between those of the individual horizons.

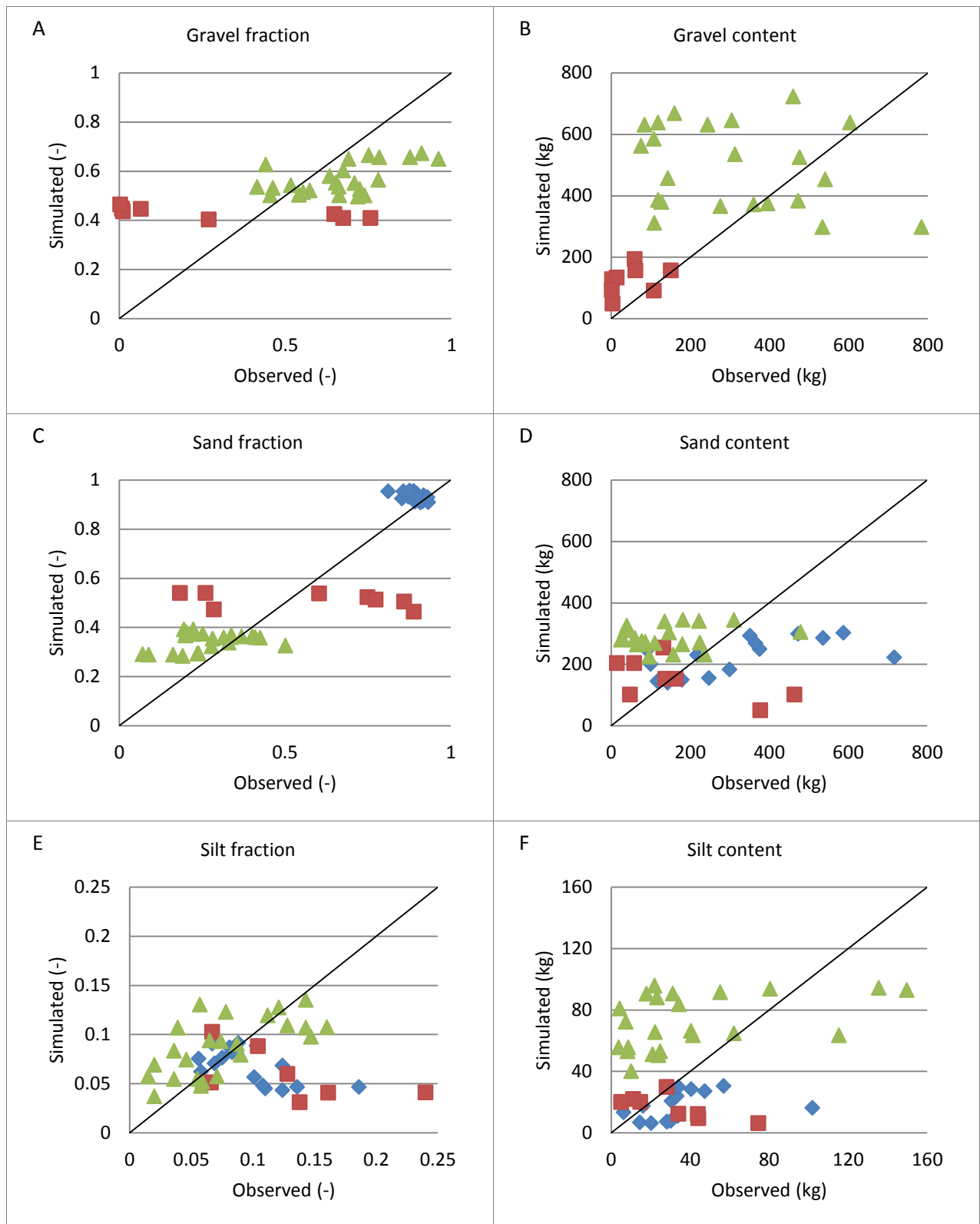


Figure 35: Scatterplots of soil properties simulated by LORICA versus field observations. The black lines indicate identity lines.

◆ : 1A horizons ■ : 2A horizons ▲ : 2BI horizons

5.3.3.6 Comparison with external data

Input parameters of LORICA are calculated using (a part of) the 30 random selected soil pits. This section compares model results for two soil pits which are not used to calibrate the model. The first soil pit, J10, is located on a ridge in the middle of the study area. The other one, J11, is located just outside the study area, above the ridge of terrace level 6 (Figure 13). Observed and predicted horizon properties of both locations are summarized in Table 13.

J10

LORICA did not simulate a 2A horizon for location J10, due to relatively low elevation. Not enough gravel was weathered into sand. However, this horizon was observed in the field and meets the criterion that the sand fraction should be higher than the gravel fraction, in order to be named a 2A horizon (Figure 36). Total soil depth observed in the field is almost 50% higher than soil depth resulting from LORICA.

Properties of 2B/ horizons are predicted quite accurate. Predicted particle size distribution differs a few percent from observed particle size distribution. Also predicted absolute contents of the three fractions do resemble field observations. The total amount of soil material is higher in the predicted 2B/ horizon, while the observed horizon is thicker. This is due to a difference in bulk density measured in the field and bulk density used in LORICA.

Table 13: Overview of observed and predicted soil properties of locations J10 and J11.

Horizon	Variable	J10		J11	
		Observed	Predicted	Observed	Predicted
	Total soil depth (m)	0.73	0.49	1.30	0.68
1A	Thickness (m)	0	0	0.95	0.21
	Sand fraction (-)	-	-	0.886	0.908
	Silt fraction (-)	-	-	0.09	0.092
	Sand content (kg)	-	-	1324.0	302.56
	Silt content (kg)	-	-	134.5	30.53
2A	Thickness (m)	0.09	0	-	0.16
	Gravel fraction (-)	0.429	-	-	0.407
	Sand fraction (-)	0.448	-	-	0.478
	Silt fraction (-)	0.123	-	-	0.116
	Gravel content (kg)	64.5	-	-	130.40
	Sand content (kg)	67.3	-	-	152.45
	Silt content (kg)	18.5	-	-	37.18
2B/	Thickness (m)	0.64	0.49	0.35	0.31
	Gravel fraction (-)	0.661	0.633	0.739	0.497
	Sand fraction (-)	0.303	0.321	0.186	0.366
	Silt fraction (-)	0.036	0.046	0.075	0.137
	Gravel content (kg)	693.8	677.0	400.9	308.7
	Sand content (kg)	318.0	339.6	100.9	225.8
	Silt content (kg)	37.8	49.4	40.7	84.7
	Total mass horizon (kg)	1049.6	1066.0	542.5	619.2

J11

Both modelled profile and observed profile of J11 contain a cover of fine material. LORICA modelled it as a cover of only aeolian sand, due its morphological setting. Observations in the field show that the material from the horizon reacts weak to moderate on HCl, while aeolian deposits in the study area react strong to extreme on HCl. Also the texture class of silty loam is finer than the usual sandy loam of most

1A horizons. This indicates a difference in parent material, where the material in the 1A horizon of J11 is probably alluvial material coming from the Wordiekammen.



Figure 36: Picture of soil pit J10, with a small, sandy 2A horizon on top of the more gravelly 2B/ horizon. Also the layering of coarse and less coarse gravel in the marine sediments is nicely visible.



Figure 37: Picture of soil pit J11, located in the colluvium captured by the highest terrace ridge. The thick cover of fine material is located on top of the beach deposits. Some gravel is captured in the 1A horizon.

Properties of predicted 2B/ horizons are different from the observed values. Taking into account the depth of the horizon, which influences the amount of gravel weathering to sand, modelled values could be expected for a 2B/ horizon located on the modelled depth. Modelled gravel fraction is lower and sand fraction is higher than the observed fractions. Also the silt fraction is higher in the model outcomes. A deeper 2B/ horizon would have a lower silt content, or could even be classified as a 2BC horizon.

6 Discussion

6.1 Processes and observed properties on the marine terraces

Age, topography and organisms are the main soil-forming factors (Jenny, 1946) influencing variability in soil properties on the marine terraces in the Ebba valley. Age of soils, controlled by isostatic uplift (Zwolinski et al., 2013), determines the period that soils are exposed to soil forming processes. Sorting and mixing of soil material by cryogenic processes is driven by water availability and topographic setting. Other processes influenced by topography are fluvial and aeolian erosion and deposition. The flat terrace levels are only to a small extent subject to fluvial erosion and sedimentation. Some beach ridges contain dissecting gullies, fluvial erosion (Mazurek et al., 2012). Lower lying beach valleys are more moist, influencing plant growth, physical weathering and dissolution of the parent material (Forman and Miller, 1984; Zwolinski et al., 2013). Vegetation in these sheltered positions captures aeolian sand, while protruding ridges are prone to wind erosion. This vegetation gets buried by aeolian deposits and, together with the decay of dead plant material, increases the amount of organic matter in the area (Zwolinski et al., 2013). Humic acids produced by vegetation growth and dissolution of carbonate-rich parent material influence pH of the soil (Kabala and Zapart, 2009; Szymański et al., 2013). A downward flux of water through the permeable soil transports silt and dissolved carbonates, forming silt caps and calcitic pendants around gravels in the subsoil.

Most dominant soil properties observed in the field were subsurface horizons enriched in silt, calcitic pendants attached to clasts, aeolian deposits in sheltered and vegetated positions and darker A horizons due to enrichment of organic matter (Figure 11). These properties were also observed in other arctic soil studies (e.g. (Forman and Miller, 1984; Courty et al., 1994; Pereverzev, 2012)).

Decrease of weathering speed of gravel in the 2B/ and 2BC horizon (Figure 22) agrees with studies showing that weathering is not a linear process (Colman, 1981; West et al., 2005). There is no supply of gravelly material in the subsurface horizons, resulting in supply limited weathering. Physical weathering is mainly driven by fluctuations in temperature. Soil depth is used as proxy for temperature fluctuations, which decrease exponentially with depth (Vanwalleghem et al., 2013). This agrees with the faster decay of gravel fraction in 2B/ horizons, compared to decay in 2BC horizons.

Particle size distribution in fresh aeolian sediments can be assumed homogenous, due to mixing in the air (Rachlewicz, 2010). However, silt fractions in both A horizons decrease with age, while the silt fractions in the 2B/ and 2BC horizon increase (Figure 23b). The amount of silt in 2B/ horizons increases faster than the total amount of silt in both 2A horizons combined, while weathering processes in the top horizons happen at a faster rate (Figure 24). These observations indicate eluviation of silt. Older soils were exposed to silt eluviation for a longer period of time. If production of new silt due to physical weathering in the top soil is lower than eluviation of silt, silt fraction decreases as the soils get older. Increase of silt in 2B/ horizons result in higher silt fractions. Moreover, the thickness and depth of the lower limit of 2B/ horizons also increase (Figure 21), agreeing with observations of Forman and Miller (1984).

Organic matter fraction in 1A horizons decreases with age (Figure 25). The total amount however increases (Figure 26). This is because the amount of aeolian sediments burying vegetation that captured them was higher than the added amount of organic material. Horizontal layers of organic matter in the soil indicate this burial process. Some initial organic matter can be expected in sediments (Kabala and Zapart, 2012). However, organic matter fractions of 2B/ and 2BC horizons increase as soils get older (Figure 25), which indicates eluviation of organic matter. This agrees with the findings of Ugolini et al. (1990), who observe brunification in arctic desert soils by high mobility of dissolved organic material in the soil solution.

Data analysis only shows correlations with age, while other soil forming factors, like topography and organism presence, also have a significant effect on soil forming processes and might explain part of the residual variation in the observed trends. These factors are indirectly taken into account by separating the vegetated 1A horizons located in valley positions from other horizons. Judging by eye, fluctuations in most trends in 1A horizons are smaller than fluctuations in trends in other horizons, showing the importance of considering the effect of other soil forming factors on soil properties.

6.2 Predicting soil properties with SEM

Thickness of the 1A horizons correlates positively with age, as is also visible in field observations (Figure 21). Thickness is negatively correlated with vegetation presence, meaning that there is a thinner aeolian cover on places with more vegetation abundance. Fearnough et al. (1998) show with their study on short term aeolian deposition that a thicker cover of aeolian deposits decreases permeability of the soil. As a consequence, deep-rooted shrubs were replaced by microbial crusts and shallow-rooted annual species. This result is supported by Ravi et al. (2007). Although texture of aeolian deposits in the study area was estimated to be coarser than texture of underlying 2A horizons, the absence of gravel in the 1A horizons still makes the top layer less permeable than horizons formed in the marine deposits. A thicker aeolian cover reduces abundance of larger plants and increases presence of lighter coloured microbial crusts. This is also visible on the aerial photograph (Figure 13), where higher terrace valleys are lighter coloured than lower lying terrace valleys.

Silt fraction correlates negatively with age, as is also visible in Figure 23. Horizon thickness correlates positively with the silt fraction. A thicker aeolian layer means that also more silt was deposited. However, this does not compensate for the negative correlation with age as the decrease in silt fraction towards the higher terraces (Figure 29b). Absence of a significant correlation with vegetation agrees with the findings presented in the conceptual model (Figure 11).

Organic matter fraction shows a negative correlation with age and thickness of the 1A horizon. This agrees with the concept of burying vegetation by aeolian material. The fraction decreases, but total amount of organic matter increases (Figure 29c and d). Negative correlation with age indicates eluviation of organic material. A positive correlation with the vegetation index shows that a higher vegetation abundance results in more organic matter in the soil, as can be expected.

The simulations of organic matter and silt fractions of the 1A horizon are biased, as the MPEs (Table 10) and scatterplots (Figure 30) indicate. Cause of this bias is an error made in converting the path model to the prediction equation (Section 4.5.1.4). Intercept j was added after the rest of the equation was converted, instead of begin cooperated in the conversion. Instead of $n = (I - B)^{-1} * (A * p) + j$, the equation should be $n = (I - B)^{-1} * (A * p + j)$. The improved equation results in an MPE of $-9.9 * 10^{-4}$ for the silt fraction, indicating an almost unbiased prediction.

6.3 Simulating soil forming processes and predicting soil properties with LORICA

Simulations of LORICA show interactions between different horizons. Especially the presence of a 1A horizon affects properties of underlying horizons (Figure 33). Weathering processes happen at a slower rate, as can be seen by lower sand fractions in 2A and 2B/ horizons when a 1A horizon is present. Silt fractions in the 2A and 2B/ horizons are higher when an aeolian cover is present. This surplus of silt originates from eluviation of silt produced by physical weathering in the top layer.

The found weathering rate of coarse material in the study area is $4.06 * 10^{-5}$ kg/kg/y. Due to absence of literature on arctic physical weathering rates, this rate could not be compared with similar studies. Most articles aim at chemical weathering rates (e.g. (Taylor and Blum, 1995; Egli et al., 2001; Egli et al., 2003)). Papers on general physical weathering rates are also scarce. Salvador-Blanes et al. (2007) estimated physical weathering rates in an area in the Southern Piedmont region of Georgia, USA, to be in the range of $8 * 10^{-4} \text{ y}^{-1}$ to $6 * 10^{-5} \text{ y}^{-1}$. However, other physical weathering processes occur in the Piedmont region. Where physical weathering in the Ebba valley is mainly frost shattering (Forman and Miller, 1984), processes in the Piedmont region are probably more influenced by thermal stress and water ablation, considering the long and warm summers and rainfall 5 times as high as in the Ebba valley (Salvador-Blanes et al., 2007; NOAA, 2014). Although the found weathering rate and the minimum weathering rate applied by Salvador-Blanes et al. (2007) are in the same order of magnitude, comparison between the two rates is difficult, due to the different underlying processes.

Initial gravel content also resulted from calculations of physical weathering rate. Initial contents of the 2B/ (90%) and 2BC horizon (89%) are similar to each other and correspond to observations of Forman and Miller (1984) (85-90%). Judging on these results, calculations of physical weathering rates in both horizons are accurate and thus the resulting physical weathering can also be assumed to be an accurate estimate.

Because no literature is available on silt translocation, I assumed it to follow the same mechanism as clay translocation. Base rate of clay translocation assumed by Vanwalleghem et al. (2013) is 0.007 kg. The found base rate for silt is 0.172 kg, which is almost 25 times as high. Silt translocation is driven by snowmelt and permeability of the soil (Forman and Miller, 1984; Frenot et al., 1995). Although soils in the study area are highly permeable, silt particles are larger than clay particles and the study area is much drier than the humid area where the base rate for clay is based upon (Alexandrovskiy, 2007). Based on these factors, it is unlikely that the base rate for silt eluviation in the study area is 25 times as high as the mentioned base rate of clay.

A general assumption is that weathering processes in the Arctic are physical in nature. However, chemical weathering processes do occur and are limited by moisture availability, and not temperature-limited (Hall et al., 2002). Especially dissolution is a common process on marine terraces, as calcitic pendants observed in the field indicate (Forman and Miller, 1984; Courty et al., 1994). Modelling only physical weathering processes leads to a bias in simulation of other soil properties. Sand content in the 2A and 2B/ horizons is overestimated for almost all locations (Figure 35d), because all weathered gravel breaks down to sand, instead of disappearing by dissolution. The amount of silt in 2B/ horizons simulated by LORICA is also overestimated. Calibration of silt eluviation has led to silt contents comparable to field observations (Figure 35f). However, the eluviation rate was heavily overestimated, to let the modelled amount of silt match the observed amount. The surplus of silt produced by LORICA is transported to the lowest layer, which is not taken into account in the analysis. Overproduction of silt in the profile also overestimated thicknesses of 2B/ horizons, which is determined by silt fraction (Figure 34, MPE=0.13). Taking into account other weathering processes like dissolution would avoid part of the simulation errors. However, there is no data available on the amount of dissolution of calcaric material in the study area.

Isostatic rebound and aeolian deposition have a significant effect on the soil properties in the area, by indicating the start of soil forming processes or by adding a 1A horizon. Erosion and sedimentation have almost no influence (Figure 32). This contradicts with the occurrence of ridges intersected by gullies in the study area. Overland erosion will not occur on these higher lying ridges, but will flow through the valley positions in search for the lowest positions. This indicates that the erosion in these ridges is not solely triggered by overland flow. Another driving mechanism could be seeping groundwater from ridge escarpments. Seepage disaggregates the coarse material. The fine material is then removed by other processes (Higgins and Osterkamp, 1990). Seepage erosion occurs in cliffs and riverbanks (Higgins and Osterkamp, 1990; Fox et al., 2007)), but its occurrence in beach ridge sequences is not described yet.

As described above, assumptions and limitations of the model have led to errors in simulating properties of the individual horizons. However, LORICA performs better on simulating properties of all horizons combined, compared to the individual horizons (Table 12 and Figure 35). This indicates that the essential soil forming processes and boundary conditions were used to simulate general patterns in the study area.

6.4 Synthesis

6.4.1 *Comparing model results*

Both models predicted thickness and silt fraction of the 1A horizon in vegetated valley positions. This analysis considers the unbiased silt fractions, calculated with the right prediction equation (Section 6.2). Analysis is performed in 16 locations, for which both LORICA and SEM simulated properties.

Validation statistics of both predictions show that the accuracy is in the same order of magnitude (Table 14). Predictions of SEM are much more precise, considering the MPE. LORICA underestimates both thickness and silt fraction (Figure 38a).

Patterns in Figure 38 indicate other model performances. There is a bias in the simulation of thickness by LORICA, but the scatter-points are more centered around the added trend-line (Figure 38a). The bias is caused by eluviation of silt and usage of different bulk densities in LORICA and in the field. Field bulk density of the 1A horizons is 1651 kg/m³ (Section 5.3.1.1). Bulk density in LORICA for pure sand is 1238 kg/m³ and decreases with added silt. Regarding these two bulk densities, LORICA should overestimate horizon thickness. However, also eluviation of silt occurs, removing a substantial part of material from the 1A horizons, leading to underestimation of horizon thickness. Thickness of 1A horizons simulated by LORICA is based on linear regression of the field observations. SEM also uses regressions with field

observations. Expected would be that SEM would give better results, because it also takes vegetation presence into account. Based on Figure 38a I would say that the prediction of LORICA is more accurate than that of SEM, when not considering the bias.

SEM predicts percentage of silt better than LORICA. A relatively low RMSE and MPE indicate a quite accurate and precise prediction. Trend in the prediction of LORICA is opposite to the observed trend, what is the main cause of the low accuracy and precision.

Table 14: Validation statistics of predictions of SEM and LORICA for 1A horizons located in valley positions (n=16)

		Average	RMSE	RMSE/ average	MPE
Thickness (m)	SEM	0.22	0.12	0.57	-0.002
	LORICA	0.15	0.13	0.87	-0.07
Silt (%)	SEM	9.8	3.1	0.31	-0.0042
	LORICA	6.7	5.5	0.81	-3.1

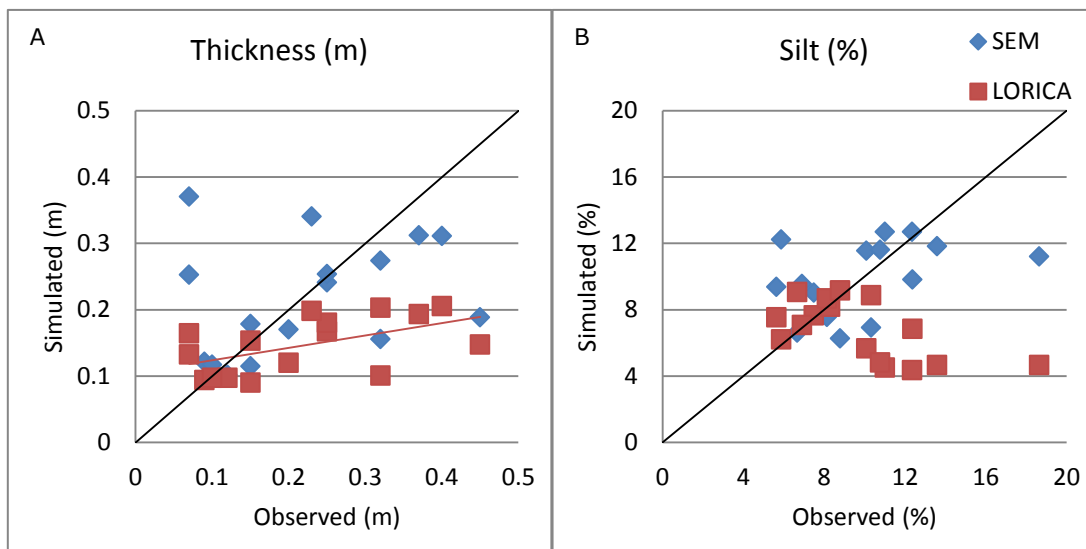


Figure 38: Scatterplots of simulated soil properties by SEM and LORICA, for 1A horizons in valley positions. The red line in window A is the trend observed in the scatter-points.

6.4.2 Performance of SEM

Parameters estimated by SEM can be explained by physical processes (Section 6.2). Next to that, predictions from SEM are quite accurate. Predictions of silt and organic matter fraction were biased, due to an error in the prediction equation. Fixing this error resulted in better predictions (Section 6.4.1).

Setting up a SEM costs a lot less time than setting up a mechanistic model. A SEM also requires less calculation time. Even if the mechanistic model already exists, SEM still has the advantages that parameters do not have to be estimated and that less process knowledge is required. Moreover, a SEM can provide this process knowledge by indicating correlations in the data. This knowledge can be used as basis for studying the mechanics behind a certain process. Separation between variances in the measurement model and path model show if the uncertainties in the model are due to errors in the data or in the prediction and indicate which part of the model can be improved.

A disadvantage of a linear and static model like SEM is that it gives a less good representation of soil forming processes compared to a mechanistic model. Next to that, this linearity also prevents a SEM of predicting the absence of a horizon. This problem is avoided in this study by using a dataset of only the valley positions to predict the properties of the 1A horizon. This would not help for e.g. the 2A horizons, where the zero thicknesses are scattered around the study area. A solution would be to expand SEM to a logistic model, which is capable of predicting the absence of a certain property.

Another disadvantage is the requirement of large datasets in order to get an accurate prediction. Where field data are used for parameterization and calibration with a mechanistic model, a SEM has to estimate correlations between different variables using the field data. An increase in target variables would mean a demand for a larger dataset. Grace et al. (2010) used 90 locations to study heterogeneity in plant recovery after a forest fire. Iacobucci (2010) state that SEMs can also perform well with 'small' sample sizes of 50 to 100. This shows the need for large sample sizes, to create a model with more relations and a better fit. The SEM used in this study was deliberately kept simple, with only three endogenous variables and two exogenous variables. Considering the small dataset of 17 samples, a more complex model could not be used. The model fit is quite good, with a P-value of 0.625. A larger dataset would probably increase the fit of the model, and give the opportunity to find more correlations in the dataset, between different exogenous and endogenous variables. This would be advised for the application of SEM on the 2A and 2B/ horizons, because they contain more target variables.

The aim of this study was to explore the use and performance of a SEM in explaining and predicting distribution of soil properties. Using structural equation models requires a steep learning curve in order to understand the terminology and get a grasp on the possibilities SEM offers. This study explored the basic functions of a SEM. Despite the error made in the prediction equation, the results are promising and show a good correlation with the field data. Comparison with LORICA shows that SEM results in predictions with more precision and accuracy (Section 6.4.1). Quantification of the variance in the predictions would give useful insights in the quality of the predictions and the strength of a SEM over other, more basic, statistical models. This study shows the potential of a SEM in helping to understand relations between different soil properties and predicting these properties based on explanatory variables.

6.4.3 Performance of LORICA

Using the mechanistic and dynamic model LORICA has given some interesting insights in the relations between processes occurring in the study area. For example, the presence of an aeolian cover not only influences the weathering rates of underlying horizons, it also has an effect on erosion processes (Figure 32) and the total amount of silt in the soil (Figure 35f).

In order to fully understand the functioning of a system, all occurring processes should be included in the mechanistic model. This was attempted in this study by modelling aeolian deposition using a linear regression with age and bulk densities observed in the field. Basing initial conditions for the model run, which still have to undergo soil forming processes, on the current situation in the field where these processes already have occurred results in prediction errors. This becomes clear from the underestimation of the thickness of the 1A horizon (Section 6.4.1). Same goes for using the present DEM as input, while this DEM also already underwent landscape and soil forming processes. This is partly compensated for, by removing the aeolian deposits from the current DEM. Using linear regressions also ignores the strength that a mechanistic model is applicable in multiple settings. This is shown by the validation using soil pit J11 (Figure 37). Other processes, like erosion by seeping groundwater, cannot be modelled by LORICA, because it does not contain a groundwater model. However, these processes do have a significant effect on the landscape and soils.

Assumed is that climatic conditions were constant. This is not the case, as analysis of calcitic pendants show (Courty et al., 1994). Traces of several episodes with differences in temperature, precipitation and vegetation were found. Knowledge on previous climatic conditions was not available and was beyond the scope of this explorative study.

Adjusting the model to enable it to model isostatic rebound and aeolian deposition cost a lot of time. Not only the processes had to be written in the right code, also the effect of the processes on other processes had to be included. There are still some errors in the model that need to be addressed in LORICA. These are the feedback between soil forming processes and changes in altitude. The error made when removing the aeolian cover from the DEM (Section 4.6.2.1) has resulted in removing 0.25 m too much from the oldest valleys. Considering the isostatic rebound, this corresponds to 54.5 years of missed soil development. This time is very small compared to the model run of 13755 years and its effect on soil properties is probably negligible. The limited amount of soil layers resulted in a constant soil depth, because the maximum thickness of a layer is fixed. This resulted in decreasing thicknesses of 2B/ horizons, while thickness should increase with age (Figure 34).

Aggregation of VI removed some important details, like smaller ridge-valley systems and local depressions on ridges, which accumulated a bit of aeolian sand. This has resulted in mispredictions of presence of a 1A horizon. Also generalization of field observations in 4 soils have led to errors in validation. Properties in the field did not always meet the decision rules imposed in LORICA (Section 4.6.3). This is visible in prediction of gravel fraction. These 2A horizons in the field had a much lower gravel fraction than could be expected from 2A horizons (Figure 35e).

As an explorative study, the results of LORICA are promising. Most simulated properties of the individual horizons are biased and not very accurate. However, considering the overall simulations, LORICA captured general trends in the field observations. Simulation of the 1A thickness also shows this. Although biased, the simulations of LORICA are more accurate than those of SEM. In general, LORICA especially contributed to the understanding of processes and interactions occurring on the marine terraces and to a lesser extent to the prediction of soil properties.

7 Conclusions

Most dominant soil forming processes occurring on marine terraces in the Ebba valley are aeolian deposition, physical weathering, dissolution and precipitation of carbonates, eluviation of silt and organic matter uptake and eluviation. This results in an aeolian 1A horizon in sheltered valley positions with decreasing silt fraction, due to eluviation. Eluviated silt forms a 2B/ horizon. Weathering decreases gravel fraction in the soil. Dissolved carbonates precipitate as calcitic pendants on subsurface rocks. The amount of organic matter increases in both top as subsurface horizons.

Parameters estimated by SEM can be explained by physical processes. Increase of aeolian material results in lower permeability, which decreases occurrence of larger plants. This explains negative correlation between vegetation index and horizon thickness. Predictions of SEM show the same patterns as field observations.

Results from LORICA show that horizons have an effect on properties of other horizons. The assumption that only physical weathering occurs led to overestimation of sand and silt content and eluviation rate of silt. This showed the importance of considering dissolution. Most important geomorphic processes affecting soil properties are isostatic rebound and aeolian deposition. In general, simulations of LORICA follow observed trends. Individual simulated properties do not correlate with observed trends.

In this study, SEM predicted the current situation in 1A horizons best. Bias in results of SEM was caused by an error in the prediction equation. LORICA predicted horizon thickness more accurate. Basing model input of a mechanistic model on the current situation leads to bias in the prediction.

SEM is more time-efficient than LORICA, both in preparation time and calculation time. Disadvantage is that it is limited by linear processes, disabling the possibility to predict absence of a certain property and leading to a less good representation of real world processes. Another disadvantage is the requirement of a large dataset needed to estimate significant correlations between the different latent variables.

Simulating interacting processes in LORICA has led to new insights in distribution of properties in the area. Predictions were not very accurate, because not all occurring processes were considered and the data were not always of sufficient quality. LORICA captures general patterns observed in soil properties.

Both models have contributed to understanding spatial and temporal distribution of soil properties in the marine terraces of the Ebba valley in their own way. The predictive power of a static and statistic model as SEM gave insight in the distribution of properties in the study area. The mechanistic and dynamic approach of LORICA contributed in the understanding of underlying processes. The gained knowledge contributes to our general understanding of arctic soil formation and forms a basis for further research on variation in soil properties in the arctic.

8 References

- Alexandrovskiy, Alexander L. 2007. Rates of soil-forming processes in three main models of pedogenesis. *Revista Mexicana de Ciencias Geológicas* 24 (2): 283-292.
- Arctic Climate Impact Assessment. 2004. *Impacts of a Warming Arctic - Arctic Climate Impact Assessment*. Cambridge University Press, Cambridge, UK.
- Arhonditsis, G. B.; Stow, C. A.; Steinberg, L. J.; Kenney, M. A.; Lathrop, R. C.; McBride, S. J.; Reckhow, K. H. 2006. Exploring ecological patterns with structural equation modeling and Bayesian analysis. *Ecological Modelling* 192 (3-4): 385-409.
- Bárcena, T. G.; Finster, K. W.; Yde, J. C. 2011. Spatial patterns of soil development, methane oxidation, and methanotrophic diversity along a receding Glacier forefield, Southeast Greenland. *Arctic, Antarctic, and Alpine Research* 43 (2): 178-188.
- Barros, V. R.; Field, C. B.; Dokken, D. J.; Mastrandrea, M. D.; Mach, K. J.; Bilir, T. E.; Chatterjee, M.; Ebi, K. L.; Estrada, Y. O.; Genova, R. C.; Girma, B.; Kissel, E. S.; Levy, A. N.; MacCracken, S.; Mastrandrea, P. R.; White, L. L.; Larsen, J. N.; Anisimov, O. A.; Constable, A.; Hollowed, A. B.; Maynard, N.; Prestrud, P.; Prowse, T. D.; Stone, J. M. R. 2014. Polar regions. *Climate Change 2014: Impacts, Adaptation, and Vulnerability. Part B: Regional Aspects. Contribution of Working Group II to the Fifth Assessment Report of the Intergovernmental Panel of Climate Change*, pp 1567-1612. Cambridge University Press, Cambridge, United Kingdom and New York, NY, USA.
- Brückner, H.; Schellmann, G. 2003. Late Pleistocene and Holocene Shorelines of Andréeland, Spitsbergen (Svalbard) - Geomorphological Evidence and Palaeo-Oceanographic Significance. *Journal of Coastal Research* 19 (4): 971-982.
- Burga, C. A.; Krüsi, B.; Egli, M.; Wernli, M.; Elsener, S.; Ziefle, M.; Fischer, T.; Mavris, C. 2010. Plant succession and soil development on the foreland of the Morteratsch glacier (Pontresina, Switzerland): Straight forward or chaotic? *Flora: Morphology, Distribution, Functional Ecology of Plants* 205 (9): 561-576.
- C'iric', M.; Senic', P. 1985. Intensity of dissolution of limestone and dolomite in different soil media (field experiment). *CATENA* 12 (2-3): 211-214.
- Colman, Steven M. 1981. Rock-weathering rates as functions of time. *Quaternary Research* 15 (3): 250-264.
- Courty, M. A.; Marlin, C.; Dever, L.; Tremblay, P.; Vachier, P. 1994. The properties, genesis and environmental significance of calcitic pendants from the High Arctic (Spitsbergen). *Geoderma* 61 (1-2): 71-102.
- Dallmann, W.K.; Piepjohn, K.; Blomeier, D. 2004. Geological map of Billefjorden, Central Spitsbergen, Svalbard with geological excursion guide 1:50,000. Norsk Polarinstituttematkart.
- Drew, J.V.; Tedrow, J.C.F. 1962. Arctic soil classification and patterned ground. *Arctic*: 109-116.
- Dunn, J. R.; Hudec, P. P. 1966. Water, Clay and Rock Soundness. *The Ohio Journal of Science* 66 (2): 153-168.
- Egli, M.; Dahms, D.; Norton, K. 2014. Soil formation rates on silicate parent material in alpine environments: Different approaches-different results? *Geoderma* 213: 320-333.
- Egli, M.; Fitze, P.; Mirabella, A. 2001. Weathering and evolution of soils formed on granitic, glacial deposits: results from chronosequences of Swiss alpine environments. *CATENA* 45 (1): 19-47.
- Egli, M.; Mirabella, A.; Fitze, P. 2003. Formation rates of smectites derived from two Holocene chronosequences in the Swiss Alps. *Geoderma* 117 (1-2): 81-98.
- Egli, M.; Wernli, M.; Kneisel, C.; Haeblerli, W. 2006. Melting glaciers and soil development in the proglacial area Morteratsch (Swiss Alps): I. Soil type chronosequence. *Arctic, Antarctic, and Alpine Research* 38 (4): 499-509.
- Elster, J.; Rachlewicz, G. 2012. Petuniabukta, Billefjorden in Svalbard: Czech-Polish long term ecological and geographical research. *Polish Polar Research* 33 (4): 289-295.
- Esau, I.; Repina, I. 2012. Wind climate in kongsfjorden, svalbard, and attribution of leading wind driving mechanisms through turbulence-resolving simulations. *Advances in Meteorology* 2012.
- Etzelmuller, B.; Sollid, J. L. 1991. The role of weathering and pedological processes for the development of sorted circles on Kvadehuksletta, Svalbard - a short report. *Polish Research* 9 (2): 181-191.
- FAO. 2006. *Guidelines for soil description*, Rome.
- Fearnehough, W.; Fullen, M. A.; Mitchell, D. J.; Trueman, I. C.; Zhang, J. 1998. Aeolian deposition and its effect on soil and vegetation changes on stabilised desert dunes in northern China. *Geomorphology* 23 (2-4): 171-182.
- Forland, Eirik J.; Benestad, Rasmus; Hanssen-Bauer, Inger; Haugen, Jan Erik; Skaugen, Torill Engen. 2011. Temperature and Precipitation Development at Svalbard 1900-2100. *Advances in Meteorology* 2011: 14.

- Forman, S. L.; Lubinski, D. J.; Ingólfsson, Ó; Zeeberg, J. J.; Snyder, J. A.; Siegert, M. J.; Matishov, G. G. 2004. A review of postglacial emergence on Svalbard, Franz Josef Land and Novaya Zemlya, northern Eurasia. *Quaternary Science Reviews* 23 (11-13): 1391-1434.
- Forman, S. L.; Miller, G. H. 1984. Time-dependent soil morphologies and pedogenic processes on raised beaches, Broggerhalvoya, Spitsbergen, Svalbard archipelago. *Arctic & Alpine Research* 16 (4): 381-394.
- Fox, Garey A; Wilson, Glenn V; Simon, Andrew; Langendoen, Eddy J; Akay, Onur; Fuchs, John W. 2007. Measuring streambank erosion due to ground water seepage: correlation to bank pore water pressure, precipitation and stream stage. *Earth Surface Processes and Landforms* 32 (10): 1558-1573.
- Frenot, Yves; Van Vliet-Lanoë, Brigitte; Gloaguen, Jean-Claude. 1995. Particle translocation and initial soil development on a glacier foreland, Kerguelen Islands, Subantarctic. *Arctic and Alpine Research*: 107-115.
- Gile, L. H.; Peterson, F.; Grossman, R. B. 1966. Morphological and Genetic Sequences of Carbonate Accumulation in Desert Soils. *Soil Science* 101 (5): 347-360.
- Grace, J. B.; Anderson, T. M.; Olff, H.; Scheiner, S. M. 2010. On the specification of structural equation models for ecological systems. *Ecological Monographs* 80 (1): 67-87.
- Grace, J. B.; Keeley, J. E. 2006. A Structural Equation Model Analysis Of Postfire Plant Diversity In California Shrublands. *Ecological Applications* 16 (2): 503-514.
- Gray, D. M.; Toth, Brenda; Zhao, Litong; Pomeroy, J. W.; Granger, R. J. 2001. Estimating areal snowmelt infiltration into frozen soils. *Hydrological Processes* 15 (16): 3095-3111.
- Gulinska, J.; Rachlewicz, G.; Szczuciński, W.; Baralkiewicz, D.; Kozka, M.; Bulska, E.; Burzyk, M. 2003. Soil contamination in high Arctic areas of human impact, central Spitsbergen, Svalbard. *Polish Journal of Environmental Studies* 12 (6): 701-707.
- Gulińska, J.; Rachlewicz, G.; Szczuciński, W.; Baralkiewicz, D.; Kózka, M.; Bulska, E.; Burzyk, M. 2003. Soil contamination in high arctic areas of human impact, central Spitsbergen, Svalbard. *Polish Journal of Environmental Studies* 12 (6): 701-707.
- Hall, Kevin; Thorn, Colin E.; Matsuoaka, Norikazu; Prick, Angelique. 2002. Weathering in cold regions: some thoughts and perspectives. *Progress in Physical Geography* 26 (4): 577-603.
- Harris, C.; Kern-Luetsch, M.; Murton, J.; Font, M.; Davies, M.; Smith, F. 2008. Solifluction processes on permafrost and non-permafrost slopes: Results of a large-scale laboratory simulation. *Permafrost and Periglacial Processes* 19 (4): 359-378.
- Hawes, T. C. 2008. Aeolian fallout on recently deglaciated terrain in the high Arctic. *Polar Biology* 31 (3): 295-301.
- Hengl, T.; Heuvelink, G. B. M.; Stein, A. 2004. A generic framework for spatial prediction of soil variables based on regression-kriging. *Geoderma* 120 (1-2): 75-93.
- Heuvelink, G. B. M.; Schoorl, J. M.; Veldkamp, A.; Pennock, D. J. 2006. Space-time Kalman filtering of soil redistribution. *Geoderma* 133 (1-2): 124-137.
- Higgins, Charles G; Osterkamp, WR. 1990. Seepage-induced cliff recession and regional denudation. *Groundwater Geomorphology: The Role of Subsurface Water in Earth-Surface Processes and Landforms, edited by CG Higgins and DR Coates, Geol. Soc. Am. Spec. Pap* 252: 291-318.
- Hijmans, R.J. 2014. raster: Geographic data analysis and modelling. Retrieved: 17-12-2014. from <http://cran.r-project.org/web/packages/raster/>
- Hobbie, S. E.; Schimel, J. P.; Trumbore, S. E.; Randerson, J. R. 2000. Controls over carbon storage and turnover in high-latitude soils. *Global Change Biology* 6 (SUPPLEMENT 1): 196-210.
- Hoffmann, U.; Hoffmann, T.; Jurasinski, G.; Glatzel, S.; Kuhn, N. J. 2014. Assessing the spatial variability of soil organic carbon stocks in an alpine setting (Grindelwald, Swiss Alps). *Geoderma* 232-234 (0): 270-283.
- Hudec, P. P. 1973. Weathering of Rocks in Arctic and Sub-Arctic Environment. *Proceedings of the Symposium on the GEology of the Canadian Arctic*: 313-335.
- Iacobucci, D. 2009. Everything you always wanted to know about SEM (structural equations modeling) but were afraid to ask. *Journal of Consumer Psychology* 19 (4): 673-680.
- Iacobucci, D. 2010. Structural equations modeling: Fit Indices, sample size, and advanced topics. *Journal of Consumer Psychology* 20 (1): 90-98.
- Ingólfsson, Ó.; Landvik, J. Y. 2013. The Svalbard–Barents Sea ice-sheet – Historical, current and future perspectives. *Quaternary Science Reviews* 64 (0): 33-60.
- Jenny, H. 1946. Arrangement of soil series and types according to functions of soil-forming factors. *Soil Science* 61 (5): 375-392.
- Jones, A.; Stolbovoy, V.; Tarnocai, C.; Broll, G.; Spaargaren, O.; Montanarella, L.; (eds). 2009. *Soil Atlas of the Northern Circumpolar Region*. European Commission, Office for Official Publications of the European Communities, Luxembourg.

- Kabala, C.; Zapart, J. 2009. Recent, relic and buried soils in the forefield of Werenskiöld Glacier, SW Spitsbergen. *Polish Polar Research* 30 (2): 161-178.
- Kabala, C.; Zapart, J. 2012. Initial soil development and carbon accumulation on moraines of the rapidly retreating Werenskiöld Glacier, SW Spitsbergen, Svalbard archipelago. *Geoderma* 175: 9-20.
- Kane, Daniel A.; Snapp, Sieglinde S.; Davis, Adam S. 2015. Ridge Tillage Concentrates Potentially Mineralizable Soil Nitrogen, Facilitating Maize Nitrogen Uptake. *Soil Sci. Soc. Am. J.* 79 (1): 81-88.
- Lambeck, K. 1995. Constraints on the Late Weichselian Ice-Sheet over the Barents Sea from Observations of Raised Shorelines. *Quaternary Science Reviews* 14 (1): 1-16.
- Lambeck, K. 1996. Limits on the areal extent of the Barents Sea ice sheet in Late Weichselian time. *Global and Planetary Change* 12 (1-4): 41-51.
- Lamigueiro, O.P.; Hijmans, R.J. 2014. rasterVis: Visualization methods for the raster package. Retrieved: 17-12-2014. from <http://cran.r-project.org/web/packages/rasterVis/index.html>
- Láska, K.; Witoszová, D.; Prošek, P. 2012. Weather patterns of the coastal zone of Petuniabukta, central Spitsbergen in the period 2008-2010. *Polish Polar Research* 33 (4): 297-318.
- Long, A. J.; Strzelecki, M. C.; Lloyd, J. M.; Bryant, C. L. 2012. Dating High Arctic Holocene relative sea level changes using juvenile articulated marine shells in raised beaches. *Quaternary Science Reviews* 48: 61-66.
- Margesin, R. 2009. *Permafrost Soils*. Springer-Verlag, Berlin.
- Matsuoka, Norikazu; Abe, Miwa; Ijiri, Manabu. 2003. Differential frost heave and sorted patterned ground: field measurements and a laboratory experiment. *Geomorphology* 52 (1-2): 73-85.
- Mavris, C.; Egli, M.; Plötze, M.; Blum, J. D.; Mirabella, A.; Giaccai, D.; Haeblerli, W. 2010. Initial stages of weathering and soil formation in the Morteratsch proglacial area (Upper Engadine, Switzerland). *Geoderma* 155 (3-4): 359-371.
- Mazurek, Małgorzata; Paluszkiwicz, Renata; Rachlewicz, Grzegorz; Zwoliński, Zbigniew. 2012. Variability of water chemistry in tundra lakes, Petuniabukta coast, Central Spitsbergen, Svalbard. *The Scientific World Journal* 2012.
- Mémin, A.; Hinderer, J.; Rogister, Y. 2012. Separation of the Geodetic Consequences of Past and Present Ice-Mass Change: Influence of Topography with Application to Svalbard (Norway). *Pure and Applied Geophysics* 169 (8): 1357-1372.
- NOAA. 2014. National Weather Service Forecast Office, Peachtree City, GA. Retrieved: 23-02-2015. from <http://www.weather.gov/climate/index.php?wfo=FFC>
- Pereverzev, V. N. 2012. Soils Developed from Marine and Moraine Deposits on the Billefjord Coast, West Spitsbergen. *Eurasian Soil Science* 45 (11): 1023-1032.
- Pereverzev, V. N.; Litvinova, T. I. 2010. Soils of sea terraces and bedrock slopes of fiords in Western Spitsbergen. *Eurasian Soil Science* 43 (3): 239-247.
- PHL, Planetary Habitability Laboratory. 2014. Visible Vegetation Index (VVI). Retrieved: 29-10-2014. from <http://phl.upr.edu/projects/visible-vegetation-index-vvi>
- Rachlewicz, G. 2010. Paraglacial modifications of glacial sediments over millennial to decadal time-scales in the high arctic (Billefjorden, central Spitsbergen, Svalbard). *Quaestiones Geographicae* 29 (3): 59-67.
- Rachlewicz, G.; Szczuciński, W. 2008. Changes in thermal structure of permafrost active layer in a dry polar climate, Petuniabukta, Svalbard. *Polish Polar Research* 29 (3): 261-278.
- Rachlewicz, G.; Szczuciński, W.; Ewertowski, W. 2007. Post-"Little Ice Age" retreat rates of glaciers around Billefjorden in central Spitsbergen, Svalbard. *Polish Polar Research* 28: 159-186.
- Ravi, Sujith; D'Odorico, Paolo; Okin, Gregory S. 2007. Hydrologic and aeolian controls on vegetation patterns in arid landscapes. *Geophysical Research Letters* 34 (24).
- Rosseel, Yves. 2012. lavaan: An R Package for Structural Equation Modelling. *Journal of Statistical Software* 48 (2): 1-36.
- Salvador-Blanes, S.; Minasny, B.; McBratney, A. B. 2007. Modelling long-term in situ soil profile evolution: application to the genesis of soil profiles containing stone layers. *European Journal of Soil Science* 58 (6): 1535-1548.
- Scheffers, A.; Engel, M.; Scheffers, S.; Squire, P.; Kelletat, D. 2012. Beach ridge systems - archives for holocene coastal events? *Progress in Physical Geography* 36 (1): 5-37.
- Schoorl, J. M.; Veldkamp, A.; Bouma, J. 2002. Modeling Water and Soil Redistribution in a Dynamic Landscape Context. *Soil Science Society of American Journal* 66 (5): 1610-1619.
- Schüllli-Maurer, I.; Sauer, D.; Stahr, K.; Sperstad, R.; Sørensen, R. 2007. Soil formation in marine sediments and beach deposits of southern Norway: Investigations of soil chronosequences in the Oslofjord region. *Revista Mexicana de Ciencias Geológicas* 24 (2): 237-246.

- Shilts, William W. 1978. Nature and Genesis of Mudboils, Central Keewatin, Canada. *Canadian Journal of Earth Sciences* 15 (7): 1053-1068.
- Sonneveld, M. P. W.; Schoorl, J. M.; Veldkamp, A. 2006. Mapping hydrological pathways of phosphorus transfer in apparently homogeneous landscapes using a high-resolution DEM. *Geoderma* 133 (1-2): 32-42.
- Strzelecki, M. C. 2012. High Arctic Paraglacial Coastal Evolution in Northern Billefjorden, Svalbard. *Department of Geography*, p 303. Durham University, Durham.
- Sturm, Matthew; Racine, Charles; Tape, Kenneth. 2001. Climate change: Increasing shrub abundance in the Arctic. *411* (6837): 546-547.
- Szpakowski, J.; Szpakowska, G.; Zwoliński, Z.; Rachlewicz, G.; Kostrzewski, A.; Marciniak, M.; Dragon, K. 2014. Character and rate of denudation in a High Arctic glacierized catchment (Ebbaelva, Central Spitsbergen). *Geomorphology* 218: 52-62.
- Szymański, Wojciech; Skiba, Stefan; Wojtuń, Bronisław. 2013. Distribution, genesis, and properties of Arctic soils: a case study from the Fuglebekken catchment, Spitsbergen.
- Taylor, Aaron; Blum, Joel D. 1995. Relation between soil age and silicate weathering rates determined from the chemical evolution of a glacial chronosequence. *Geology* 23 (11): 979-982.
- Temme, A.J.A.M.; Vanwalleghem, T. 2015. LORICA – A new model for linking landscape and soil profile evolution: development and sensitivity analysis.
- Temme, A.J.A.M.; Lange, K. 2014. Pro-glacial soil variability and geomorphic activity - the case of three Swiss valleys. *Article in press*.
- Ugolini, FC; Sletten, RS; Marrett, DJ. 1990. Contemporary pedogenic processes in the Arctic: Brunification. *Sci. du Sol* 28 (4): 333-348.
- Ugolini, Fiorenzo C. 1986. Pedogenic zonation in the well-drained soils of the arctic regions. *Quaternary Research* 26 (1): 100-120.
- Vanwalleghem, T.; Stockmann, U.; Minasny, B.; McBratney, A. B. 2013. A quantitative model for integrating landscape evolution and soil formation. *Journal of Geophysical Research-Earth Surface* 118 (2): 331-347.
- Vanwalleghem, T.; Temme, A. J. A. M. 2014. New possibilities for soil and landscape evolution modelling by coupling LAPSUS and MILESD. *Geophysical Research Abstracts* 16.
- West, A. J.; Galy, A.; Bickle, M. 2005. Tectonic and climatic controls on silicate weathering. *Earth and Planetary Science Letters* 235 (1-2): 211-228.
- White, S. L. 1976. Is frost action really only hydration shattering? A review. *Arctic and Alpine Research* 8 (1): 1-6.
- Zwoliński, Z.; Gizejewski, J.; Karczewski, A.; Kasprzak, M.; Lankauf, K.R.; Migon, P.; Pekala, K.; Repelewska-Pekalowa, J.; Rachlewicz, G.; Sobota, I.; Stankowski, W.; Zagorski, P. 2013. Geomorphological settings of Polish research stations on Spitsbergen. *Landform Analysis* 22 (1): 125-143.

Appendix A: Field form

The field form used during the fieldwork. The listed numbers refer to the page where they can be found in the soil classification booklet.

SOIL DESCRIPTION FORM - Svalbard 2014 <i>Adjusted</i>															
Site no:		GPS-reading (WGS 84 UTM 33N coordinates)													
Date:		UTM Zone 33 X		Easting [m]:			Northing [m]:			Altitude [m]:		Waypoint nr.:			
Surveyor: Marijn / Christian / Both															
Picture Nr. Before:					After:					Picture of Soil itself:					
Presumed Location: Terrace (nr.) / Moraine (nr.) / Other:															
Landscape Setting: 10-11															
Slope [%]		Inclinometer		Surface stoniness [%]				Effective depth			Depth of Siltated layers/Pebble layers				
Profile curvature		12		Gravel:	Stone:	Bould:	Rock:		Rooting Depth			Silt:			
Plan curvature		12		21-22				24-25			Pebbles:				
Aspect [°]		Compass		Geomorphological setting: 16-18				Erosion / Deposition: 22-23							
Crusts		23		Drainage class: 50-52				Vegetation type: 16			Coverage [%]				
Salts		24		Permeability: 50-52				Sample Bag nr.:							
Expected main soil forming processes:							Remarks:								
Differences in Parent Material?:															
<i>Soil Profile Description</i>															
Horizon		Colour	Mottles		Texture	Stones in prof.		Structure			HCL	Carbonate (Forman)	Soil Moist	Siltation	Bulk Density
Symb	Depth (cm)	Moist	%	Type	Class	%	Nodules	Type	Grade	Size	Class	Class	[%]	Class	g/100cm ³
67	Measurement tape	33-34	35-	37	25-29	29-	31	44-	48		38	Forman	SM-meter	Forman	Ring/Scale
FAO Classification:							Specifiers:								

Appendix B: R-scripts used for SEM

B1: Horizon 2A

```
LAVAAN_hor2A <- '  
# measurement model  
  thick_2A_r =~ 1*thick_2A  
  silt_2A_r =~ 1*silt_2A  
  OM_2A_r =~ 1*OM_2A  
  initial_2A_r =~ 1*initial_2A  
  
# residual variances observed variables  
  thick_2A =~ 1*thick_2A  
  silt_2A =~ 0.15*silt_2A  
  OM_2A =~ 1.9*OM_2A  
  initial_2A =~ 0.058*initial_2A  
  
# path analysis (regressions)  
  thick_2A_r ~ age+veg_index  
  OM_2A_r ~ veg_index+age  
  silt_2A_r ~ OM_2A_r+thick_2A_r+veg_index  
  initial_2A_r ~ age+veg_index+silt_2A_r+thick_2A_r  
  
#factor variances  
  thick_2A_r =~ thick_2A_r  
  silt_2A_r =~ silt_2A_r  
  OM_2A_r =~ OM_2A_r  
  initial_2A_r =~ initial_2A_r  
  
#intercepts  
  thick_2A_r~1  
  silt_2A_r~1  
  OM_2A_r~1  
  Initial_2A~1  
,
```

B2: Horizon 2B/

```
LAVAAN_hor2Bl <- '  
# measurement model  
  thick_2Bl_r =~ 1*thick_2Bl  
  silt_2Bl_r =~ 1*silt_2Bl  
  OM_2Bl_r =~ 1*OM_2Bl  
  initial_2Bl_r =~ 1*initial_2Bl  
  
# residual variances observed variables  
  thick_2Bl =~ 1*thick_2Bl  
  silt_2Bl =~ 0.00205*silt_2Bl  
  OM_2Bl =~ 0.035*OM_2Bl  
  initial_2Bl =~ 0.0125*initial_2Bl  
  
# path analysis (regressions)  
  thick_2Bl_r ~ age+veg_index  
  initial_2Bl_r ~ age  
  silt_2Bl_r ~ age+initial_2Bl_r  
  OM_2Bl_r ~ veg_index+thick_2Bl_r  
  
#factor variances  
  thick_2Bl_r =~ thick_2Bl_r  
  silt_2Bl_r =~ silt_2Bl_r  
  OM_2Bl_r =~ OM_2Bl_r  
  initial_2Bl_r =~ initial_2Bl_r  
#intercepts  
  thick_2Bl_r~1  
  silt_2Bl_r~1  
  OM_2Bl_r~1  
  Initial_2Bl~1  
,
```

B3: Horizon 2BC

```
LAVAAAN_hor2BC <- '  
# measurement model  
silt_2BC_r ~ 1*silt_2BC  
OM_2BC_r ~ 1*OM_2BC  
initial_2BC_r ~ 1*initial_2BC  
  
# residual variances observed variables  
silt_2BC ~ 0.094*silt_2BC  
OM_2BC ~ 2.3*OM_2BC  
initial_2BC ~ 4.4*initial_2BC  
  
# path analysis (regressions)  
OM_2BC_r ~ veg_index+age  
silt_2BC_r ~ OM_2BC_r+age  
initial_2BC_r ~ age  
  
#factor variances  
silt_2BC_r ~ silt_2BC_r  
OM_2BC_r ~ OM_2BC_r  
initial_2BC_r ~ initial_2BC_r  
  
#intercepts  
silt_2BC_r ~ 1  
OM_2BC_r ~ 1  
Initial_2BC_r ~ 1  
,
```

B4: Applying model on field data

```
##setting up matrices  
{B <- matrix(c(0,coef(fit1A1)["silt_1A_r~thick_1A_r"],coef(fit1A1)["OM_1A_r~thick_1A_r"],  
coef(fit1A1)["thick_1A_r~silt_1A_r"],0,coef(fit1A1)["OM_1A_r~silt_1A_r"],  
coef(fit1A1)["thick_1A_r~OM_1A_r"],coef(fit1A1)["silt_1A_r~OM_1A_r"],0),  
ncol=3,nrow=3)  
B[is.na(B)] <- 0} #Matrix endogenous variables B  
{I <- diag(nrow=3,  
ncol=3)} #Identity matrix  
{A <- matrix(c(coef(fit1A1)["thick_1A_r~age_hy"],coef(fit1A1)["silt_1A_r~age_hy"],  
coef(fit1A1)["OM_1A_r~age_hy"],coef(fit1A1)["thick_1A_r~VI"],  
coef(fit1A1)["silt_r~VI"],coef(fit1A1)["OM_1A_r~VI"]),  
nrow=3,ncol=2)  
A[is.na(A)] <- 0  
} #Matrix exogenous variables  
  
##Apply model  
thick_1A <- age_valley #create target rasters with the same dimensions as the input rasters  
silt_1A <- age_valley  
OM_1A <- age_valley  
  
for (i in 1:nrow(age_valley)) {  
for (j in 1:ncol(age_valley)) { #for every column j in row i  
p = matrix(c(age_valley[i,j],VI_valley[i,j]),nrow=2,ncol=1)  
n = c(0,0,0)  
n = (solve(I-B))%*%(A%*%p)  
thick_1A[i,j] <- n[1]  
silt_1A[i,j] <- n[2]  
OM_1A[i,j] <- n[3]  
}  
}  
  
thick_1A <- thick_1A + coef(fit1A1)["thick_1A_r~1"] #add intercepts to predicted values  
silt_1A <- silt_1A + coef(fit1A1)["silt_1A_r~1"]  
OM_1A <- OM_1A + coef(fit1A1)["OM_1A_r~1"]
```

B5: Cross validation

```
cross_valid<-as.data.frame(matrix(nrow=nrow(V_data),ncol=4))
colnames(cross_valid)<-c("sample","thickness","silt", "OM")

count<-1
for (i in c(V_data$nr)){
  temp<-subset(V_data,(nr!=i))
  fit1AI<- lavaan(LAVAAN_horA1, data=temp)
  print(paste("sample = ", i,sep=""))
  summary(fit1AI)

  B <-matrix(c(0,coef(fit1AI)["silt_1A_r~thick_1A_r"],coef(fit1AI)["OM_1A_r~thick_1A_r"],
  coef(fit1AI)["thick_1A_r~silt_1A_r"],0,coef(fit1AI)["OM_1A_r~silt_1A_r"],
  coef(fit1AI)["thick_1A_r~OM_1A_r"],coef(fit1AI)["silt_1A_r~OM_1A_r"],0),
  ncol=3,nrow=3)
  B[is.na(B)] <- 0

  coef(fit1AI)
  I<-diag(nrow=3,
  ncol=3)

  A<-matrix(c(coef(fit1AI)["thick_1A_r~age_hy"],coef(fit1AI)["silt_1A_r~age_hy"],
  coef(fit1AI)["OM_1A_r~age_hy"],coef(fit1AI)["thick_1A_r~VI"],
  coef(fit1AI)["silt_r~VI"],coef(fit1AI)["OM_1A_r~VI"]),
  nrow=3,ncol=2)
  A[is.na(A)] <- 0

  p=matrix(c(V_data$age_hy[count],V_data$VI[count]),nrow=2,ncol=1)
  n=c(0,0,0)
  z<-(I-B)^-1
  z[is.infinite(z)] <- 0
  n=(solve(I-B))%*%(A%*%p)
  cross_valid$sample[count]<-i
  cross_valid$thickness[count]<-n[1]+coef(fit1AI)["thick_1A_r~1"]
  cross_valid$silt[count]<-n[2]+coef(fit1AI)["silt_1A_r~1"]
  cross_valid$OM[count]<-n[3]+coef(fit1AI)["OM_1A_r~1"]
  count<-count+1
}
```


C3: Physical weathering

```
void soil_physical_weathering() //calculate physical weathering
{
    int cells = nr * nc;
    int layer, tex_class;
    double depth;
    try
    {
        for (row = 0; row < nr; row++)
        {
            for (col = 0; col < nc; col++)
            {
                if (dtm[row,col] != -9999) //MEIJ bij elke soil development code deze voorwaarde
                //toegepast, zodat het alleen werkt als er een DEM-waarde aanwezig is. Dit zal ook de snelheid van
                //LORICA verhogen, omdat anders op de cellen met NoData ook bodems worden berekend
                {
                    int tempcol = col;
                    depth = 0;
                    for (layer = 0; layer < max_soil_layers; layer++)
                    {
                        if (layerthickness_m[row, tempcol, layer] > 0)
                        {
                            int templayer = layer;
                            depth += layerthickness_m[row, tempcol, templayer] / 2;
                            for (tex_class = 0; tex_class <= 1; tex_class++) //for (tex_class = 0; tex_class
                            <= 2; tex_class++) //we only physically weather the coarse and sand fractions. MEIJ
                            {
                                int tempclass = tex_class;
                                // calculate the mass involved in physical weathering
                                weathered_mass_kg = texture_kg[row, tempcol, templayer, tempclass] *
                                physical_weathering_constant * Math.Exp(Cone * depth) * -Ctwo /
                                Math.Log10(upper_particle_size[tempclass]) * dt;
                                if (weathered_mass_kg > texture_kg[row, tempcol, templayer, tempclass]) {
                                weathered_mass_kg = texture_kg[row, tempcol, templayer, tempclass]; }
                                total_phys_weathered_mass_kg += weathered_mass_kg;
                                //Debug.WriteLine(" weathered mass is " + weathered_mass + " for class " + tempclass );
                                // calculate the products involved
                                if (tex_class == 0) {
                                    texture_kg[row, tempcol, templayer, tempclass + 1] += 1.00 *
                                    weathered_mass_kg; //MEIJ used to be 0.975
                                    //texture_kg[row, tempcol, templayer, tempclass + 2] += 0 * weathered_mass_kg;
                                }
                                if (tex_class == 1)
                                    texture_kg[row, tempcol, templayer, tempclass + 1] += 1.00 *
                                    weathered_mass_kg; //all weathering material turns to silt MEIJ
                                    // texture_kg[row, tempcol, templayer, tempclass + 2] += 0.04 *
                                    weathered_mass_kg; //no clay produced MEIJ
                                }
                                // if (tex_class == 2) No weathering of silt MEIJ
                                // {
                                // texture_kg[row, tempcol, templayer, tempclass + 1] += weathered_mass_kg;
                                // }
                                texture_kg[row, tempcol, templayer, tempclass] -= weathered_mass_kg;
                            }
                            depth += layerthickness_m[row, tempcol, templayer] / 2;
                        }
                    }
                }
            }
        } // end for cells
    }
    catch { Debug.WriteLine(" Soil physical weathering calculation threw an exception");
    }
}
```

C4: Silt eluviation

```
void soil_silt_translocation()
{
    //in Spitsbergen, it is mostly silt (with attendant clay) that gets translocated in
    the profile. Clay is not modelled in itself

    int layer;
    double eluviated_kg;
    try
    {
        for (row = 0; row < nr; row++)
        {
            for (col = 0; col < nc; col++)
            {
                for (layer = 0; layer < max_soil_layers - 1; layer++) // we loop
                through all layers except the lower one - silt translocation there has no lower recipient
                {
                    if (layerthickness_m[row, col, layer] > 0 && layerthickness_m[row,
                    col, layer + 1] > 0) //both source and sink layers have to exist.
                    {
                        if (texture_kg[row, col, layer, 2] > 0)
                        {
                            //calculate the mass of eluviation
                            eluviated_kg = max_eluviation * (1 - Math.Exp(-Cclay *
                            texture_kg[row, col, layer, 2])) * dt * dx * dx;
                            if (eluviated_kg > texture_kg[row, col, layer, 2]) {
                                eluviated_kg = texture_kg[row, col, layer, 2]; }
                            texture_kg[row, col, layer, 2] -= eluviated_kg;
                            if (texture_kg[row, col, layer, 2] < 0) {
                                Debug.WriteLine("error: too much silt eluviation "); }
                            texture_kg[row, col, layer + 1, 2] += eluviated_kg;
                        }
                    }
                }
            }
        }
    }
    catch { Debug.WriteLine(" Problem occurred in translocation calculation"); }
}
```